

1-1-2016

Sub-Picogram, Inline Detection Of Proteins Using Microfluidic Drop Generators And Shape-Based Detection

Razieh Kebraei
Wayne State University,

Follow this and additional works at: https://digitalcommons.wayne.edu/oa_dissertations



Part of the [Biomedical Engineering and Bioengineering Commons](#)

Recommended Citation

Kebraei, Razieh, "Sub-Picogram, Inline Detection Of Proteins Using Microfluidic Drop Generators And Shape-Based Detection" (2016). *Wayne State University Dissertations*. 1645.
https://digitalcommons.wayne.edu/oa_dissertations/1645

This Open Access Dissertation is brought to you for free and open access by DigitalCommons@WayneState. It has been accepted for inclusion in Wayne State University Dissertations by an authorized administrator of DigitalCommons@WayneState.

**SUB-PICOGRAM, INLINE DETECTION OF PROTEINS
USING MICROFLUIDIC DROP GENERATORS AND
SHAPE-BASED DETECTION**

by

**RAZIEH KEBRIAEI
DISSERTATION**

Submitted to the Graduate School,

Wayne State University,

Detroit, Michigan

in partial fulfillment of the requirements

for the degree of

DOCTOR OF PHILOSOPHY

2016

MAJOR: BIOMEDICAL ENGINEERING

Approved By:

Advisor Date

© COPYRIGHT BY

RAZIEH KEBRIAEI

2016

All Rights Reserved

DEDICATION

Dedicated to:

All the ones who have supported me during my breath taking hardships.

To all the ones who have shared my moments with smile and kindness.

To all the ones who have inspired me and strengthen me.

*To all the ones who have loved me and taught me to be kinder, wiser and better than last year and the years
before.*

ACKNOWLEDGEMENTS

I would like to express my sincere appreciation to Dr. Amar Basu for his valuable contributions to my research. Being a PhD student in his group has been a very precious opportunity for me.

I would also like to thank Dr. Armant for his constant help and encouragement during the past year. I would like to thank Denis Ceh and Priyan Weerappuli for their great help and support. I am very fortunate to have amazing lab mates, friends and family. Last but not least, I appreciate valuable suggestions and constructive inputs from committee members.

TABLE OF CONTENTS

DEDICATION.....	ii
ACKNOWLEDGEMENTS	iii
LIST OF TABLES.....	vii
LIST OF FIGURES	viii
Chapter 1. INTRODUCTION	1
Chapter 2. PROTEIN SEPARATION METHODS	4
Structure of Proteins.....	4
Protein Detection Methods	5
Chemical Detection Methods.....	7
Ion Exchange Chromatography (IEXC).....	19
Reversed Phase Chromatography (RPC).....	21
Detectors in Liquid Chromatography	26
UPLC	31
Continuous Detection Methods in Microfluidics.....	33
Chapter 3. THEORY.....	35
Interfacial Tension	36
Temperature Effect on Surface Tension	39
Surfactants Effect on Surface Tension.....	40
The Effect of Proteins on Interfacial Tension	42
Langmuir Isotherm.....	44

Gibbs Isotherm	45
Young- Laplace Equation: Pressure Difference Due to Interfacial tension	46
Dimensionless Numbers.....	47
Fabrication of Microfluidic Drop Generators.....	52
Theory of Droplet Generators	54
Flow Driven Versus Pressure Driven Systems.....	56
Impact of Interfacial Tension on Drop Formation	63
Proteins	65
Carrier Phases	65
Chapter 4. EXPERIMENTAL RESULTS.....	68
Pendant Drop Experiment	69
Drop Generation.....	77
Effect of Proteins on Drop Size.....	87
HPLC System Connected To Microfluidic Chip.....	90
Protein Measurement without HPLC.....	100
Chapter 5. SIMULATION.....	107
Fixed Flow System	107
Fixed Pressure System	109
Comparison of Pressure Profiles	113
3D simulations.....	115
Chapter 6. Application	117

Chapter 7. Future work.....	119
Chapter 8. CONCLUSION.....	122
BIBLIOGRAPHY	124
ABSTRACT	136
AUTOBIOGRAPHICAL STATEMENT	139

LIST OF TABLES

Table 2-1. List of different fractionation methods [5].....	6
Table 2-2. Common types of spectroscopy [6], [15]	13
Table 2-3. Important parameters in chromatographic separations [22], [23], [24]	15
Table 2-4. Limitations and selectivity of major detector groups	30
Table 2-5. Limit of detection and linear range of various detectors [27].....	30
Table 2-6. List of different continuous methods used in microfluidics [13]	34
Table 3-1. Properties of the proteins used in the experiments.....	65
Table 3-2. Chemical and physical properties of different carrier phases.....	67
Table 4-1. Experimental results for change in drop size versus pressure ratio	80
Table 7-1. Possible continuous phases for drop generation [103]	120

LIST OF FIGURES

Figure 2-1. A typical amino acid structure	5
Figure 2-2. Summary of different detection methods. Types of detectors used in liquid, gas chromatography as well as spectroscopy are shown underneath.....	7
Figure 2-3. Radiation through a sample and blank [20]	10
Figure 2-4. Schematic of Beer Lamber's law [20]	11
Figure 2-5. Positive and negative divergence from ideal calibration curve [6].....	13
Figure 2-6. Schematic of a chromatographic separation with mobile and stationary phases. The two red arrows show diffusion from mobile phase to stationary phase and from stationary phase to mobile phase.....	14
Figure 2-7. Schematic of a typical chromatogram with retention time of t_R and width of W_h	16
Figure 2-8. Schematic of signal to noise ratio [30].....	17
Figure 2-9. Symmetry of a chromatogram [27]	17
Figure 2-10. Schematic of peak to valley ratio [27]	18
Figure 2-11. Positively charged protein binds to negative beads and negatively charged protein can pass through the column	22
Figure 2-12. Shows the difference in peak capacity in HPLC (top) Vs. UPLC (bottom) graph [53]	32
Figure 2-13. Comparison of HETP in different LC systems [52]	33
Figure 3-1: Interaction of molecules at a liquid interface (from [63])	37
Figure 3-2: Molecular forces in bulk and surface of water	38
Figure 3-3. Interface motion associated with regions of different temperature (from [63]).....	40
Figure 3-4. Schematic of surfactants on the surface of a water droplet (from [63])	40
Figure 3-5. Change in surface tension with different concentrations(from [63])	41
Figure 3-6. Schematic of Marangoni convection due to difference in concentration (from [63]) .	42
Figure 3-7. A droplet of water in oil. Molecules of BSA are adsorbed to water side from their hydrophilic head and their hydrophobic head is facing the oil side.	43

Figure 3-8. Adsorption of proteins on the interface of a droplet (from[72])	43
Figure 3-9. Schematic of a droplet with proteins adsorbing to its surface	44
Figure 3-10. Liquid drop which is immersed in another immiscible liquid increase in the volume causes increase in surface area (from [63])	47
Figure 3-11. Schematic of a plug inside a channel	49
Figure 3-12. a) The process of replica molding for making PDMS stamps. These PDMS stamps can be bounded to a plain PDMS layer or glass. b) A single channel with two inlets and one outlet is made by PDMS. A photograph of a two channel PDMS chip is shown(from [83])	53
Figure 3-13. Schematic of gaseous silanization process A. Hydrophilic surface after treating with plasma B. step 1 in silanization reaction. When the surface of pdms is treated with FDTS Si bonds to OH groups C. over time Si-O-Si groups are formed. These groups will make the surface hydrophobic.....	54
Figure 3-14. Schematic of different drop generation approaches a) coflowing systems b) cross flowing in a T junctionc) Elongational flow in a flow focusing channel (from [80])	55
Figure 3-15. Schematic of 3 steps in drop formation.	58
Figure 3-16. Drop formation process in a T shaped channel (from [91])	59
Figure 3-17. Flow rate controlled system versus pressure controlled system (from [90])	59
Figure 3-18. Dimensionless drop length versus pressure ratio(from [90])	60
Figure 3-19. Dimensionless drop length versus flow rate ratio (from [90])	61
Figure 3-20. Droplet diameter vs. water pressure at three different oil pressures. The filled markers are experimental data and the unfilled markers refer to predicted data by following equation (from [90]).....	62
Figure 3-21. System set up for studying the dynamic interfacial tension (from[91])	63
Figure 3-22. Different concentrations of surfactant inside a droplet (from [91]).....	63
Figure 4-1. Pendent drop experiment set up	70
Figure 4-2. 3D design for syringe holder in pendent drop experiment	70
Figure 4-3. Schematic of surfactants on the surface of a water droplet	71
Figure 4-4. Different percentages of methanol in water with FC-40 and 2% surfactant.....	71
Figure 4-5. Different percentages of methanol in water with Oleic acid	72

Figure 4-6. Effect of different concentrations of protein on IFT	73
Figure 4-7. Effect of different concentrations of blood plasma on IFT	74
Figure 4-8. Effect of different concentrations of protein LGAL- 14 on IFT (water in oleic acid)...75	
Figure 4-9. Effect of different concentrations of protein PGF on IFT (water in oleic acid)	75
Figure 4-10. HPLC pump calibration with different flow rates	76
Figure 4-11 Microfluidic chip design and dimensions	77
Figure 4-12. Pressure regulators used for oil and water input	77
Figure 4-13. Schematic of the block diagram used for controlling pressure regulators	78
Figure 4-14. The drop generation zone considering the water/oil pressure ratio.....	79
Figure 4-15. Schematic of the closed loop drop generation system.....	82
Figure 4-16. Characterization of open loop system. (A) Model. (B) The open-loop system shows a nonlinear relation between water pressure and plug length (C) open loop testing of response time, using a 3-3.2 PSI pressure and step function at 1Hz. (D, E) Open loop characterization of plug spacing and plug velocity, under the same experimental conditions as (C).	84
Figure 4-17. Characterization of closed loop system. (A) Model. (B) The closed-loop system provides precise, linear control of drop size. (C) Step response with proportional gain (KP) set to 0.0005, showing a critically damped response. (D) Step response with KP doubled to 0.001, resulting in oscillations on the low to high transition.	86
Figure 4-18. Dynamic, in situ tuning. The closed loop system is used to generate a tri-disperse population 150, 200, and 250 μm plugs. (A) Plug length vs. time, (B) histogram of plug lengths.	87
Figure 4-19. The drop generation zone considering the water/oil pressure ratio.....	88
Figure 4-20. A. Using Hexadecane as carrier phase doesn't cause considerable change in drop size B. Oleic acid shows a limit of detection of 10^{-7} g/ml with Thyroglobulin. Velocity of droplets also changes with the amount of protein D Using octanol the limit of detection is about 10^{-5} g/ml.....	89
Figure 4-21. Total amount of protein detected.....	90
Figure 4-22. Comparison between various detection methods	90
Figure 4-23. HPLC detector based on drop shape morphometry. A drop generator is attached inline after the HPLC column, and the drop shape/size is monitored in real time.....	91
Figure 4-24. Proteins accumulate at the end of droplet. This is due to Marangoni flows inside the droplet.....	93

Figure 4-25. Drop size change with protein elution in HPLC.....	94
Figure 4-26. The outlet of HPLC goes to the inlet of the chip. The other tube (with resistance) is to bypass the extra liquid to a syringe.	95
Figure 4-27 (A) The UV absorbance detector shows no signal for the 0.1 mg/ml; (B) Drop length vs. time (C) Shape eccentricity vs. time.....	96
Figure 4-28. Major axis length peak area vs. concentration for three different injections	97
Figure 4-29. Shape Eccentricity peak area vs. concentration for three different injections	98
Figure 4-30. Confined drop (plug) generator. (A) Plug length vs. time (B) Plug shape eccentricity vs. time.....	99
Figure 4-31. (A) Plug length vs. injected protein concentration in a confined drop generator. As the protein concentration increases, the plug length decreases. (B) Drop shape vs. protein concentration in an unconfined drop generator. With increasing protein, the drop elongates to a teardrop shape.....	99
Figure 4-32. Injection to the tube using a 10 μ l Hamilton syringe	100
Figure 4-33. The pattern of drop size change by injecting protein to the tube. This graph represents drop size change at concentration 0.001 gr/ml	100
Figure 4-34 Schematic of protein injection to the chip. We are using the buffer inlet to inject protein to the chip.	101
Figure 4-35. Drop size doesn't show any change with pristine solution or very low concentrations (10-5 gr/ml) of protein.....	102
Figure 4-36. Graphs show the change in major axis length change with protein injection. The peak time varies with concentration.	103
Figure 4-38. Calibration curve for Log (time) Vs. Log (concentration).....	105
Figure 4-39. Drop size during different times after injection of protein. This figure shows that drop size returns to its original size at about 846 seconds.	106
Figure 5-1. Change in drop size with increasing water flow rate (oil flow rate is kept constant at 0.02 m/s).....	108
Figure 5-2 Demonstration of increase in drop size with increase in interfacial tension, the amounts of interfacial tension are shown on each channel	109
Figure 5-3. Drop size increase with increase in water pressure at constant oil pressure	110
Figure 5-4 Shows a schematic of fluid fraction inside microfluidic channel with different amounts of interfacial tension	112

Figure 5-5. Comparison of droplet size vs. interfacial tension both in flow driven and pressure driven systems 113

Figure 5-6 Pressure profile at one point of the microfluidic chip 114

Figure 5-7. Comparison of pressure profiles at three different inlet points 115

Figure 5-8. 3D simulation of drop generation with $\sigma=0.02$ 116

Figure 7-1 Chip design for antibody coating 119

Chapter 1. INTRODUCTION

Proteomic workflows rely on sensitive and precise methods for detecting proteins. In the most common workflow, proteins are separated by liquid chromatography and detected with an inline detector. However, the most commonly used detector, UV-Vis absorbance, provides relatively low sensitivity and requires long path lengths in the flow cell. Mass spectrometry-based detectors provide high sensitivity, but are more expensive and require some optimization of protein ionization and fragmentation [1]. Other sensitive detection methods such as ELISA (Enzyme Linked Immunosorbent Assay) cannot be easily integrated into 'inline' continuous measurements where we need continuous monitoring and analyzing samples [2].

Detection and diagnosis of various diseases is dependent on sensitive and specific detection of proteins relevant to them. Quantitative monitoring of proteins is shown to be one of the most promising approaches for biomarker discovery [3]. Better detection and quantification techniques can lead to better understanding of metabolic cycles and biological reactions inside the body. Secreted extracellular enzymes and metabolites can also be analyzed by better protein detection techniques. This can potentially lead to molecular fingerprinting and early diagnosis of diseases[4], [5].

Recent advances in patient inspired techniques obligates scientists and engineers to design technologies compatible with patient needs. This applies to samples taken from patients and also the tests. Evaluating known serum biomarkers such as galectin-14 (LGALS14), and placental growth factor (PGF) can be a great way of predicting

pregnancy loss. Previous research has reported a decrease in the amounts of these two biomarkers in woman who experience pregnancy loss in comparison to control group [6].

In this research we present a highly sensitive, label-free method to detect proteins in continuous flow, using a pressure-driven microfluidic droplet generator. This continuous detection method is based on the difference in interfacial tension of different proteins. We have applied our method to different protein mixtures such as blood plasma. Problem statement, research objectives and research contributions are summarized here:

Problem Statement:

Lack of a sensitive, reproducible, inexpensive method for detecting proteins

- Low sensitivity of UV absorbance detectors in microfluidic devices.
- ELISA methods perform in batch mode and cannot be integrated to continuous detections such as HPLC.
- Mass spectrometry-based detectors provide high sensitivity, but are very expensive and require optimization for each protein.

Research Objectives:

- Inexpensive, sensitive, reproducible, continuous method for protein measurement (fg-ng ranges).
- Testing different proteins to investigate the domain of presented method.
- Presenting a real world application for this method.

Research Contributions:

- Presented a label free inline protein detection method which is sensitive to globular proteins encapsulated inside water-oil droplets

- This method was effective only using oleic acid and octanol. Other nonpolar oils such as Hexadecane and FC-40 are not effective for this experiment.
- This method has shown promising results with placental protein galectin (LGAL-14)

After this introduction, chapter 2 will provide an overall review of the protein detection methods. Chapter 3 will talk about the theory of our detection technique. Many of the fundamental aspects of microfluidic devices are also discussed here. Dimensionless numbers and definitions for them are also included. Reading this chapter will provide a core understanding of microfluidic devices and their physics. Experimental results are presented in chapter 4. These results are also discussed with potential conclusions. Chapter 5 includes simulation results and chapter 6 presents one of the applications of the proposed method. Future goals for this project are discussed in chapter 7. The conclusion chapter talks about different outcomes of experiments and the limitations for the suggested method.

Chapter 2. **PROTEIN SEPARATION**

METHODS

Understanding the chemical structure of proteins can aid us to engineer better techniques for protein detection. This chapter presents information about chemistry of proteins and available detection methods. Protein detection methods can be divided into physical and chemical subgroups. They can also be divided into batch and continuous unit operations. Chemical protein detection methods are discussed next. After that we will introduce physical methods with their various subgroups such as liquid chromatography, gas chromatography and mass spectrometry.

For each of these methods, this chapter will discuss the operational principle, strengths and limitations, limit of detection, specificity and selectivity. Various types of chromatography and their applications are discussed in this section. Finally, a comparison between various detectors is demonstrated. Considering the fact that physical methods such as liquid chromatography have performed in continuous pattern, continuous microfluidic protein detection methods are listed at the end.

Structure of Proteins

Proteins, also called polypeptides, are polymers consisting of long chains of amino acids which are connected to each other by peptide bonds. Generally, if a protein chain has less than 40 amino acid residues it is called peptide. Amino acids have the same fundamental structure; however, they vary in their linked R group. For instance, glycine has hydrogen for its R group and alanine has a methyl as its R group (Figure 2-1). The R groups can carry a positive or negative charge in physiological pH range. Different R

groups can enforce different charges on the structure of amino acid. For instance, amine groups are always positive while hydroxyl groups are negative. Proteins have secondary structure which is defined by patterns of hydrogen bonding between the peptide groups. Tertiary structure is a completely folded structure of protein[7], [8]. Fibrous and globular proteins (such as BSA, ovalbumin, Thyroglobulin) have quaternary structure. Variety of bonding interactions holds globular proteins in a clumped shape.

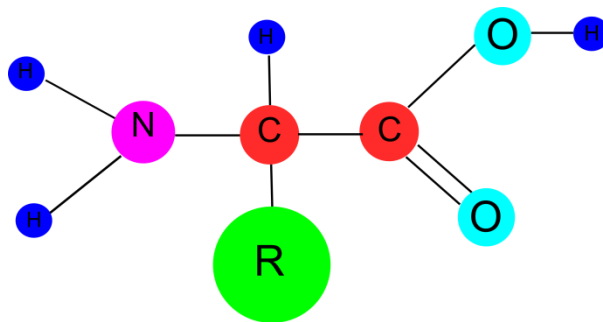


Figure 2-1. A typical amino acid structure

Protein Detection Methods

Protein assays are performed based on single physical/ chemical characteristic as mentioned in Table 2-1. In order to increase the capacity of assays scientists have tried to add 2D and multidimensional assays to their separation systems. Integration of two or more separation system will have challenges such as compatibility of systems and control of the interface between two systems. Specific applications of multidimensional separations are in analysis of metabolites and proteins [9]. Proteins can be fractionated from cell lysate or any kind of protein mixture. It is possible to separate proteins according to their physical or chemical properties such as isoelectric point, refractive index, density, molecular weight, charge or stokes radius.

Some of these methods are designed only for separation and not for quantification of proteins. However, any type of protein quantification may need a separate step for purification as well. Thus some of these methods can be combined together for multidimensional assays.

Table 2-1. List of different fractionation methods [10]

Separation method	Physical/Chemical property
Ultracentrifugation	Density
Size-exclusion chromatography	Stokes radius
Isoelectric focusing	Isoelectric point
Hydrophobic interaction chromatography	Hydrophobicity
Reversed phase chromatography	Hydrophobicity
Ion exchange chromatography	Charge
Affinity chromatography	Specific biomolecular interaction
Gel electrophoresis	Stokes radius

As Figure 2-2 shows, protein detection methods are categorized into two major groups depending on the nature of the separation/detection method. Chemical methods include ELISA and all the detection methods which are based on a chemical reaction between a specific reagent and protein. Physical methods are divided into chromatography and spectroscopy methods.

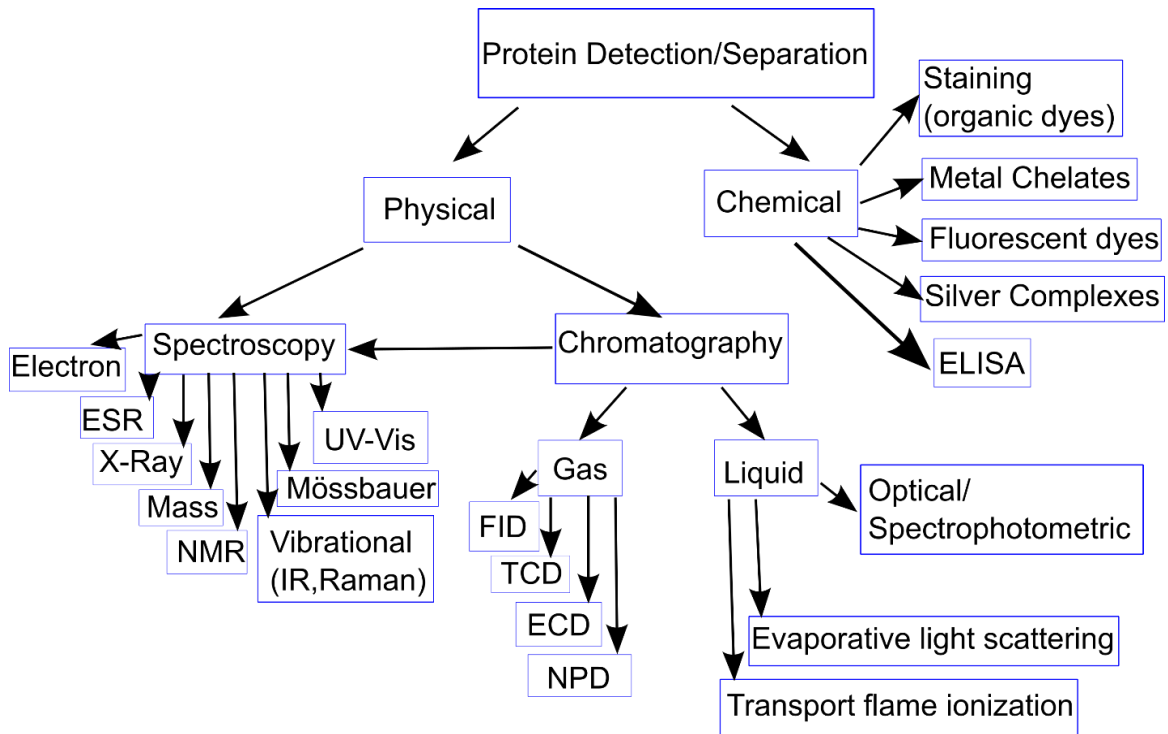


Figure 2-2. Summary of different detection methods. Types of detectors used in liquid, gas chromatography as well as spectroscopy are shown underneath.

Chemical methods can be used in combination (after) physical methods. Since chemical methods are irreversible (due to chemical reactions), it is not possible to apply them before physical methods.

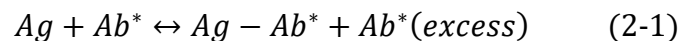
Chemical Detection Methods

Many chemical and enzymatic methods have been used to detect the amino acid bounds and chemical structure of proteins [11]. Protein labels covalently attach to a specific binding site in protein chemical structure and promote detection and separation of the desired protein. Depending on their active sites and chemical structures, proteins may have various reactions to different labels. In order to maintain specificity and selectivity, each label should be designed for a certain protein with best linear dynamic range. This will cause a signal depending on the characteristics of the protein. For instance, in Bradford method the dye Coomassie blue binds to arginyl and lysyl residues

of protein. Interference from other compounds and lack of specificity are major drawbacks of these methods [12].

Enzyme linked immunosorbent assays (ELISA) are used for detection of peptides, proteins and antibodies. ELISA is typically performed in batch mode, in 6, 24, 96 or 384, 1536 well plates [13]. It has become clear that batch mode is not a proper choice for continuous flow of high throughput screening assays due to limitations such as sample handling, assay time, evaporation and expense. Most of the mentioned chemical methods can be performed in batch mode and it is not possible to combine them with another detection/separation method in a continuous operation [14].

In these methods an antigen is immobilized on a solid surface (in commercial products the plates are pre coated). A corresponding antibody linked to an enzyme will complex to antigen (in a lock and key mechanism Ab-Ag). Enzyme activity will be measured. For this purpose, usually enzyme is incubated with a substrate to produce a measurable product. Horse radish peroxidase (HRP) and alkaline phosphatase (AP) are commonly used in ELISA kits. These enzymes are compatible with a large number of substrates. Selection of the proper substrate depends on required sensitivity and available instrumentation. [15]. In formula (2-1) Ab^* is a symbol for the labeled antibody.



Immunological assays such as ELISA have many applications in clinical, scientific and pharmaceutical studies since 1960s. These techniques are capable of detecting important biomarkers, hormones, proteins, enzymes and microbes in biological mixtures [8].

Fluorescent detection is the most utilized signal transduction method for immunosorbent assays; however, bulky instrumentation used in these methods (fluorescent scanners) are another barrier for performing handy health care experiments or diagnostics. For most specific immunoassays the sensitivity of the assay is dependent to the label and its complex with Ag/Ab. Considering this phenomena, label free methods have the privilege of quantifying proteins in their primary state without conducting chemical reactions. Some of the ELISA versions are applied to microfluidic chips for better automation and high throughput screening [16],[17]. All ELISA versions need 5-30 minutes incubation time dependent on the labels they are using. This makes the ELISA not compatible with inline continuous screenings.

Proteomics research demands sensitive inline fractionation and detection techniques for complex proteins in different body fluids or biological systems. A typical human cell can express up to 20,000 proteins at any given time [18]. Continuous flow separations are useful for online monitoring and linking upstream and downstream samples. These methods are playing a key role in point of care analysis devices.

Physical Methods

Some of the chemical methods are discussed in previous section, here we will focus on physical methods and their varieties. For this purpose spectroscopy and its concept is studied initially. This includes Beer Lambert's law and related equations. Afterwards, we will investigate liquid and gas chromatography techniques.

Spectroscopy

After chemical methods, spectroscopy is the most common method of protein detection[19]. Traditionally, spectroscopy was referred to all the methods dependent on

absorption and emission of the visible and UV radiation; however, spectroscopy methods have been extended to other types of electromagnetic waves (X-rays, microwaves, radio waves or even energetic particles and plasma spectrometers) after 1900 [20]. The nature of electromagnetic radiation can be described in terms of waves and particles. When they pass through different media the light can be described as waves. In case of absorption or emission the light is explained as particles [21].

Different spectroscopic techniques operate at different ranges of spectrum. For instance UV-visible spectroscopy only operates at wavelengths 10^{-6} - 10^{-7} m. UV or visible light can be absorbed by many compounds depending on their chemical structure. Absorption of light in different molecules corresponds to various structural groups such as carbonyl, amine etc. Figure 2-3 shows monochromatic radiation passing through a sample (PT) or blank (P0).

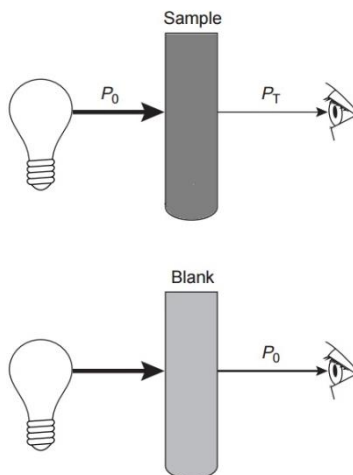


Figure 2-3. Radiation through a sample and blank [20]

The amount of light absorbed to the sample is measured by different formulas.

Transmittance is defined as:

$$T = \frac{P_T}{P_0} \quad (2-2)$$

Absorbance is defined as:

$$-\log\left(\frac{P_T}{P_0}\right) = \log\left(\frac{P_0}{P_T}\right) = A \quad (2-3)$$

Besides absorption by solute, there are some other reasons for depletion of radiation power after passing the sample. For instance, the solvent itself may have some absorption or a small amount of reflection may happen. Having a blank sample of solvent without any solute can reduce these errors.

Colorimetric detections are based on Beer Lambert's law. Passing monochromatic radiation through a sample with finite length involves decrease in power corresponding to sample's length (thickness) as shown in Figure 2-4.

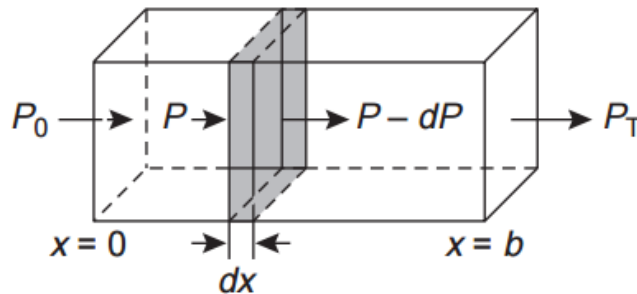


Figure 2-4. Schematic of Beer Lambert's law [20]

A simple energy balance in the defined boundary conditions results in:

$$\frac{-dp}{p} = \alpha C dx \quad (2-4)$$

Where α is the proportion constant. Integrating the two sides of equation can result in:

$$\int_{p=p_0}^{p=p_T} \frac{-dp}{p} = \int_{x=0}^{x=b} \alpha c dx \quad (2-5)$$

$$\ln\left(\frac{p_0}{p_T}\right) = \alpha bc \quad (2-6)$$

Considering the absorbance formula:

$$A = abc \quad (2-7)$$

Where α is the absorptivity of the solute defined by $\text{cm}^{-1}\text{Conc}^{-1}$. If concentration is presented in molarity then the units of α will be $\text{cm}^{-1} \text{M}^{-1}$ and it is replaced by ϵ . ϵ is extinction coefficient, c is concentration in mol/L and b is optical path length in cm. Thus if the ϵ is known measurement of A can define the concentration of sample. In spectrophotometers the path length is usually set as 1 cm.

Limitations of beer's law can be instrumental or chemical. One of the chemical limitations is the sample concentration. At relatively high concentrations absorption peaks broaden and they are not accurate enough. Particles in the sample interact with each other which leads to variations in extinction coefficient. This phenomena can also be explained due to the change in refractive index at higher concentrations which both affects and causes positive or negative divergence from an ideal linear calibration curve as shown in Figure 2-5.

One of the instrumental limitations is that the radiation is not always purely monochromatic and it varies with percentage of bandwidth. Maintaining the 1 cm distance is not possible for many microfluidic chips or high throughput screening applications. If light doesn't pass through sample but reaches the detector it can cause a stray effect. This is another instrumental barrier which relates to wavelength selector in the system.

Spectroscopic methods are very powerful tools for defining chemical structure of unknown molecules. They are used for identifying different chemical structures and reactions especially in organic chemistry. One of the examples of the spectroscopic

methods is calorimetry which is very common. Calorimetry is based on absorbance of light in the sample and it shows a linear signal with increasing concentration.

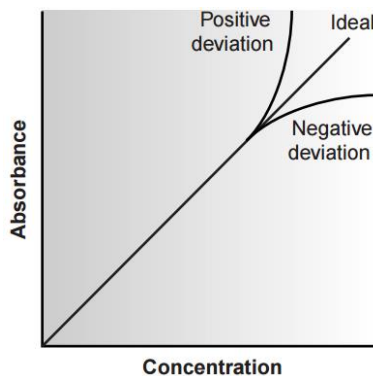


Figure 2-5. Positive and negative divergence from ideal calibration curve [6]

Here we will introduce different classifications of spectroscopy methods and compare them. Mass spectroscopy has limit of detection 1-50 fg of protein with dynamic range of 10^5 . This can vary with protein or type of detector. Certain modifications are being done on new versions which causes better limit of detection and dynamic range [11].

Mass spectrometer located in Wayne state proteomics core offers detection limit in the range of fg-pg for proteins. They digest the proteins using trypsin which is a protease enzyme. Then they will compare the ion spectra of the sample with standard curves. This method is not reversible and it cannot be used before other detection methods. Common types of spectroscopy are shown in Table 2-2.

Table 2-2. Common types of spectroscopy [11], [20]

Absorption	The power of light is measured before and after passing a sample. It is also referred as tunable diode laser absorption spectrometry (TDLAS)
Fluorescence	This technique uses high energy photons to pass through a sample which will emit lower energy photons [22].
X-ray	Inner shell electrons can be excited to outer empty orbitals when the atoms are excited with x-ray.
Flame	This category includes three subdivisions. Flame emission spectroscopy, flame atomic absorption spectroscopy and atomic fluorescent spectroscopy. This method uses the intensity of the light emitted from a flame or spark to quantify the amount of a certain component in a sample [23].

Visible	Many atoms absorb visible light in their gas phase. This type of spectroscopy is usually combined with UV spectroscopy [24].
Ultraviolet	Ultra violet photons are very energetic and all atoms can absorb UV radiation. This type of spectroscopy is often used for protein/DNA quantification[19], [21].
infrared	This type of spectroscopy has many applications in organic chemistry for studying the inter molecular bonds in the sample[19].
Raman	Raman spectroscopy is using monochromatic and inelastic radiation (often from a laser source) to analyze vibration and rotation states of molecules. Shift in the frequency of the reemitted light can provide information about the intermolecular transitions.
Nuclear magnetic resonance (NMR)	NMR refers to absorption and emission of radio frequency by a nucleus in a magnetic field. Complete structural and conformational analysis and quantification of complicated mixtures is possible by this technique [25].
Photoemission	This technique is based on photoelectric effect to study the electronic structure of molecules, surfaces. Measuring the energy of electrons emitted from solids can verify the binding energy of various electrons in a compound [26].

Chromatography:

In general chromatography is separation of different components in a mobile phase which are eluted at different rates through the stationary phase (Figure 2-6). While mobile phase is traveling through stationary phase, each component in mobile phase will have different migration velocity. This is the principle for separation in chromatographic techniques.

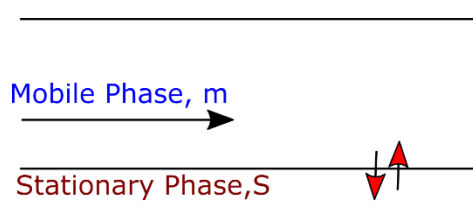


Figure 2-6. Schematic of a chromatographic separation with mobile and stationary phases. The two red arrows show diffusion from mobile phase to stationary phase and from stationary phase to mobile phase.

Some components tend to adsorb to the stationary phase by building temporary bonds depending on their affinity to mobile phase and stationary phase. These separation techniques vary by type of mobile phase (liquid or gas) and type of stationary phase and

the detector used to detect the components in the system. Different chromatographic techniques are listed below [27]:

- Paper chromatography
- Thin layer chromatography
- Gas chromatography
- Liquid chromatography
- Size exclusion chromatography
- supercritical fluid chromatography

Here we will introduce important parameters in chromatographic separation techniques. Liquid chromatography and Gas chromatography will be discussed afterwards.

Important Parameters in Chromatography:

Table 2-3 shows the popular parameters for describing the observations in chromatographic separations. Chromatograms are the signals presented by detectors to measure eluent concentration or any other physical/chemical characteristic as mentioned before. Ideal chromatograms should represent Gaussian peaks.

Table 2-3. Important parameters in chromatographic separations [27], [28], [29]

Parameter	Description
Retention time	The amount of time for a peak in the chromatogram (Figure 2-7). $V_R = V \cdot t_R$ Retention volume is directly calculated from flow rate (V) and retention time.
Hold up time	Hold up time is the amount of time required for elution of a certain component in mobile phase.
Mass distribution ratio	This parameter is also called retention factor k and it's defined as the volume of solute in stationary phase and volume of solute in mobile phase. $D_m = K_c \frac{V_S}{V_m}$ where K_c is the distribution coefficient
Retardation factor	Retardation factor is the distance traveled by fraction of injected component (analyte) in the mobile phase to the distance traveled by solvent.
Column performance	For all separation techniques performance of the system is calculated in terms of number of theoretical plates. $N = 5.54 \left(\frac{t_R}{w_R} \right)^2$ As shown in figure 2-7.

Peak to valley ratio	This test is to confirm system's performance in separating two different components. $\frac{p}{v} = \frac{H_p}{H_v}$
Signal to noise ratio	The precision of the separation is affected by this parameter. $\frac{S}{N} = \frac{2.H}{h}$ As shown in figure 2-8.
Symmetry	This factor is also called tailing factor and it is calculated by $w_{0.05}/2d$ in figure 2-9.
Resolution	Each peak should start from baseline and end in baseline in ideal situation, however in some cases especially when components have similar characteristics (such as molecular weight) peaks are merged together or they do not separate completely. Figure 2-10

Figure 2-7 shows a typical chromatogram. Generally chromatograms are a demonstration of signal (Y axis) versus time (X axis). The amount of time for a chromatogram is called retention time and width of the chromatogram at half of its height is called W_h .

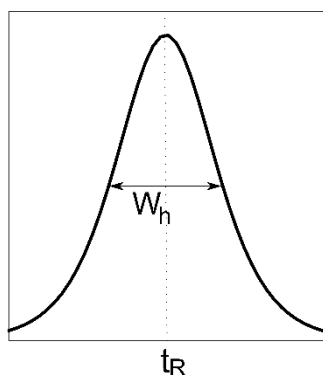


Figure 2-7. Schematic of a typical chromatogram with retention time of t_R and width of W_h

Parameters mentioned in Table 2-3 are essential for characterization and comparison of experimental results. Figure 2-8 shows a demonstration of signal to noise ratio. This ratio should be at least more than 2, otherwise there wouldn't be any distinction between signal and noise. Figure 2-9 shows the symmetry of the chromatogram. Symmetry factor is also called tailing factor (symmetry) as mentioned in Table 2-3.

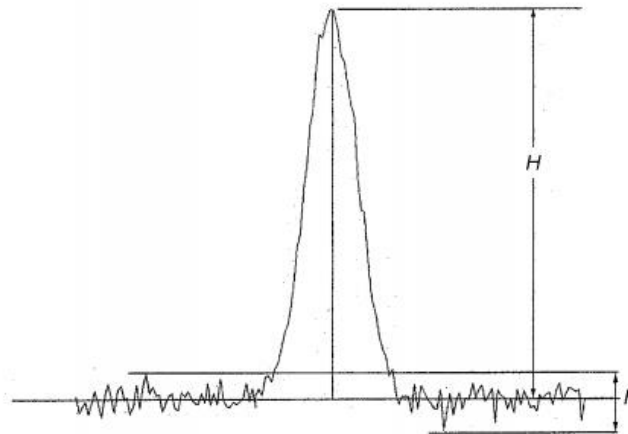


Figure 2-8. Schematic of signal to noise ratio [30]

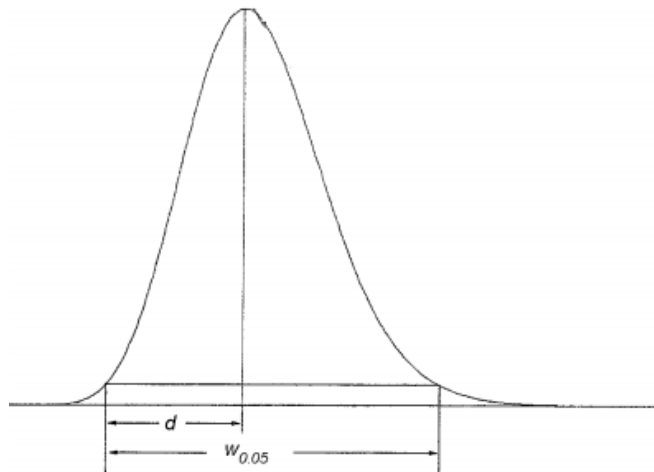


Figure 2-9. Symmetry of a chromatogram [27]

Another important parameter in chromatography experiments is the peak to valley ratio as shown in Figure 2-10. This ratio defines the resolution of peaks. If we don't have a good resolution peaks will merge to each other and we cannot define a separate peak. This happens for various reasons such as contamination in the column.

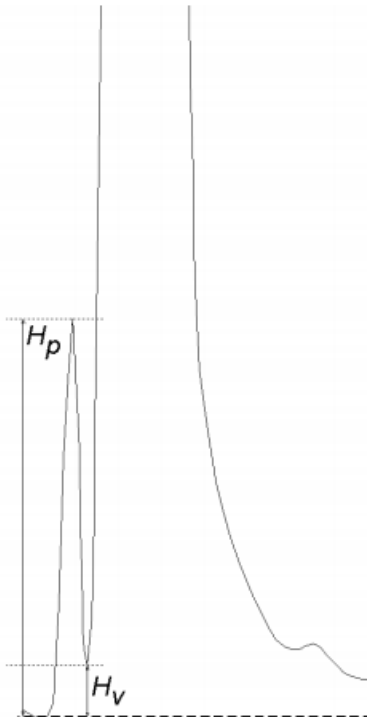


Figure 2-10. Schematic of peak to valley ratio [27]

Liquid Chromatography:

Liquid chromatography is widely used for purifying individual proteins in a mixture. Basically in this method, the mobile phase and the eluent are passed through a packed column. Liquid chromatography is modeled using mass balance equations in mobile and stationary phases in the column [31]. Depending on the column type and chemical structure the mobile phase can be eluted faster or slower. Interactions between stationary phase and mobile phase are also responsible for separation. There are several methods used for protein and peptide separation by HPLC [28], [29], [31], [32]:

- Ion exchange chromatography
- Chromatographic methods based on hydrophobicity
- Reversed phase chromatography
- Affinity chromatography

- Size exclusion chromatography

These different methods in liquid chromatography are discussed and compared here. Choosing a proper chromatography is dependent to the application and specific demands of the experiment. For instance if we want to keep the structure of protein we may not use reversed phase chromatography; however, we can use ion exchange chromatography or size exclusion chromatography.

Ion Exchange Chromatography (IEXC)

Proteins are amphiphilic structures and they have both positive and negative charges. The sum of charges of different amino acids in protein structure will produce the net charge of protein which varies depending on the pH of the solvent. Ion exchange chromatography is based on ionic charges of proteins on their surface which defines their isoelectric point (PI). Proteins with different charged groups interact with the ion exchange adsorbent.

Charge characteristics of proteins depend on ionizable amino acid residues in protein structure. Generally any free amine group in an amino acid R group can cause positive charge and any carboxyl group can cause negative charge. In addition to the net charge of proteins, the charge distribution and strength in different locations of the molecule is important. If there is a strong charge in a specific region of the molecule, binding to ion exchanger can happen in spite of the fact that the net charge of the molecule is zero. Properties of the ion exchanger, mobile phase and elution process can affect the separation as well [33].

This method is one of the most powerful separation techniques for charged biomolecules such as proteins, peptides and nucleic acids. Due to mild conditions of

separation, a protein can maintain its conformation. Selectivity, simple performance and controllability of ion exchange resins are other advantages of this type of chromatography. These resins are more powerful than other adsorbents used in protein chromatography and they can perform hundreds of separation cycles [34].

Chromatographic Methods Based on Hydrophobicity

Chromatography methods can also be based on hydrophobic interactions between carrier phases and the stationary phase. Chromatographic methods based on hydrophobicity are divided to two groups: Hydrophobic interaction chromatography (HIC) and Reversed phase chromatography (RPC).

Proteins generally have various hydrophobic and hydrophilic groups. In a hydrophilic solvent the hydrophobic groups try to bury themselves in a cover of hydrophilic groups which have active hydrogen bonding sites and link to water molecules. However, some of these hydrophobic groups are still in contact with water molecules.

Generally when a hydrophobic residue is added to a water phase several phenomena is observed [35]:

- Negative entropy change ($-\Delta S$)
- A small enthalpy change that is usually negative ($-\Delta H$)
- An increase in heat capacity ($-\Delta C_p$)
- Decrease in volume ($-\Delta V$)

Hydrophobic chromatography uses minimizing the interface as a driving force. From an energy perspective, this will lead to increase in entropy of the system ($\Delta G = \Delta H - T\Delta S$) [36].

The stationary phases are usually alkane chains with or without amino groups. Phenyl ligands have also shown a good selectivity to aromatic proteins [36]. Increase in the length of the alkane chain causes stronger bonding of hydrophobic protein residues. Interactions in RPC are usually stronger than HIC. Polarity of the solvent is very important in both RPC and HIC.

Reversed Phase Chromatography (RPC)

This type of chromatography is the opposite of the traditional normal phase chromatography in which the stationary phase is usually hydrophilic while the solvent is hydrophobic. RPC is closely related to the principles in HIC and it is based on polarity of molecules. The adsorbents in RPC are usually more hydrophobic than HIC. In RPC molecular interactions are high enough to adsorb molecules even from water to the adsorbent. This technique was originally developed when very small molecules of protein were non dissolvable in organic phases (in HIC).

In RPC the stationary phase is usually nonpolar while the mobile phase is relatively polar. Mobile phases can vary depending on the stationary phase and the analyte. However, the principle of reversed phase chromatography is adsorption of hydrophobic (non polar) analyte on hydrophobic (non polar) stationary phase as shown in Figure 2-11. Polarity of the mobile phase can be adjusted by varying the percentage of water or organic phase inside it. Estimated retention time of a particular protein/polypeptide varies by using different of mobile phases. The following solvents are nonpolar to polar from left to right [37]:

Methanol < Ethanol < Acetonitril < isopropanol

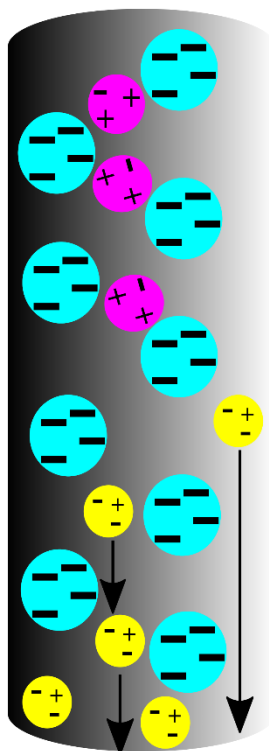


Figure 2-11. Positively charged protein binds to negative beads and negatively charged protein can pass through the column

It is clear that more percentage of nonpolar solvent will result in more linkage of analyte to stationary phase. Organic phase will cause denaturation of the proteins as they alter the three dimensional structure of proteins. Gradient elution is used in RPC to decrease the polarity of the mobile phase by increasing the fraction of organic phase [34].

This technique is usually used for checking the purity of protein samples or quantifying purposes while recovering the protein structure is not necessary afterwards.

Affinity Chromatography

Besides the fact that proteins can interact with the stationary phase based on their charge and hydrophobicity they can also interact with molecules called ligands. Each molecule has binding sites specific for interactions with its ligand. These interactions may be Van der Waals forces, hydrogen bonds or electrostatic forces. These ligands can be proteins as well. Selectivity of ligands can be as unique as only one protein but they can

also be selective to limited number of target molecules depending on their binding sites [33].

It is important to be able to detach the complex of ligand-protein after chromatography by changing the medium without affecting ligand or protein. The mobile phases for affinity chromatography is usually optimized for ideal binding. By changing this ideal binding condition such as pH of the solution it is possible to detach adsorbed proteins. Ligands should be compatible with the carrier phases as well. Flow rate of the mobile phase can cause huge differences in protein binding process. If the flow rate is too high proteins will not find adequate time for attachment and a portion of target proteins will elute without binding to stationary phase [38].

The stationary phase in affinity chromatography should have large surface area available for covalent bonding with ligands. It should also be stable both chemically and physically. Gel material also needs to be inert and stable. Agarose is one of the most popular stationary phases for affinity chromatography. Attachment of a specific ligand to the stationary phase accelerates binding of the desired protein to the surface. This ligand should be compatible with carrier phases used in the procedure. Proteins can be used as ligands since they are very selective; however, synthetic molecules have the advantage of being stable and cheap.

Spacer arms are used as a link between ligands and column (stationary phase). The length of spacers is usually 6-10 carbon atoms. Spacers will prevent binding of the target molecules directly to the stationary phase.

This type of chromatography is often used for purification of proteins such as immunoglobulins, glycoconjugates, DNA binding proteins, receptor proteins, enzymes and synthetic ligands. Isolation of cells or nucleotides [39].

Immobilized metal affinity chromatography is based on the similar concept as affinity chromatography; however, the immobilized phase is metal ions which interacts with some of the protein residues such as histidines. This method relies on specific interaction between metal ions and proteins (mostly histidine groups on the surface of the protein).

Size Exclusion Chromatography (SEC)

In all previously described methods, separation is based on interactions between protein structure and the stationary phase. However, in SEC, Size and shape of the protein molecules are the important factors in this type of chromatography. This technique is also called gel filtration. SEC columns contain different size range beads packed together. As small molecules and large molecules pass through these beads. It is clear that small molecules are able to pass through more channels than larger molecules, therefore larger molecules pass quickly and elute faster than smaller molecules.

Shape of the protein molecule is responsible for SEC separations. Proteins tend to have globular shapes while DNA molecules maintain linear structure. Linear structures elute much faster than globular shapes due to their shape (hydrodynamic volume). Considering this description, a DNA molecule will elute much faster than a protein with same molecular weight [33], [40].

The stationary phase used in SEC is usually made up of synthetic polymers such as polyacrylamide or natural polymers such as agarose. Different amounts of cross linking inside the polymer can cause various pore sizes. These synthetic gels are commercially

available with different ranges of porosity. They are usually categorized by their capacity to separate globular proteins. The upper range shows the largest protein molecular weight and the lower range shows the smallest protein molecular weight [27], [30], [40].

In this type of separation there is no adsorption involved. Choosing the proper pore size in the stationary phase is a key parameter for optimal separation. For best results it is recommended to have a good control over the range of pore sizes in the stationary phase. Unlike the previous methods changing the mobile phase conditions will not affect separation process since separation is based on molecular weight (shape). However we still need a solvent which carries the molecules of interest without changing their structure or affecting the stationary phase. These systems don't need any gradient pumping since proteins are eluted and not adsorbed.

This method offers the least resolution in comparison to other methods, however it is used due to ease of operation and lack of interaction with protein structures. This type of chromatography has a wide range of applications such as buffer exchange, protein fractionation and determination of molecular size. However, protein fractionation is not expected for proteins of globular shape with less than 30% difference in size. The resolution of the two separate peaks in the SEC column increases with the square root of column length. In general the diameter of the column is chosen based on the eluted volume and the length depends on the resolution needed [34].

SEC chromatography (separation by size) is independent of solubility, charge and polarity of the proteins [33]. Coupling this method with another detection method such as mass spectrometry, gel electrophoresis or chromatographic separations has been shown to make better identifications and separations [2], [42], [8], [43] .

Detectors in Liquid Chromatography

Having discussed the different types of liquid chromatography we will now move on to chromatography detectors which are responsible for converting a physical or chemical property of the injected samples to measurable signals. Different detectors can be used in HPLC for defining separate peaks of individual protein in a mixture. Detectors can function according to various parameters as listed below [44].

- Bulk property
- Analyte properties
- Carrier phase properties
- Combined techniques

Bulk property detectors calculate the difference between the properties of the carrier phase with and without sample. For instance refractive index detectors are considered as bulk property detectors.

Analyte property detectors are sensitive to analyte properties. Fluorescence detectors or electrochemical detectors are some of the examples of this group.

Mobile (carrier phase) property detectors are based on some modification or change in carrier phase properties post column. Corona discharge or evaporative light scattering detectors are in this category of detectors.

Combined techniques refers to coupling a different measurement/separation technology to an HPLC system. Some of the popular hyphenated techniques are (LC-MS), (LC-NMR) and (LC-IR).

An ideal detector needs to satisfy the following qualifications [8]:

- Sensitive: Response should be sensitive to certain property or characteristic of the sample
- Selective: It should have selectivity for a certain sample over another
- Wide dynamic range: Which is linear can help the response to be predictable
- Reproducible: Results should be reproducible and predictable
- Reliable: Response should not be affected by environmental parameters such as temperature
- Fast: High speed response enables the detection of short peaks

Each principle detection parameter may have different versions and subgroups. In addition to mentioned types, there are also other versions of detectors which are not the focus of this research such as electrochemical, density and radioactivity detectors. Detectors based on density are not very sensitive and they have many other disadvantages. Electrochemical detectors are very sensitive and specific to reduction of hydro peroxide groups in the molecules. Among various electrochemical methods, electrochemical impedance spectroscopy (EIS) and cyclic voltammetry (CV) are two methods characterized for protein detection. They have reported that with increase in the amount of proteins in the sample the surface charge density will increase [45]. In spite of their high sensitivity (less than 0.1 ng) these methods have some disadvantages such as no selectivity in complex biochemical solutions and interaction of proteins with other molecules.

Seventy five percent of all the detectors used in HPLC systems are UV detectors [32]. Finding the best wavelength for each molecule is essential. For instance at wave lengths between 215 and 230 nm conjugated double bonds are not showing a distinguished

absorbance with UV detector and only esteric groups are absorbed. Table 2-4 shows the major detector groups and their subgroups accompanied with limitations and selectivity of each one. Table 2-5 introduces other methods besides UV absorbance method. UV absorbance happens as a result of transition of electrons from one molecular orbital to another. For instance n to σ . Aromatic samples (such as Benzene) absorb at or below 260 nm. Samples with double bonds such as olefins absorb at 215 nm.

Fluorescent detectors have about 100 times better limit of detection than absorption detectors. They are considered as second most common detectors commercially used (15%) [46], [47]. They are very selective due to the limited number of fluorescent proteins and lipids. Methods mentioned in table 2-4 can also be used together. For instance spectrophotometric detection methods are used as a post column detection system. The content of a specific sample in the HPLC column can be monitored by applying a reaction after the column. Different enzymes, lipids or proteins can be quantified by using the proper reagents for the reaction.

Mass spectrometer can be used as HPLC detector. Mass spectrometer can define chemical structure, formula and molecular weight in addition to quantifying the amount of the protein present in the sample. These instruments are still very costly but they can separate and quantify components of about 160 ng in a sample.

Evaporative light scattering detectors are also known as evaporative analyzers or mass detectors. They are based on nebulization of the solute through a chamber which has a light source. Detector response increases linearly with concentration inside small droplets. The peaks can be modified by tuning the size distribution of droplets. Different calibration curves are reported for the same chemical structure under different

nebulization conditions and sample sizes [48]. They can be used for any solute which does not evaporate before the light scattering chamber. Due to various noise parameters their sensitivity is poor. As reported in this research the minimum amount of sample needed for this experiment is sometimes less than its dynamic range. This means the minimum amount which can form droplets for light scattering tube is lower than the detectable amount by the detector.

Some of the parameters which are considered in selecting detectors are as follows [44]:

- Chemical and physical characteristics of samples
- Potential interferences and noises
- Cost
- Compatibility with the system
- Throughput or number of assays needed

Table 2-4 shows the limitations of each detector subgroup. Depending on the nature of detection method it can be sensitive only to certain molecular structures. Table 2-5 shows the limit of detection and linear range of different detectors such as refractive index, conductivity, light scattering, corona discharge, UV visible, photodiode array, fluorescent, radioactivity electrochemical, interfacial tension (our proposed detection method) and mass spectrometry.

Table 2-4. Limitations and selectivity of major detector groups

Detector	Sub group	Selectivity	Limitations
Optical/Spectrophotometric	Refractive index detector	Lipids	Temperature dependent
	Ultraviolet detector	Aromatic rings, conjugated double bonds	Misses some chemical structures
	Fluorescent detector	Fluorescent molecules, Fluorescent proteins and lipids	Limited application
	Infrared spectrophotometric detector	Non polar molecules	High back ground noise
Evaporative/light scattering		Ketons, Esters, Chlorinated and Aromatic compounds	Nonlinear signal with concentration, No salts or buffers can be used in the solvent
Transport flame ionization		Monomer, dimer and polymeric acids	Many disadvantages such as interfering parameters and non-reproducible results

Table 2-5. Limit of detection and linear range of various detectors [32]

	Range of application	LOD	Linear range
RI	Universal	µg	10 ³
Conductivity	Selective	High ng	10 ⁴
Light scattering	Universal	High ng	10 ³
Corona discharge	Universal	Low ng	10 ⁴
UV/ VIS/PDA	Selective/Universal at low λ	ng	10 ⁵
FL	Very selective	pg	10 ³ -10 ⁴
Radioactivity	Selective	pg	10 ³ -10 ⁴
EC	Very selective	Fg-pg	10 ⁵
IFTD	Very selective	Fg-pg	10 ⁻⁴
MS	Very selective	Fg-pg	Up to 10 ¹⁵

Gas Chromatography

The concept of all chromatographic methods is similar. They are based on elution of a sample through a stationary phase called column via a carrier phase, which is always a neutral gas like nitrogen or Helium. Gas Chromatography or GC is used for analyzing and identifying the compounds that can evaporate without decomposition. The sample injected to the instrument passes the heating chamber to vaporize it. Usually proteins of

secondary and tertiary structure denature with heat because of the disruption of hydrogen bonds and weak intermolecular bonds, chemicals such as alcohols have similar effect and they can cause denaturation of proteins which is irreversible. However, peptide bonds (primary structure) are usually stronger and they don't break with heat [49], [50]. Most of the protein studies using GC have focused on number of amino acids in the protein structure [51]. GC detectors can produce signals which can be mass or concentration dependent. The detectors used in gas chromatography are listed as bellow [50]:

- Thermal conductivity detector
- Flame ionization detector
- Electron capture detector
- Nitrogen Phosphorous Detector
- Atomic Emission Detector
- Photoionization Detector
- Flame Photometric Detector

UPLC

In recent years scientists have tried to improve HPLC units by modifying packing materials, detectors and performance conditions. UPLC (Ultra performance liquid chromatography) is based on the evolution of packing materials which causes better separation with injection volumes less than 1 μ l. According to published articles by Waters Corporation, UPLC has up to 8 times faster speed, up to 3.4 better sensitivity and better resolution. UPLC system uses sub- μ m particles and operates at higher pressures than traditional HPLC.

These changes lead to an improvement in sensitivity, resolution and frequency of analysis. Figure 2-12 is a comparison between peaks for the same sample in UPLC and HPLC. As reported in [52] the peak capacity (number of peaks per unit time) increases about 2.5% in UPLC Vs. HPLC. Efficiency of LC systems is usually described using Van Deemter equation which is an empirical relationship between flow rate and plate height. Height equivalent to theoretical plates or HETP is a measurement for column efficiency.

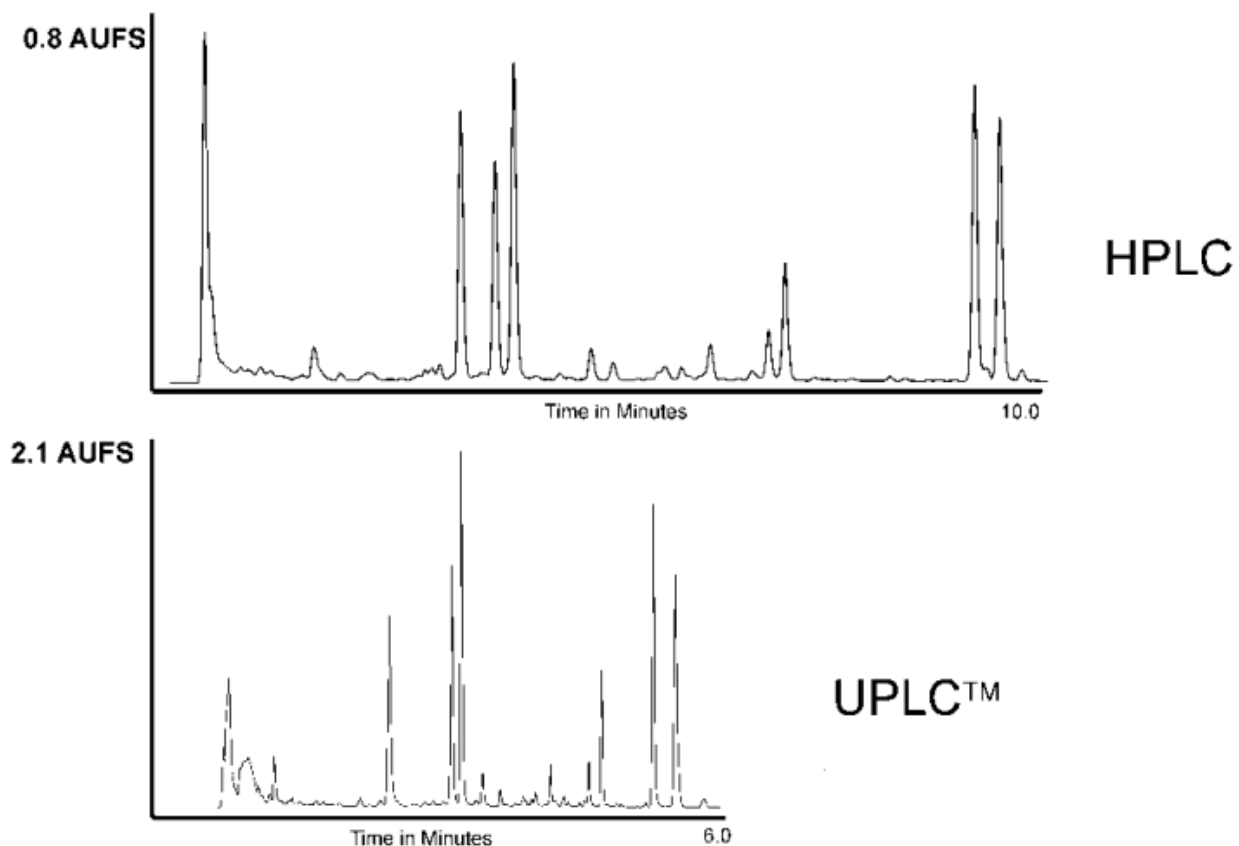


Figure 2-12. Shows the difference in peak capacity in HPLC (top) Vs. UPLC (bottom) graph [53]

Mass spectrometer (MS) detectors are used in UPLC systems causing improved detection limits and sensitivity. Traditionally absorbance detectors are used in HPLC systems and these detectors are sensitive to concentration and they have limitations of Beer's law.

Figure 2-13 shows the history of HPLC systems since 1970. Size of packing materials is decreasing while achieving uniform velocity and better HETP. UPLC systems have minimum particle sizes.

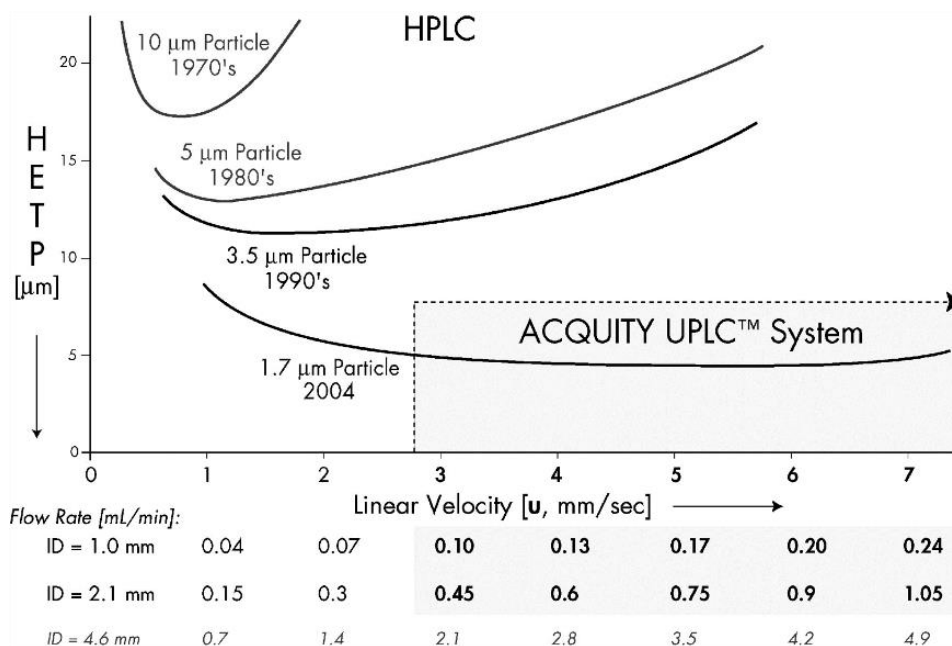


Figure 2-13. Comparison of HETP in different LC systems [52]

Continuous Detection Methods in Microfluidics

Integration between upstream and downstream can lead to other possible analysis or reactions. Microfluidic platforms are in favor of continuous, sensitive and portable screening. A list of continuous flow separations are listed in Table 2-6.

Current continuous protein detection/fractionation methods monitor the existence or lack of existence of a certain component/ substrate inside the samples. Recently, multidimensional separation techniques have gained attention due to better fractionation of proteins in a continuous mode. For instance they combine liquid chromatography and mass spectroscopy to get better limit of detection [9], [54]

Table 2-6. List of different continuous methods used in microfluidics [18]

Method	Separation induced by	Separation based on	Sample	Flow rate/throughput
Pinched flow fractionation	Laminar flow regime	Size	Microparticles, cells	70 cm s ⁻¹ 40 000 particles h ⁻¹
Hydrodynamic filtration	Laminar flow regime	Size	Microparticles	1 mm s ⁻¹ 100 000s particles h ⁻¹
Bifucation	Laminar flow	Size, shape	Blood	5 mL h ⁻¹ 1-3 mm s ⁻¹
Filtration obstacles	Diffusion and obstacles	Size	Blood	5-12 μ L min ⁻¹ 10-20 mm s ⁻¹
Lateral displacement	Obstacle array	Size	Particles (0.8, 0.9, 1.0 μ m) DNA (61 kbp, 158 kbp)	20 μ m s ⁻¹ (DNA) 100 pg h ⁻¹ (DNA)
Brownian ratchet	Diffusion and obstacles	Size	DNA	2 μ m s ⁻¹ 10 pg h ⁻¹
Hydrophoretic separation	Pressure gradient from slanted obstacles	Size	Microparticles	1 to 3 cm s ⁻¹ 10 000s beads h ⁻¹
DNA prism	Obstacle array and electric field	Size	DNA	10 ng h ⁻¹
Entropic trap array	Dams and electric field	Size	DNA	10 pg h ⁻¹
Repulsion array	Dams, electric double layers	Charge to size ratio	Proteins	300 pg h ⁻¹
Free-flow electrophoresis	Homogeneous electric field	Charge to size ratio	Proteins, amino acids	6 mm s ⁻¹
Free-flow isoelectric focussing	pH gradient	Isoelectric point	Proteins and cells	9 mm s ⁻¹
Magnetophoresis	Inhomogeneous magnetic field	Size, magnetisation	Magnetic particles, cells	up to 1.2 mm s ⁻¹ 10 000s cells h ⁻¹
Dielectrophoresis	Inhomogeneous electric field	Size, polarisability	Microparticles, cells	up to 4 mm s ⁻¹ 100 000s cells h ⁻¹
Acoustophoresis	Acoustic pressure	Size, density, compressibility	Microparticles, cells	11 cm s ⁻¹
Optical lattice	Optical force	Size, refractive index	Microparticles, cells	30 μ m s ⁻¹ 90 000 particles h ⁻¹
Sedimentation	Gravity	Density, size	Microparticles, droplets	6 mm s ⁻¹ slowed to 1 mm s ⁻¹

Chapter 3. THEORY

In this chapter, we will discuss some of the concepts related to experimental results. Our drop-based detection system relies on several fundamental phenomenon. When a droplet is formed at a flow focusing junction, its size depends on the interfacial tension. Hence, the first section discusses the concept of interfacial tension and related parameters. There are several parameters having impact on interfacial tension such as temperature and surfactants. Since protein molecules are also amphiphilic (like surfactants) the effect of proteins on interfacial tension is further investigated.

Microfluidic devices are desirable for protein assays due to less sample preparation time, high surface to volume ratio, less consumption of expensive reagents and minimum analysis time [55]. In this research we will focus on droplet microfluidics because each droplet can be considered as a micro container for dissolved materials such as protein mixtures. To understand the physics of drop generation, the Laplace equation is driven by a simple model of a droplet inside a channel. The Langmuir and Gibbs isotherms are shown in the next section for better demonstration of protein adsorption on the interface of water-oil. Dimensionless numbers are key concepts in fluid mechanics (both macro and micro). In order to work in appropriate microfluidic flow rates we need to have a good knowledge of dimensionless numbers and their changes. For instance, we need to work at laminar flow zone (dimensionless numbers in proper range).

Next section describes the fabrication techniques and process of modifying microfluidic chip surfaces. After that we move on to drop generation techniques and common microfluidic chip geometries used for drop generation. Droplets can maintain a well-defined structure for studying small amounts of protein secreted by cells in volumes

of $< \text{pL}$ [42], [56]. In the latter study, the activity of enzyme B-Galactosidase secreted by entrapped cells inside droplets can be measured by fluorescent labeling. Measurement of extracellular protein secretion has been used for amplification of DNA molecules [42], [57]. For this measurement, the clonal amplified DNA in each separate droplet is analyzed for enzymatic activity of certain proteins in order to verify the cloning efficiency.

Most reported protein detection methods for reading out the amount of protein inside droplets are based on fluorescence labeling. These approaches are limited to certain species and cannot be used for complicated mixtures such as blood serum. In fact traditional fluorescence detection methods may lack the sensitivity to detect small amounts of protein molecules [42], [58].

Fluid handling and delivery is one of the big questions in every microfluidic setup. Some of the common methods for injecting fluids to the microfluidic chip include using peristaltic pumps, syringe pumps, pressure regulators, and vacuum pumps [15], [59]. Some of these methods may encounter limitations such as non-uniform velocity profile or pulses in the flow. For instance syringe pumps show repeated pulses in the flow which is not in favor of our experiments. It has been proven that fluctuations made by syringe pumps are the source of polydispersity in droplets [60]. In this section we summarized two of the most common used methods syringe pumps and pressure regulators and compared these two strategies.

At the end we discussed the chemical and physical properties of some of the carrier phases. This chapter will offer a better view of the concept of experimental results in next chapter.

Interfacial Tension

An interface is the geometrical boundary around a certain object (this object can be a droplet or plug). Ideally, an interface doesn't have any thickness or roughness as shown in Figure 3-1. Molecules in the interface always have interactions with neighbor molecules of all sides as shown in Figure 3-2. These interactions can be Van der Waals forces for nonpolar molecules and hydrogen bindings for polar molecules. Interactions between two adjacent fluids (oil-water, water-air) can define the interface. Generally in equilibrium conditions, atoms in the interface will have different energy level than the ones in the bulk. The excess energy of atoms in the interface (also called interfacial excess energy) is equal to surface stress, therefore, this energy is called surface tension [61], [62]. In simple words surface tension defines how easy or difficult it is to extend a surface. If this surface has very strong molecular forces (like water), then it is difficult to extend it and hence surface tension is high.

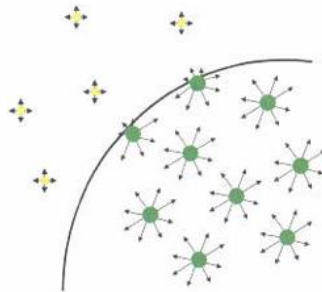


Figure 3-1: Interaction of molecules at a liquid interface (from [63])

For instance, water molecules have strong attractive forces toward each other. The two hydrogen molecules have positive net charge and they are strongly attracted to the oxygen atom of the other water molecule. The net force for each molecule is zero in the bulk; however, there is no upside force (pull) in the surface of water. This cohesive forces cause the surface molecules to behave like a blanket attaching to each other and resisting the external forces, therefore, a light object like a paper clip placed on the surface of pure

water remains suspended. Surface tension, an ignorable (weak) force in macro scale, gains a considerable attention in microscale [64]. This is because they scale as length squared, whereas weight and other mass-based phenomena scale as length cubed [65].

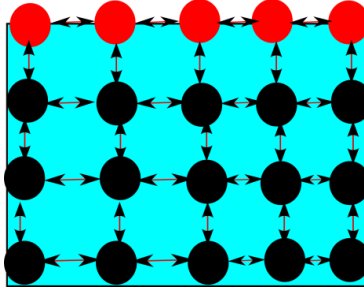


Figure 3-2: Molecular forces in bulk and surface of water

In terms of energy, molecules tend to reduce their energy state. When a molecule is in the bulk of water in contact with adjacent molecules it has the lowest possible energy. However, when a molecule is alone it is in its highest energy level. In water droplets, it is energetically favorable to have a smooth surface in addition to minimizing the surface area. Any curvature in the surface will elevate the molecule's energy level.

If each molecule has a total energy of U , in the bulk, a molecule in the interface will have total energy of $U/2$. If δ is the dimension characteristic of a molecule then δ^2 presents the surface area of that molecule.

$$\gamma = \frac{U}{\delta^2} \quad (3-1)$$

Interfacial tension in the liquid-liquid interface (γ) can be defined as a linear force ($\text{N}\cdot\text{m}^{-1}$) which forms a tensile skin holding the liquid inside. The other definition for interfacial tension is as surface energy ($\text{J}\cdot\text{m}^{-2}$). This energy tries to minimize the surface area and reduce the energy in the interface [66].

When two immiscible surfaces face each other they tend to maintain the minimum possible interfacial area. For any given volume, an enclosing surface with the minimum area is a sphere. In the absence of gravitational forces, droplets in nature are usually in this shape. However, inside a microfluidic chip, the drop shape is also affected by viscous and pressure forces. This will be discussed in more detail later.

Temperature Effect on Surface Tension

Since we learned about the definition of surface tension in previous section here we will discuss parameters having impact on surface tension. One of these parameters is temperature. Surface tension can decrease to zero at a critical temperature T_c [63]. Figure 3-3 shows a demonstration of internal flows inside a droplet with temperature difference on its surface. Equation (3-2) describes the effect of temperature on surface tension:

$$\gamma = \gamma_0(1 + \beta(T - T_0)) \quad (3-2)$$

Surface tension in a reference state is measured as (γ_0, T_0) and the linear change with temperature can be defined using the above equation. If T is equal to T_c then $\gamma=0$:

$$\beta = \frac{1}{T_0 - T_c} \quad (3-3)$$

As mentioned before, surface tension can be considered as a force. Heating a spot on the surface of a fluid decreases surface tension at that region. This phenomena, referred to as the Marangoni Effect, can cause imbalance of surface tension forces and create a flow from low surface tension areas to high surface tension areas. If this heating is temporary, gradient of temperature will result in uniform surface tension around the interface [63].

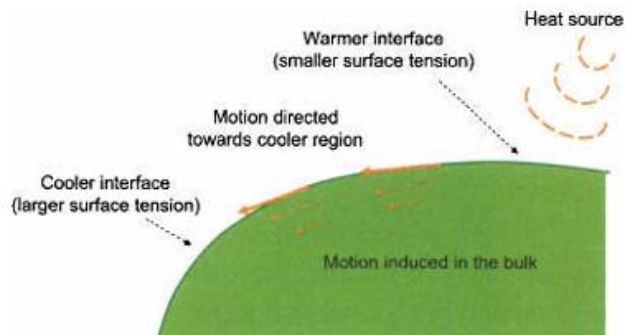


Figure 3-3. Interface motion associated with regions of different temperature (from [63])

Surfactants Effect on Surface Tension

Another important factor which impacts the surface tension is the amount of surfactant inside it. “Surface active agents” are called surfactants. Surfactants are usually amphiphilic molecules with hydrophilic head groups and hydrophobic tails [67]. Due to this chemical structure, it is energetically favorable for them to accumulate at the water-air or water-oil interface. Figure 3-4 shows a droplet with surfactants on its surface. Surfactants have many applications in biological sciences [42], [68].

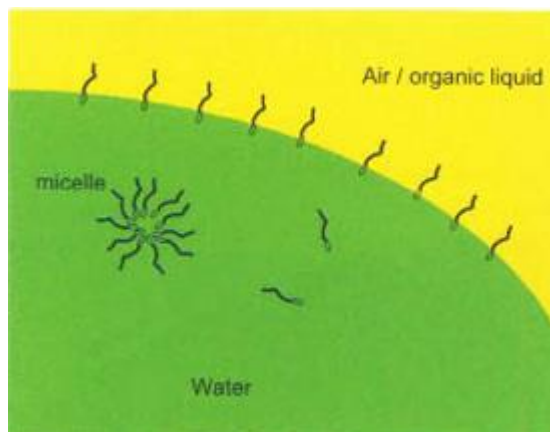


Figure 3-4. Schematic of surfactants on the surface of a water droplet (from [63])

Above a certain concentration called critical micelle concentration (CMC), surfactants saturate the surface [69]. At concentrations above the CMC, excess surfactants group

together in the bulk, forming micelles. A sample micelle of surfactants is shown in Figure 3-4. Above the CMC level, adding additional surfactant has minimal effect on surface tension. At concentration less than CMC, there is a linear relationship between surface tension and concentration. This phenomena is clearly shown in Figure 3-5:

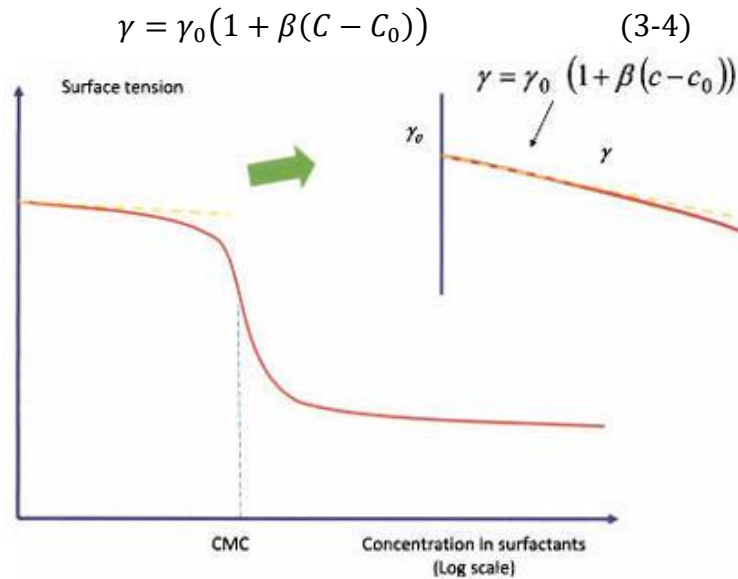


Figure 3-5. Change in surface tension with different concentrations(from [63])

The term surface energy relates to the number of active sites on the surface of a molecule. We can modify the surface energy of a liquid by adding polar or nonpolar groups to its chemical structure. Also the difference in the molecules of the two phases (for instance the oil and the surfactant) can cause a driving force for adsorption of surfactants.

Various temperatures on the surface of droplet will cause internal flows in the droplet. These movements are due to gradient in interfacial tension. This phenomena is true for surfactants too. Nonhomogeneity of surfactants on the surface of droplets will cause internal flows called Marangoni flows inside the droplet [70]. This is shown in Figure 3-6.

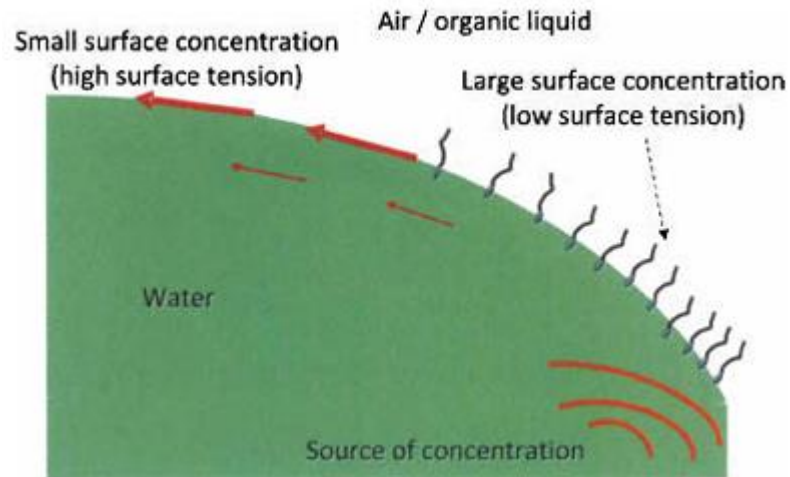


Figure 3-6. Schematic of Marangoni convection due to difference in concentration (from [63])

The Effect of Proteins on Interfacial Tension

After studying the effect of surfactants on surface tension, we are ready to investigate the impact of protein molecules which behave similar to surfactants. Proteins are large molecules with polar and nonpolar head groups. Depending on the number of polar and nonpolar groups on their surface area they adsorb to different phases. Figure 3-7 shows molecules of protein BSA adsorbed to the interface of water in oil droplet. They stick to water side from their polar group and to oil side from their nonpolar tail[71].

Figure 3-8 shows the molecules of adsorbate (molecules which are being adsorbed) and adsorbent (the surface which has empty sites of adsorbing the adsorbate).

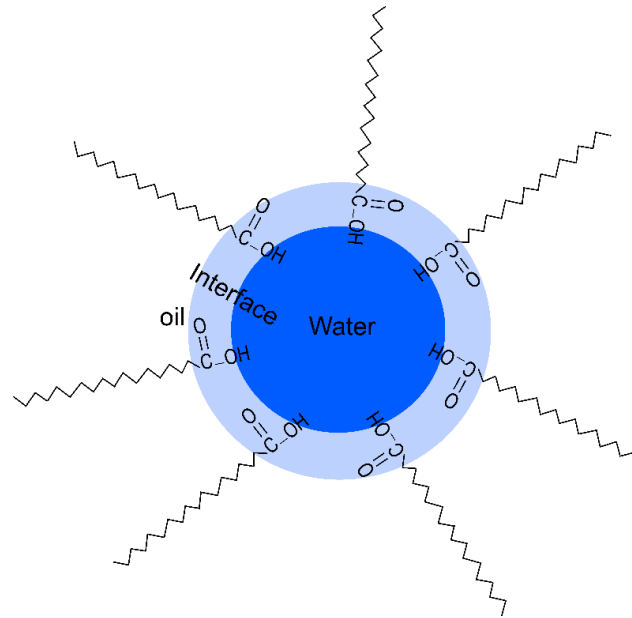


Figure 3-7. A droplet of water in oil. Molecules of BSA are adsorbed to water side from their hydrophilic head and their hydrophobic head is facing the oil side.

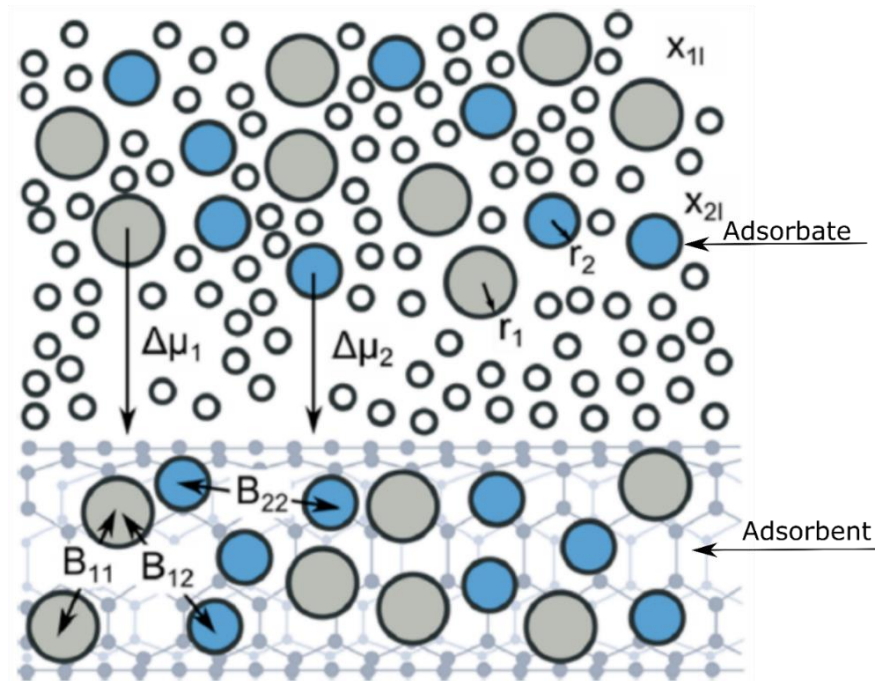


Figure 3-8. Adsorption of proteins on the interface of a droplet (from[72])

The difference in the energy (μ) of molecules in the bulk and on the surface defines the rate of adsorption. Interaction between adsorbate molecules B_{11} , B_{22} and their interaction with other molecules B_{12} is important as well. Previous researchers have

identified these relations using molecular simulations. Here we will describe the adsorption process only with Langmuir and Gibbs isotherms. Ulissi et al. [72] have reported the detailed relations between molecular interactions and their energies.

Langmuir Isotherm

Adsorption of protein (A) onto the surface (S) is considered as a reversible reaction on the surface of a droplet (Figure 3-9). This means surface concentration of protein molecules is in equilibrium with the dissolved proteins inside the droplet.

$$\theta = \frac{K[A]}{1 + K[A]} \quad (3-5)$$

K is the adsorption to desorption rate constant and Θ is the surface coverage of protein molecules.

$$K = \frac{k_a}{k_d} = \frac{[AS]}{[A][S]} \quad (3-6)$$

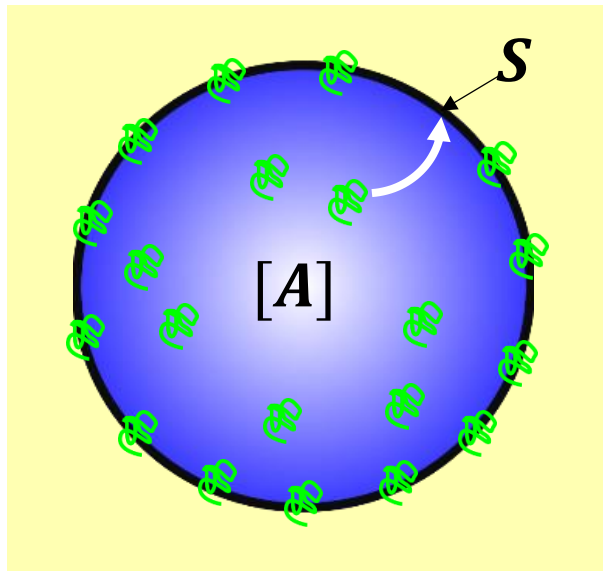


Figure 3-9. Schematic of a droplet with proteins adsorbing to its surface

The Langmuir isotherm has some limitations, for instance it is designed for adsorption of molecules of an ideal gas on a solid surface. It considers only one layer of adsorption and not multilayers [73]. This theory doesn't deal with molecular interactions between the adsorbate molecules themselves. No matter how weak these interactions are, they exist in experimental conditions. All of the adsorption sites are assumed to be equal which may not be true for different materials [74].

Gibbs Isotherm

The Gibbs Isotherm defines the relationship between the changes in concentration of a component with changes in surface tension. This isotherm is usually considered for a binary system. Based on the following formula interfacial tension falls logarithmically with protein concentration. In this equation Γ refers to the surface concentration of the protein molecules. C is the concentration of component in the bulk. T is temperature and R is gas constant.

$$\frac{d\gamma}{d(\ln C)} = -\Gamma RT \quad (3-7)$$

In other words Gibbs isotherm describes the relationship between chemical potential of components present in the surface and the amount of surface tension of that material [75]. Some components can increase the interfacial tension while others decrease it. For instance inorganic salts generally increase the interfacial tension while surfactants decrease it to a critical point and then they don't show any effect. Generally alcohols decrease the interfacial tension continuously. Carbohydrates such as sugar haven't shown any impact on the interfacial tension [69].

Young- Laplace Equation: Pressure Difference Due to Interfacial tension

Young- Laplace equation relates the pressure difference across the interface of binary phases such as oil and water to the shape of the surface and interfacial tension between two phases. One of the applications of this equation is in pendent drop experiments when we are measuring the interfacial tension between two phases. The shape of the pendent drop is fitted to Laplace equation through a user interface and the amount of interfacial tension is calculated. The same concept is used for calculating contact angle [76].

The interfacial tension on the surface of a closed droplet results in a pressure difference between the inside and outside of the drop. The relationship between the two (Young- Laplace equation), can be driven from first principles. There are three types of work associated with increase in volume: To model the work needed to expand a droplet with radius of R to $R+dR$ as shown in Figure 3-10:

The amount of work associated with volume increase is:

$$\delta w_i = -p_0 dv_0 \quad (3-8)$$

dv_0 is the increase in volume.

The work to pull out the external layer is:

$$\delta w_e = -p_1 dv_1 \quad (3-9)$$

Where dv_1 is equal to dv_0 . The work associated with increased interfacial area is [63]:

$$dw_s = \gamma dA \quad (3-10)$$

The sum of work is:

$$\delta w = \delta w_i + \delta w_e + \delta w_s = 0 \quad (3-11)$$

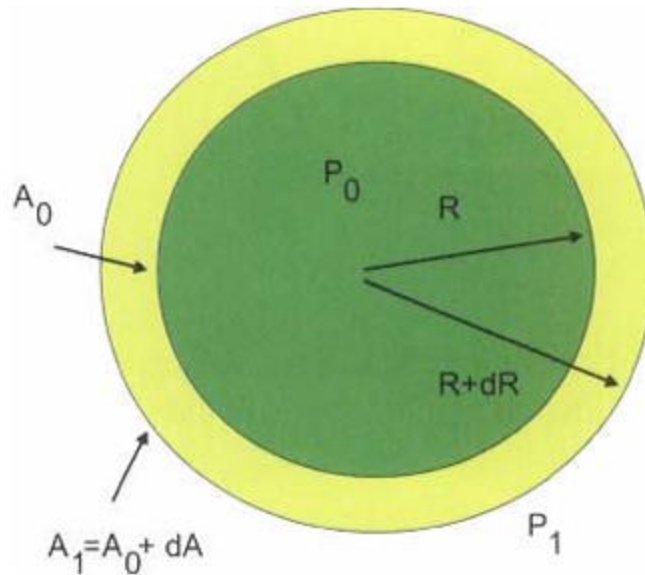


Figure 3-10. Liquid drop which is immersed in another immiscible liquid increase in the volume causes increase in surface area (from [63])

$$\delta P = P_1 - P_0 = \frac{2\gamma}{R} \quad (3-12)$$

$$\delta P = \gamma \left[\frac{1}{R_1} + \frac{1}{R_2} \right] \quad (3-13)$$

For a cylindrical shape this equation will change due to infinite curvature of one surface:

$$\Delta P = \frac{\gamma}{R} \quad (3-14)$$

Laplace equation will be discussed further in next section.

Dimensionless Numbers

Dimensionless numbers are always associated with fundamentals of fluid mechanics. They usually represent the ratio of one force to another. To maintain a certain flow characteristics we need to maintain these dimensionless numbers inside a certain zone.

Some of the important dimensionless numbers in microfluidics are Reynolds (Re), Capillary (Ca), Weber (We) Marangoni (Ma) Peclet (Pe) and Bond (BO) number [77].

Re is the ratio of inertial forces to viscous forces. In microfluidic applications usually this number is very small to maintain the laminar flow inside microfluidic chip.

$$Re = \frac{VR}{\nu} \quad (3-15)$$

Where V is the average velocity of the fluid and R is the length of the channel. ν is the kinematic viscosity of the fluid. Re number less than 2000 is considered as laminar flow.

Ca is especially important in two phase flow microfluidics. It is the ratio of viscous/elongation forces to surface tension forces.

$$Ca = \frac{\mu V}{\gamma} \quad (3-16)$$

Where μ is the fluid viscosity (kg/m/s) and V is fluid velocity (m/s) and γ is the interfacial tension (N/m). It is possible to define two Ca numbers (for dispersed phase and continuous phase). They are called internal and external Ca numbers. Usually the external Ca is more dominant and it is used in calculations. When Ca is smaller than a certain amount (0.01-0.1) interfacial/surface tension forces break the liquid into droplets in order to minimize the interfacial area. This process is called "Rayleigh-Plateau instability"[77].

The shape of droplets/plugs in microfluidic channel is determined by the balance of surface tension forces and viscous forces, described by Ca . As shown in figure 3-11, for a plug moving with velocity of V inside a channel there are two important angles:

advancing (front) and receding (back) angles which are defining the menisci of plug. This menisci usually has spherical shape. When a drop of liquid is in contact with a solid surface dynamic contact angle shows the significance of these forces [78].

Chip geometry, ratio of continuous to dispersed phase and viscosity of the two fluids are important in this case [79]. Usually in an identical confined T junction with the ratio of 1/1 continuous and dispersed phase droplets tend to choose the plug shape in microfluidic chip as Figure 3-11 shows. According to Young Laplace equation, the difference in pressure of a plug is related to the radius of its curvatures. Greater curvatures in the plug are the result of imbalance between internal and external surface energy forces [79], [66].

$$P_0 - P_1 = \frac{\gamma}{R_1} \quad (3-17)$$

$$P_0 - P_2 = \frac{\gamma}{R_2} \quad (3-18)$$

Since $R_2 < R_1$

$P_1 > P_2$

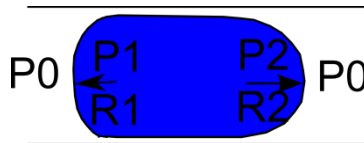


Figure 3-11. Schematic of a plug inside a channel

Therefore this system is imbalanced and plug will move from high pressure to low pressure. In a cylindrical tube with radius R , the pressure drop for a plug (along the plug) with length L is defined with Washburn's law [78]:

$$\Delta P = \frac{8\mu UL}{R^2} \quad (3-19)$$

$$F_{drag} = \Delta P \pi R^2 \approx \mu UL \quad (3-20)$$

Ca force can be driven as

$$F_{Ca} \approx \gamma R \quad (3-21)$$

$$\frac{F_{drag}}{F_{Ca}} \approx \frac{\mu UL}{\gamma R} \approx Ca \frac{L}{R} \quad (3-22)$$

The ratio of inertial forces to surface tension forces is described by Weber number. It is possible to predict deformation of drops using *We* number [77]:

$$We = \frac{\rho V^2 R}{\gamma} \quad (3-23)$$

Pe number is very important when we have diffusion in the microfluidic channel because it represents the ratio of convective forces to diffusive forces [80], [81].

$$Pe = \frac{LU}{D} \quad (3-24)$$

Where *L* is the characteristic length, *U* is the velocity of the fluid and *D* is the diffusion coefficient. If diffusive forces are high enough then diffusion will be the dominant mechanism and $Pe < 1$.

When droplets have a strong surface tension they maintain a rigid object with a convex interface. Decrease in surface tension will cause depression on the back of the plug and this depression waves will continue progressively, until the shape of plug is totally disturbed. At this point plug generation will become impossible.

Usually gravitational forces are not very significant in microfluidics (due to small channel sizes). However, bond number introduces the ratio of surface tension forces to gravitational forces. It is clear that very high *Bo* numbers show that system is not affected by surface tension forces.

$$Bo = \frac{\Delta\rho g R^2}{\gamma_i} \quad (3-25)$$

Where $\Delta\rho$ is the density difference between the two fluids, g is the gravitational constant, R is the dimension characteristic of the fluid, and γ is the interfacial tension.

The significance of convective forces inside a droplet is determined by the Marangoni Number Ma . A gradient of interfacial tension forces can cause convective motion inside droplet even when droplet is not moving. These interfacial forces include gradient of interfacial tension, gradient of heat in the interface or gradient of concentration. These are described by Ma :

$$Ma = \frac{\Delta\gamma R}{\rho\vartheta\alpha} \quad (3-26)$$

In the above formula $\Delta\gamma$ represents the gradient of interfacial tension $\gamma = \gamma_0 \left(1 + \frac{\beta}{T}\right)$, $\beta = 1/T_c$, R is the length of droplet (m), α is the diffusivity constant (m^2/s), ρ is density and ϑ is the kinematic viscosity (m^2/s) [77].

The interfacial tension of an oil-water interface is inversely related to protein concentration. Globular proteins such as bovine serum albumin (BSA) adsorb to the interface, reducing its interfacial tension [42]. This reduction in the interfacial tension in the surface of the droplet will cause the droplet to deform to its lower energy shape. To measure the changes in interfacial tension, we utilize a flow focusing droplet generator coupled to the HPLC column. The size of droplets produced in the drop generator, is highly sensitive to interfacial tension. Prior to the microfluidic chip the blood serum is fractionated into protein using SEC column. As a result, the size and shape of the generated drops changes as proteins elute from the HPLC.

Fabrication of Microfluidic Drop Generators

In this section we will talk about fabrication process for microfluidic chips. After fabrication, surface modification may be essential depending on the application.

The most promising materials for microfluidic devices are polymers. They are compatible with most replication processes such as injection molding, casting and laser micromachining. Since the original objective of microfluidics is high throughput screening, so the polymer should be optically clear for screening purposes.

Polydimethylsiloxane (PDMS) is a flexible, clear, gas permeable polymer which is used in all our experiments. No visible swelling has observed for PDMS however it has shown very low swelling with alcohols and some salts [82]. Replica molding is used very often for creating microfluidic chips. A thin layer of photosensitive material (photoresist) is spin coated on a silicon wafer. A photomask (transparent glass which is patterned with opaque regions) is placed over this photoresist. The photomask exposes some regions to high intensity UV light while protecting other regions. The UV exposed regions dissolve in developer solution and create a micro pattern etched on the photoresist. Liquid polymer in contact with this micro pattern will have the complementary pattern to the etched surface. This technique is called replica molding [83]. Figure 3-12 shows the process of fabrication.

Oxygen plasma or Corona treatment is used for their surface treatment before bonding; however, oxygen plasma increases the hydrophilicity of the surface. Depending on the experimental requirements, another step for surface treatment is needed after bonding the two layers. This step is discussed in next section.

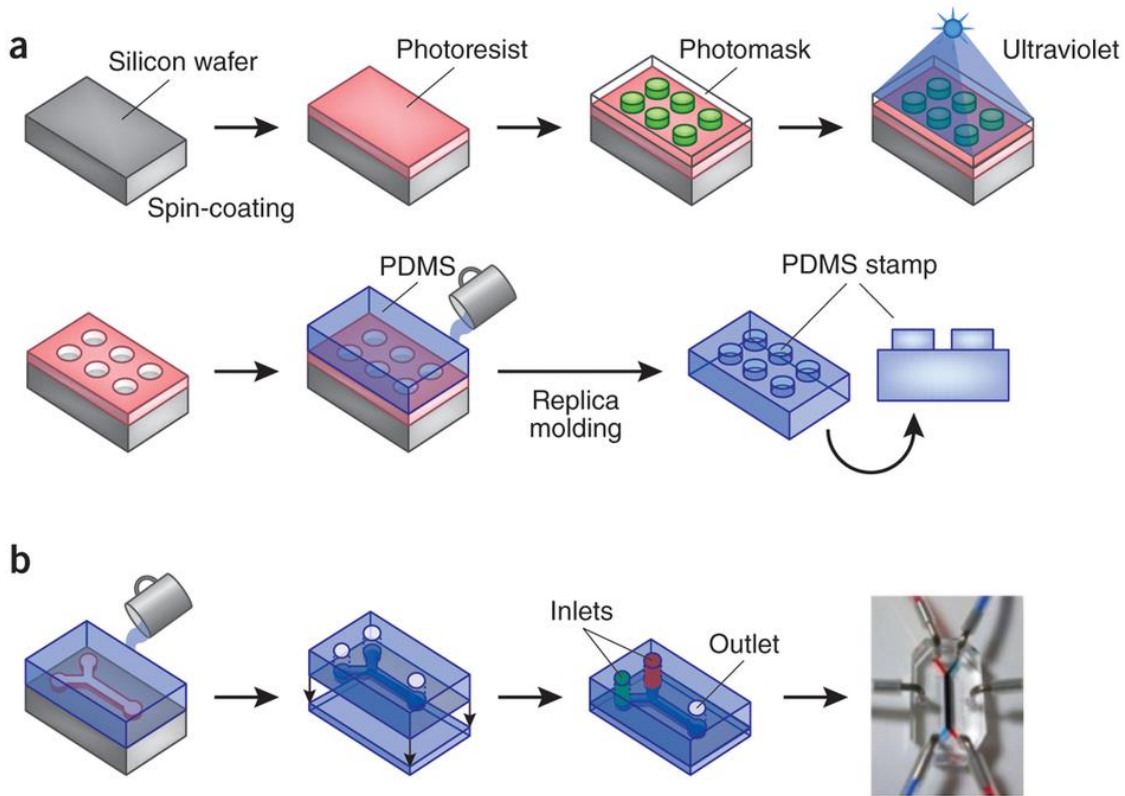


Figure 3-12. a) The process of replica molding for making PDMS stamps. These PDMS stamps can be bounded to a plain PDMS layer or glass. b) A single channel with two inlets and one outlet is made by PDMS. A photograph of a two channel PDMS chip is shown(from [83])

In order to prevent droplets from attaching to PDMS surface certain modification steps are necessary. Silanization is used to cause hydrophobic characteristics to the walls of microfluidic channel. A monolayer of silane is grafted on the surface of the PDMS. First the surface is wetted with water to produce Si-OH bonds and in next step it is silanized to produce Si-O-Si bonds. Figure 3-13 shows a schematic of silanization process, there are different silanization protocols available [84]; however, the schematic shown in this figure 3-13 shows the process of grafting PDMS surface with a thin layer of FDTS (PerFluoroDecylTrichloro-Silane $\text{CF}_3(\text{CF}_2)_7(\text{CH}_2)_2\text{-SiCB}$) at 35 °C in a vacuum chamber. Si-O-Si bonds are very flexible and heating will help their formation as well. Heating the

microchips for 4 hours after treating with corona bonder (plasma) can also recover hydrophobicity.

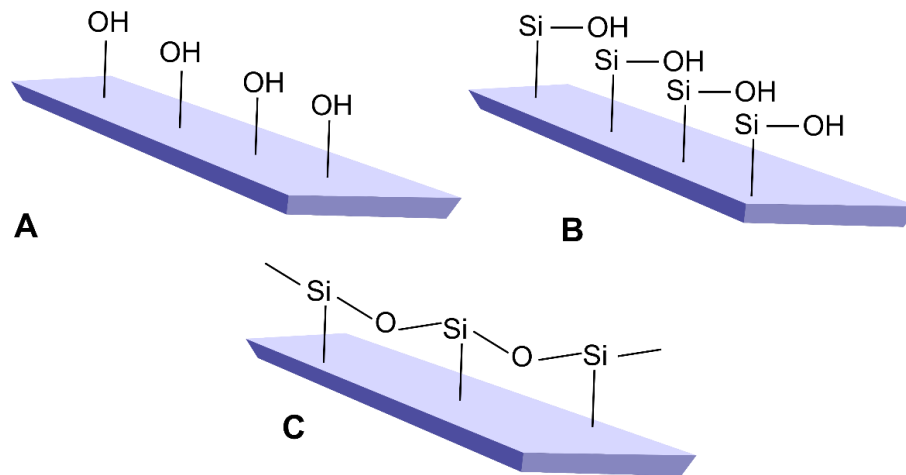


Figure 3-13. Schematic of gaseous silanization process A. Hydrophilic surface after treating with plasma B. step 1 in silanization reaction. When the surface of pdms is treated with FDTs Si bonds to OH groups C. over time Si-O-Si groups are formed. These groups will make the surface hydrophobic.

Theory of Droplet Generators

After studying the fabrication process, we will discuss different drop generation techniques and geometries in this section. In general, drop generation happens when two immiscible fluids flowing in separate channels meet each other at a junction and build a finger or jet. The droplet size is determined by a number of factors, including the geometry of the junction, interfacial tension of the fluids, flow rate ratio and viscosity.

The two immiscible fluids are driven at constant flow or constant pressure. In the former case, syringe pumps have been used very often for maintaining a fixed flow rate in the channel inlets. The pressure of inlet channels can be also controlled via a pressure source (regulator). In single phase microfluidic systems, it can be assumed that at low Re numbers pressure gradient and flow rate are related to each other linearly. However, due

to the influence of interfacial tension there are significant differences in drop formation process in multiphase flow [85], [86].

There are three main approaches for drop generation as stated in [66],[87]. Generally droplet break up is the competition between two major forces: local fluid stresses, which cause deformation of the interface, and interfacial forces which resist this deformation (higher interfacial tension means higher resistance):

- Coflowing systems
- Cross flowing systems
- Elongational flows

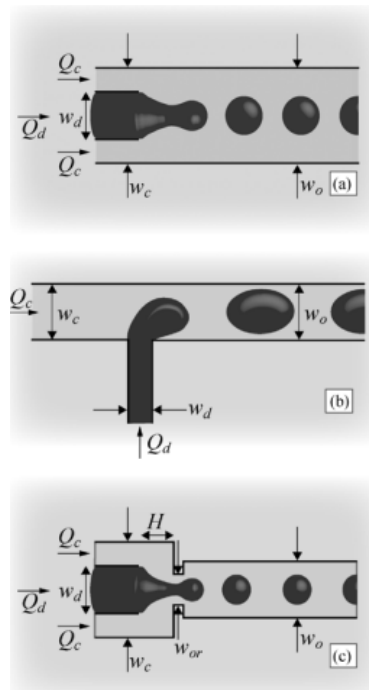


Figure 3-14. Schematic of different drop generation approaches a) coflowing systems b) cross flowing in a T junction c) Elongational flow in a flow focusing channel (from [80])

As stated by Christopher and Anna [88] in cross flowing systems if the width of oil and water channels are the same they are considered as confined channels and if water channel is less than one fifth of the oil channel they are called unconfined channels.

Flow Driven Versus Pressure Driven Systems

In this section we will do a comparison between two main drop generation systems, flow driven and pressure driven. This information is necessary for analyzing experiments in the next chapter.

In our experiments we have investigated the size, shape, frequency and velocity of drop formation (by tracking the center of mass in each droplet using DMV software [89]) by varying the dispersed to continuous pressure ratios. These experiments are performed with various continuous phases with different viscosities, refractive indexes and chemical properties.

Previous research [90] has explored the impact of dispersed to continuous phase pressure and flow rate ratio in flow focusing channels. In flow rate controlled system, oil flow rate is constant and water flow rate is varying. In pressure controlled system oil pressure is constant while water pressure is varying. Increasing flow rate up to ten orders of magnitude causes drop size increases slightly (only 1.5) orders of magnitude, while increases pressure (slightly) causes significant change in drop size.

Pressure driven flow has a strong dependence to geometry of the channel since the minimum drop size is the same as the size of cross junction (or orifice) where oil and water phases meet each other. Ward et al., have suggested that in pressure driven flows the main resistance for drop generation comes from surface tension and not viscous forces [90].

Experimental study of the production of micrometer-sized droplets in a flow-focusing geometry shows there are two distinct methods of flow control: (i) control of the flow rates of the two phases and (ii) control of the inlet pressures of the two phases. In each type of experiment, the drop size l , velocity U and production frequency f are measured and compared as either functions of the flow-rate ratio or the inlet pressure ratio. The minimum drop size in each experiment is on the order of the flow focusing channel width. The variation in drop size as the flow control parameters are varied is significantly different between the flow-rate and inlet pressure controlled experiments [62].

Figure 3-15 shows the 3 steps in drop formation. The first step is Nucleation when a curved surface of dispersed phase is formed at the end of water channel. At this point, pressures of oil and water are related to the amount of interfacial tension ($P_W - P_O = \frac{\gamma}{2R}$ where P_W is the pressure of water inside the curved surface, P_O is the pressure of oil which is outside the curved surface, γ is the interfacial tension at the surface and R is the radius of the curved surface). In this step, pressure inside the droplet is larger than the pressure outside the droplet. This will lead to the second step which is called expansion and at this stage the dispersed phase expands more into the middle of the junction. Pressure inside the dispersed phase will cause more expansion and as a result more elongation and eventually droplet pinch off happens. During the third step elongation of the drop will cause concave surfaces on both sides of the elongated drop. Inside these concave surfaces pressure of water is less than pressure of oil. If the oil pressure is high enough it can pinch off the droplet.

Figure 3-16 shows different steps in drop formation in a T shaped microchannel versus time. Wang et al. have recorded drop generation in four different time steps. Their

model is very similar to our model; however, we have considered the first two steps as one [91].

Figure 3-17 is a general comparison between flow driven system and pressure driven system. In a typical pressure-driven junction, a 10% increase in dispersed phase pressure (water) causes a 4 fold increase in plug size. By comparison, in a flow-driven junction, increasing the dispersed phase flow by a factor of 10 will only cause <30% increase in plug size.

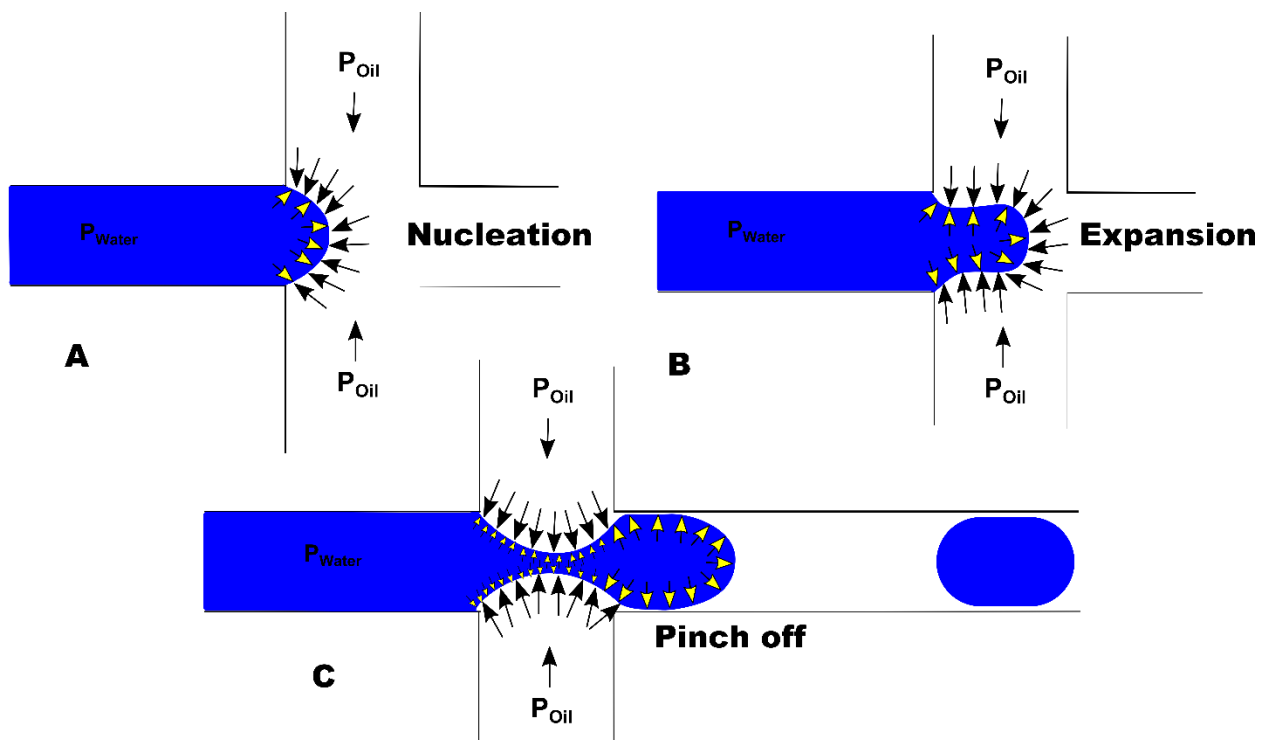


Figure 3-15. Schematic of 3 steps in drop formation.

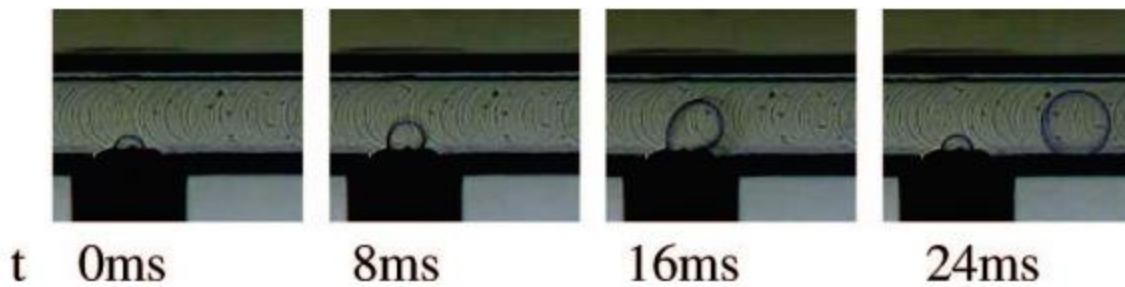


Figure 3-16. Drop formation process in a T shaped channel (from [91])

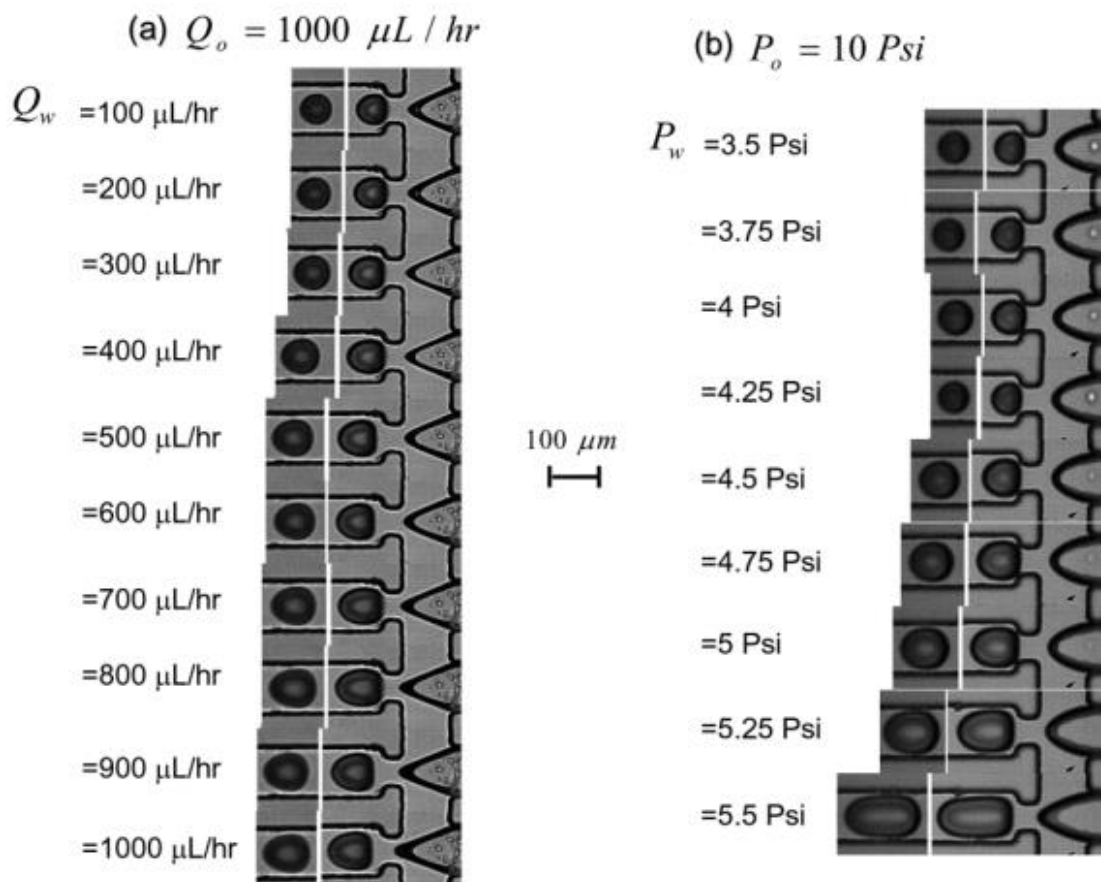


Figure 3-17. Flow rate controlled system versus pressure controlled system (from [90])

Graph in Figure 3-18 shows the dimensionless droplet length (length divided by the width of orifice) versus the ratio of water flow to oil pressure (water flow rate to oil in Figure 3-19). In this research [90], they have also investigated the frequency and velocity profiles

versus flow rate or pressure ratios. The changes in drop size by changing the pressure is much sharper than flow rate. These figures confirm the fact that pressure variation have a strong impact on droplet size.

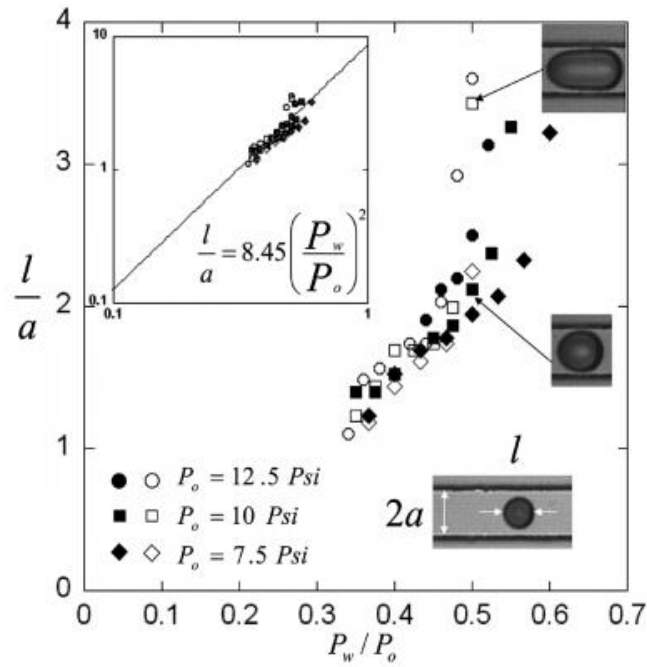


Figure 3-18. Dimensionless drop length versus pressure ratio(from [90])

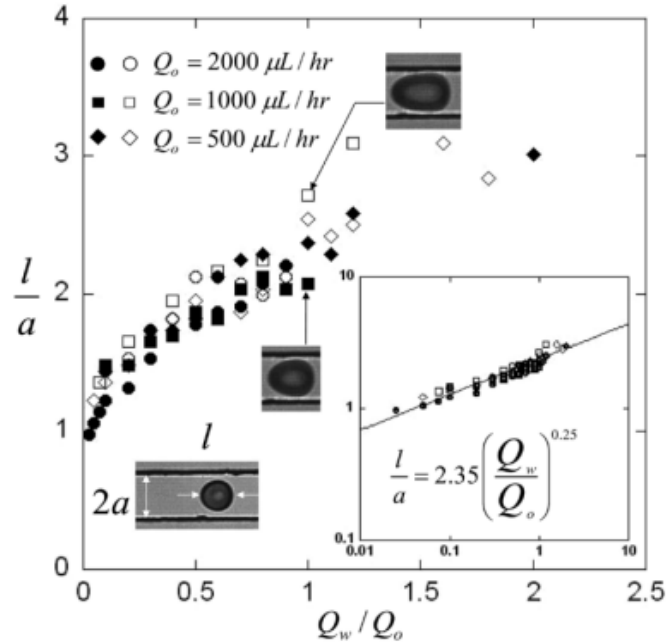


Figure 3-19. Dimensionless drop length versus flow rate ratio (from [90])

Drop velocity increases in a linear manner with the water flow rate. In pressure driven flow droplets cannot be generated below a certain minimum pressure ratio. Below this critical pressure ratio the dispersed phase is not able to diffuse into continuous phase and a static flow condition is observed in which a static spherical cap of dispersed phase is formed. The velocity difference between two phases is proportional to small powers of external phase Ca number ($Ca^{1/3}$) at small ranges of Ca number [90]. In our applications Ca number is 0.01-0.1. This phenomena shows the significance of interfacial forces. For estimating the size of droplet in a pressure driven flow, Thorsen et al., have suggested the following equation [92]. Equating Laplace pressure with shear force:

$$r \approx \frac{\sigma}{\mu \varepsilon} \quad (3-27)$$

Here r is the droplet radius, σ is the interfacial tension between two phases, μ is the viscosity of continuous phase and ϵ is the shear rate. Figure 3-20 shows the droplet diameters versus oil and water pressures.

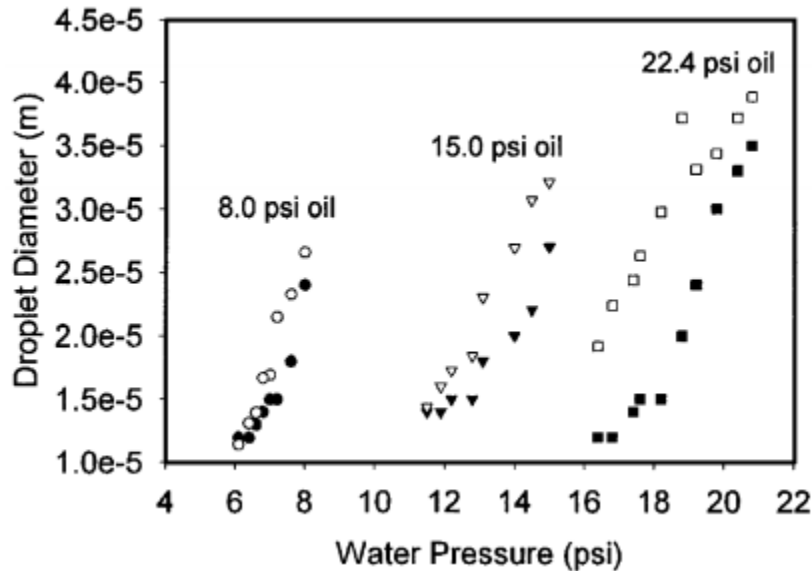


Figure 3-20. Droplet diameter vs. water pressure at three different oil pressures. The filled markers are experimental data and the unfilled markers refer to predicted data by following equation (from [90])

Ward et al., have suggested a microscopic force balance at the interface of oil-water [90].

$$\Delta P + \tau = Ca^{-1}\kappa \quad (3-28)$$

ΔP is the difference between dispersed and continuous phase pressures, τ is the viscous stress and κ is the mean curvature at the interface. When the droplet is forming at the cross section area the mean curvature will decrease until the pressure of outer fluid and viscous forces break the drop.

After certain pressure, size of droplets is not dependent to pressure any more. Velocity tends to be constant at this point too. The experimental results agree with literature reports. This will be discussed in next chapter.

Impact of Interfacial Tension on Drop Formation

Interfacial tension is an important physical characteristic which impacts Ca number and drop formation process. Previous researchers [91] have reported that different concentrations of surfactant (Figure 3-22) can cause variation in size of droplets in a T junction channel. They have conducted these experiments in a microfluidic chip with a needle for dispersed phase. Dispersed and continuous phases are injected using syringe pumps (Figure 3-21).

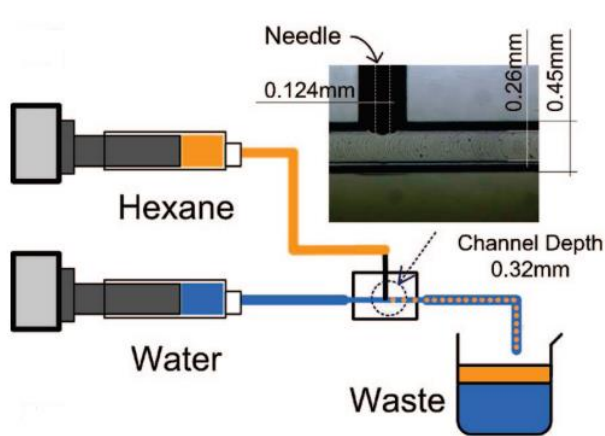


Figure 3-21. System set up for studying the dynamic interfacial tension (from [91])

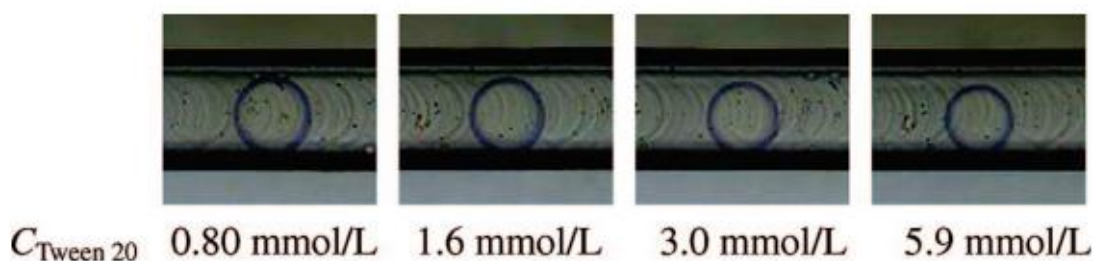


Figure 3-22. Different concentrations of surfactant inside a droplet (from [91])

Surfactants can be transported either by advection of flow or by molecular diffusion. This can happen either in the bulk or in the surface of the droplet. In addition to their

transport, their partition coefficient (bulk and surface concentrations of the surfactant in the equilibrium condition) and rates of adsorption or desorption of surfactant in the interface (chemical kinetics) are some of the physico-chemical properties which characterize different surfactants. Interfacial tension has a nonlinear relation with the concentration of surfactant in the fluid interface. This is usually described by Langmuir model [66]. The process of adsorption of surfactant to the surface of droplet can be described in three steps. [63].

1. Convection and diffusion of surfactant molecules from the bulk to the surface. This layer is also called the subsurface and it has a thickness equal to one surfactant molecule.
2. Surfactant molecules will then self-assemble themselves from sublayer to the interface.
3. The gradient in the concentration of micelles and molecules will cause disaggregation of micelles inside the bulk of droplet.

The process of surfactant absorption happens simultaneously with drop formation. The relative adsorption rate of surfactant is dependent to the expansion time of the droplet. Short expansion time will prevent adsorption of the surfactant to the surface of droplet. Besides expansion time, dispersed phase velocity (flow rate) plays a key role in the mass transfer phenomena. Higher flow rates may still maintain the flow in the laminar flow zone but rupturing the dispersed phase will prevent proper mass transfer in the interface.

Proteins

Proteins used in the experimental work include BSA, Uridine, blood plasma, Thyroglobulin, Galectin and PGF (shown in Table 3-1). Researchers have used affinity labeling in order to identify the long chain fatty acid binding sites of BSA. Albumin is able to carry 0.5-2 moles of fatty acid/mole of albumin. The binding is characterized as heterogeneous binding which involves various sites with different affinities. The major fatty acid binding site of albumin is located at the half of molecule adjacent to COOH terminal. Long chain fatty acids bind to the hydrophobic core of the albumin with their tail and their hydroxyl head will be exposed and able to interact with polar surface [93].

Table 3-1. Properties of the proteins used in the experiments

BSA	A single chain poly peptide. Average mass: 66.5 KDa
Uridine	Chemical formula: C ₉ H ₁₂ N ₂ O ₆ . Average mass: 244.201 Da
Blood plasma	55% of the total volume of blood is plasma 90% of plasma is water and the rest of it is composed of proteins and lipids. Blood plasma powder is from sigma and it contains following proteins. Prealbumin, Albumin, Retinol binding protein, Galactoglycoprotein, α-Globulins, B-Globulins, Low molecular weight proteins, Coagulation proteins and Immunoglobulins.
Thyroglobulin	Dimeric protein chain. Average mass: 660-690KDa
Galectin	Human galectin also called LGAL-14. Released in placental tissue. Average molecular mass: 16 KDa
PGF	Placental growth factor, Consists of immunoglobulin like domains in its extracellular portion. Average mass: 32KDa

Carrier Phases

To understand the impact of interfacial tension on drop formation process we need to study the chemistry of two phases. Polar and nonpolar groups in the carrier phase can interact with proteins and result in different adsorption profiles on the interface. Partitioning coefficient of proteins varies in different carrier phases. This can result in better adsorption of proteins on droplet surface. Here we discuss chemical and physical properties of different carrier phases. Table 3-2 shows properties of different carrier phases. We have used oleic acid, Octanol, Hexadecane and FC40 as carrier phases.

The famous guide “like dissolves like” is a good representation for this topic. Intermolecular forces between two species with similar chemistry causes smaller endothermic enthalpy of the solution than molecules with different chemistry. When the process of dissolution happens the system shifts to lower endothermic enthalpy. In addition to activity of a substance, solubility also depends on the fugacity of the pure solid. Escaping tendency of a substance is known as its fugacity. Fugacity is a function of vapor pressure in pure liquids and solids. Fugacity of the ideal gasses is the same as their pressure.

In the equilibrium state the fugacity of the pure solid should be equal to the fugacity of the solute in liquid solution.

$$f(\text{pure solid})=f(\text{solute in the liquid solution}), f(\text{pure solid})=\gamma x f_0$$

X is the mole fraction of the solute in the solvent, γ is the activity coefficient of the liquid phase and f is the fugacity. So

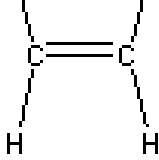
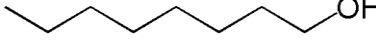

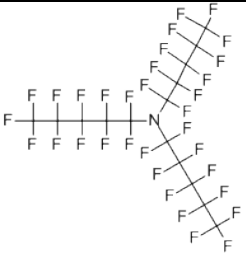
$$f = \frac{f(\text{pure solid})}{\gamma f_0} \quad (3-29)$$

This equation shows that solubility depends on both activity coefficient and fugacity [73].

We have tested various oils to see the impact of oil selection on this experiment. Alkanes such as Hexadecane didn't show successful results. Tested proteins didn't show any IFT change when they were used with Alkane carrier phase. One of the probable reasons for this phenomena is the fact that alkanes are lacking the COOH group in their structure. Previous researchers have shown that long-chain hydrocarbons which didn't contain carboxyl group were only bounded to BSA very weakly and to a small extent [94].

For choosing the appropriate oil we have to consider critical parameters such as miscibility in water, interfacial tension and refractive index.

Table 3-2. Chemical and physical properties of different carrier phases

Oleic acid	Chemical formula	$C_{18}H_{34}O_2$	$CH_3(CH_2)_7$ $(CH_2)_7COOH$ 
	Density	895.00 kg/m ³	
	Molar mass	282.4614 g/mol	
	Boiling point	680°F (360°C)	
	IFT (with water)	15.59 (dyn/cm)	
	Log (P) (with water)	7.64	
	Refractive index	1.459	
	Viscosity	0.04 (Pa.S)	
Octanol	Chemical formula	$C_8H_{18}O$	
	Density	824 kg/m ³	
	Molar mass	130.23 g/mol	
	Boiling point	383 F (195°C)	
	IFT (with water)	8.52 (dyn/cm)	
	Log (P) (with water)	3	
	Refractive index	1.429	
Viscosity	7.65e ⁻³ (Pa.S)		
Hexadecane	Chemical formula	$C_{16}H_{34}$	
	Density	770.00 kg/m ³	
	Molar mass	226.44 g/mol	
	Boiling point	549 F (287°C)	
	IFT (with water)	53.3 dyn/cm	
	Log (P) (with water)	8.859	
	Refractive index	1.434	
Viscosity	3.03e ⁻³ (Pa.S)		
Fc-40	Chemical formula		
	Density	1855 kg/m ³	
	Molar mass	650	
	Boiling point	329 F (165 °C)	
	IFT (with water)	52.06 dyn/cm	
	Log (P) (with water)	11.2	
	Refractive index	1.290	
Viscosity	0.0041 (Pa.S)		

Chapter 4. **EXPERIMENTAL RESULTS**

In previous chapter, we reviewed the fundamentals of drop generation and different drop generation techniques. In this chapter we present experimental results.

We begin with measurements of interfacial tension (IFT) vs. protein concentration for proteins in various continuous phases. IFT is measured using the pendant drop method, and IFT is calculated using the Young-Laplace equation which is already discussed in chapter 3.

The next set of experimental results illustrate the operation of a pressure driven droplet generator. These initial experiments focus on flow regimes where droplets are generated. The pressure control system for drop generation is discussed next. We have used pressure driven flow for most of our experiments. We can define the size of droplet by tuning the pressures of dispersed and continuous phases. We developed two variants of the pressure-controlled system: an open loop version with fixed pressure, and a feedback control system which can perform closed loop drop size control using image feedback.

Next, we demonstrate droplet generation with various proteins and carrier phases, showing variations in droplet size. In some cases, proteins inside droplets behave similar to surfactants and they decrease the interfacial tension between the two phases. This will decrease the size of droplets. However, this theory is not true for all carrier phases. As discussed in previous chapter, the partitioning coefficient of proteins inside the carrier phase has a key role in adsorption of proteins to the interface. Our method is compared with other detection methods at the end.

In the next section we introduce our protein detection system as an inline detector for HPLC. We connect the drop generator system to the outlet of HPLC, and monitor droplet size chromatograms. Different chromatography techniques are discussed in first chapter. Results show a better limit of detection (40% more signal) in our drop generator in comparison to the conventional HPLC system.

Pendant Drop Experiment

Pendant drop experiments are used to measure interfacial tension of proteins in various carrier oils. These measurements are used throughout the remaining experiments. In order to generate droplets, we need to maintain Ca number in a certain range ($0.01 < Ca < 0.1$), otherwise jetting will occur at very high Ca numbers or we will have no drop formation at low Ca numbers. For calculating Ca we must know the interfacial tension between two fluids. Figure 4-1 shows the system set up of the pendant drop experiment set up in our lab.

This system must be very stable since even a small movement can cause errors in the calculations. For this purpose, a syringe holder is designed using AutoCAD 2015 and 3D printed that (Figure 4-2). A plastic cuvette is placed on a stage which can move in three dimensions (X, Y and Z) for adjusting focal point of the camera. This cuvette holds the denser fluid. A typical 10 ml syringe with a 30 gauge needle is prefilled with a lighter fluid to produce a 3 μL pendant drop immersed inside the cuvette. The shape of the droplet is imaged with a horizontally arranged microscope and camera. The IFT is calculated by fitting a numerical solution for Young-Laplace equation to the digital profile of the hanging drop [95].

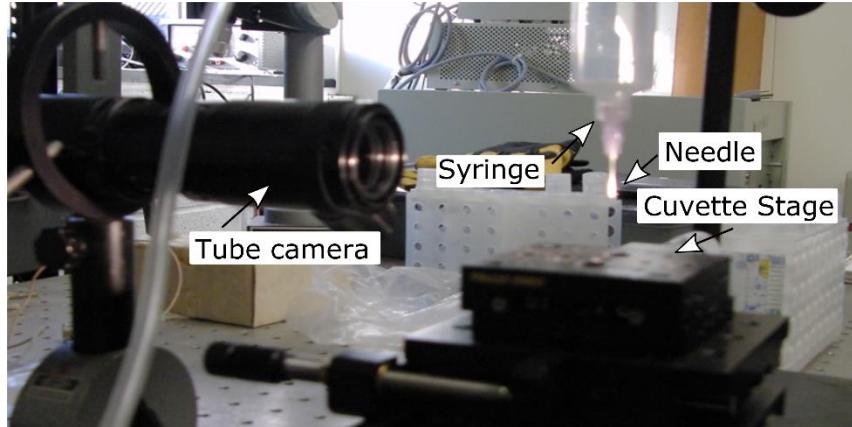


Figure 4-1. Pendent drop experiment set up

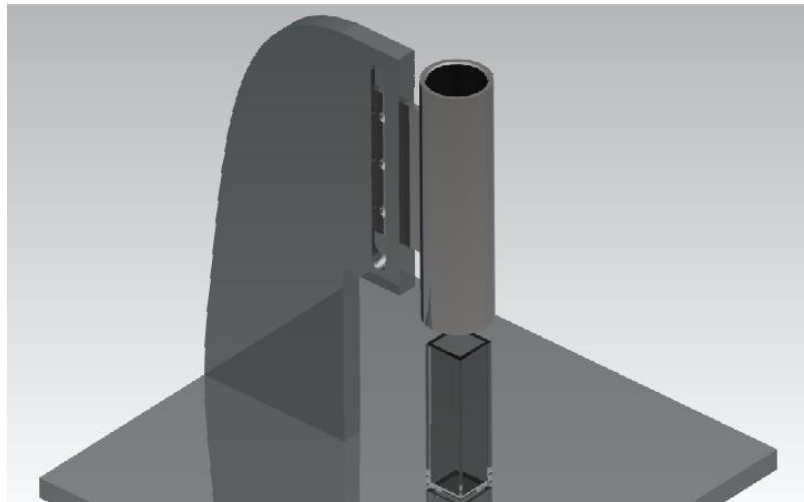


Figure 4-2. 3D design for syringe holder in pendent drop experiment

Figure 4-3 shows interfacial tension profile versus different concentrations of surfactant (Krytox, DuPont). Since different surfactant molecules have different chemical and physical characteristics, changing surfactants can lead to major impacts in drop generation process. CMC point happens at about 5% V/V of surfactant where we can see a very sharp reduction in interfacial tension. After this point the slope reduces much slower (25 degrees or less at higher concentrations). Eventually this slope will be zero after 75% V/V of surfactant in FC-40.

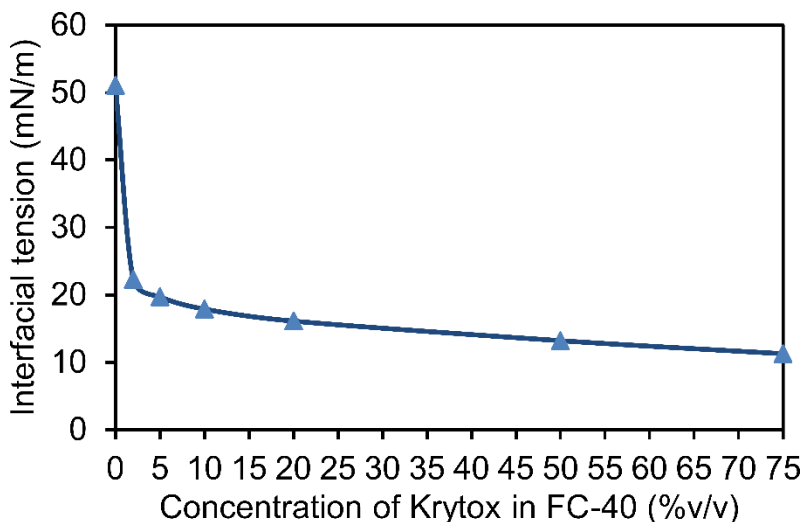


Figure 4-3. Schematic of surfactants on the surface of a water droplet

In our studies, we found that alcohols can decrease IFT of the two phases (water-oil) progressively, unlike surfactants which can impact IFT primarily below the critical micelle concentration (CMC). Figure 4-4 shows the effect of different percentages of alcohol on IFT. Increasing the alcohol percentage will cause decrease in IFT. This is something that must be considered when performing gradient solutions in HPLC, as it would lead to baseline shifts in droplet size.

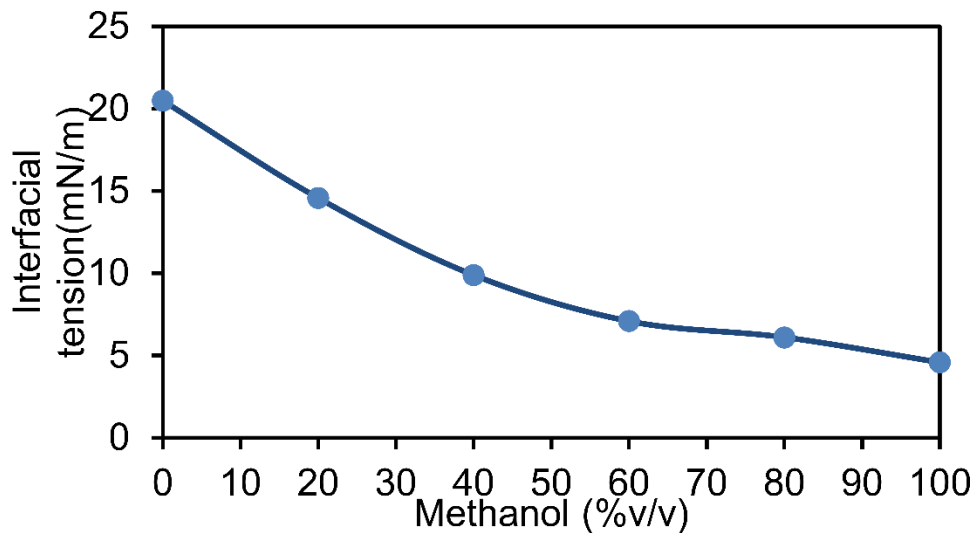


Figure 4-4. Different percentages of methanol in water with FC-40 and 2% surfactant

Methanol has the similar effect on water-Oleic acid droplets. We observed that after certain percentage (40% V/V Methanol in water) the two phases (oil and water) are completely miscible and generating droplets is impossible (Figure 4-5).

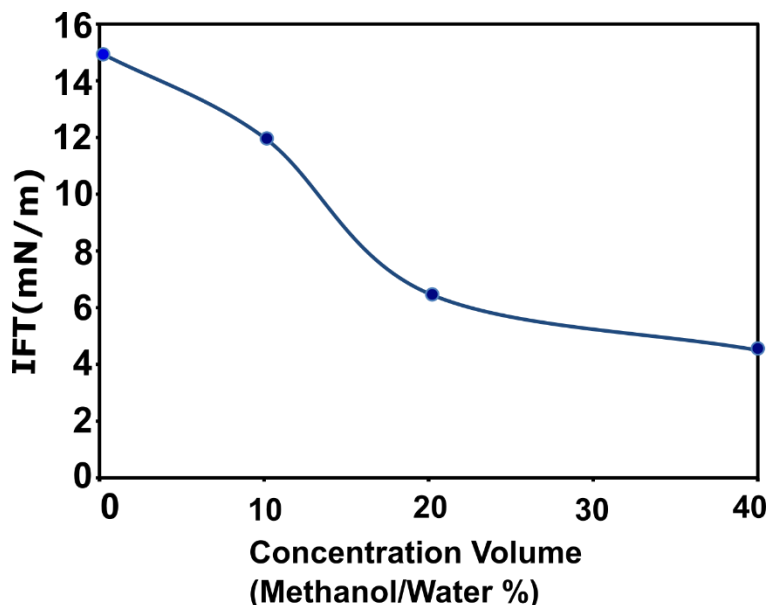


Figure 4-5. Different percentages of methanol in water with Oleic acid

As mentioned in the previous chapter, some proteins behave similar to surfactants since they have both hydrophilic and hydrophobic heads. However, other proteins do not have this structure, and consequently there is no considerable change in IFT versus concentration of protein. For instance, different concentrations of uridine dissolved in water didn't show any change of IFT from 0 to 4.01 mM of protein (with oleic acid). This may be because of the fact that Uridine is totally hydrophilic, soluble in water and the total charge of this protein is zero [96]. This will prevent the protein from migrating to the interface and interacting with oil. Chemical structure and physical properties of all 6 proteins are reported in Table 3-1. The same experiment was performed for other proteins such as BSA and Thyroglobulin, we observed expected changes in IFT versus the changes in protein concentration. Figure 4-6 shows changes in IFT for BSA and

Thyroglobulin. Also different carrier phases may cause different results. For instance, no change was observed in IFT when we used same proteins with hexadecane. Considering the chemical structure of Hexadecane (Table 3-2), this hydrocarbon is nonpolar and includes 18 carbon atoms. This heavy and nonpolar structure of hexadecane prevents it from bonding to BSA. Change in interfacial tension of BSA solutions in oleic acid is due to binding fatty acids (oleic acid) to BSA [94], [97].

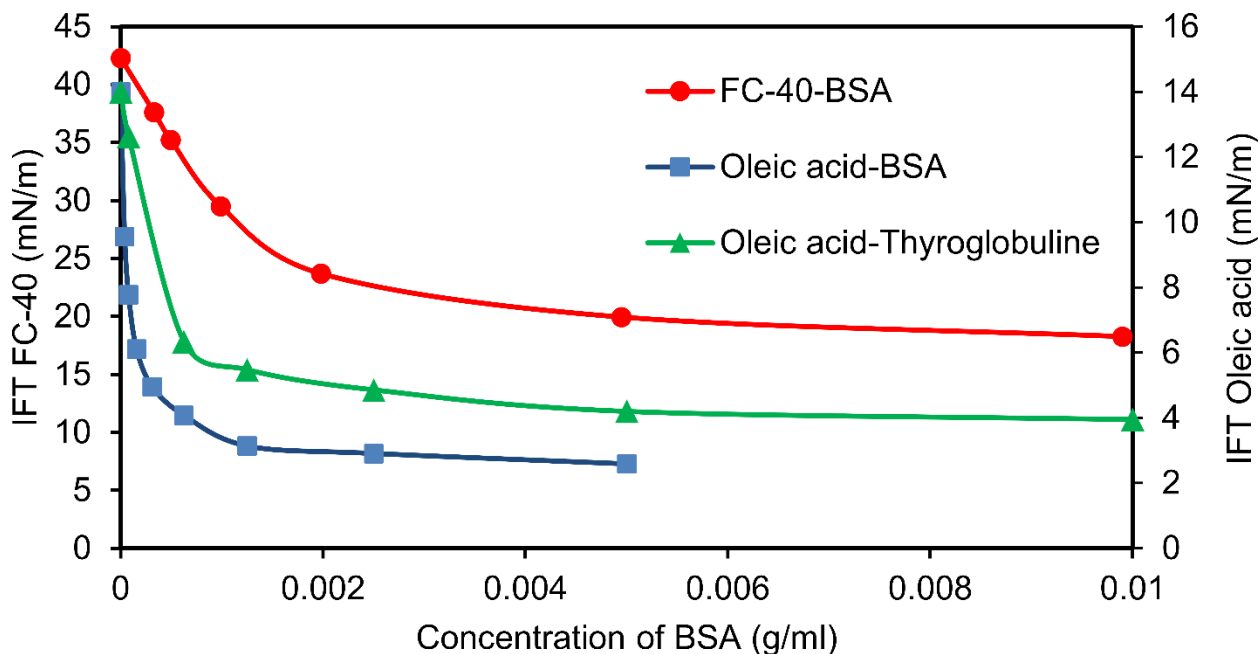


Figure 4-6. Effect of different concentrations of protein on IFT

The pendant drop experiments have therefore shown that protein concentration decreases IFT. This experiment motivated us to investigate if the similar phenomena happens inside the microfluidic chip, which is covered later in this chapter. For this purpose we performed experiments to show the drop formation zone using pressure driven flow.

Figure 4-7 shows IFT change with different concentrations of blood plasma. Blood plasma contains globulins and albumins (globular proteins) which is why it can impact IFT.

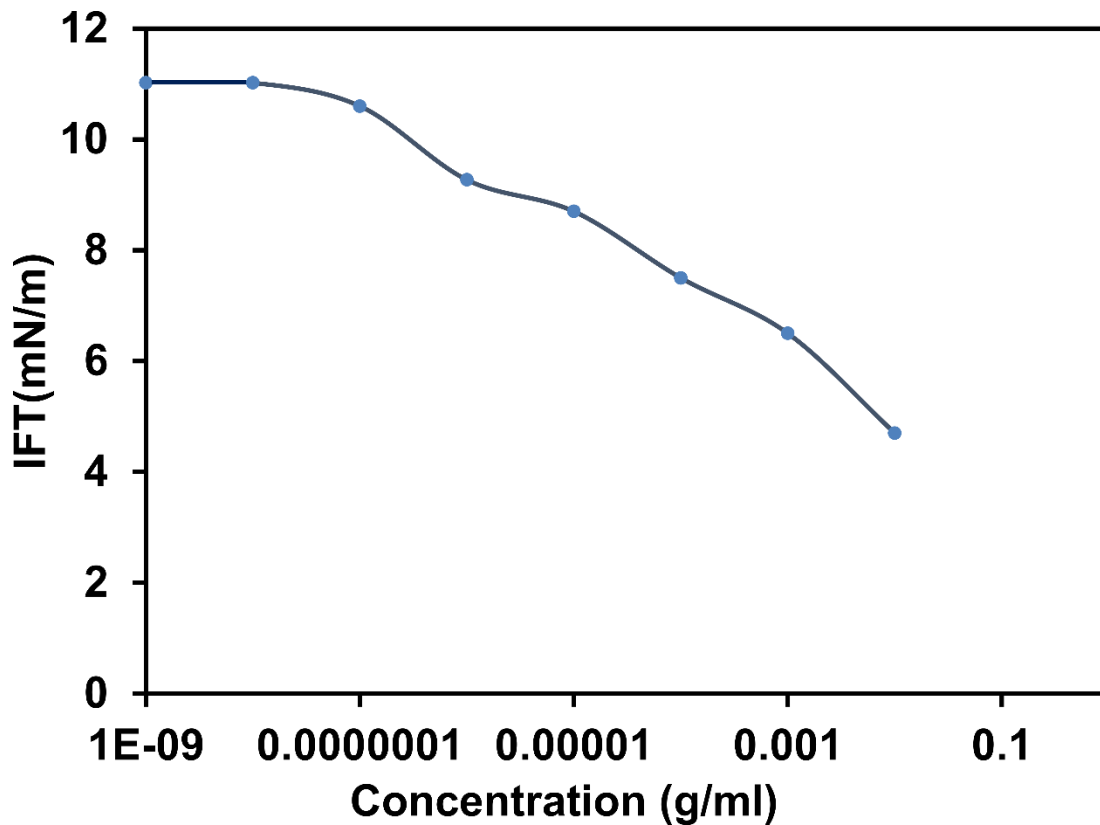


Figure 4-7. Effect of different concentrations of blood plasma on IFT

Figure 4-8 shows the impact of human galectin (LGAL 14) on IFT. We also tried another protein (PGF), a biomarker for miscarriage in pregnant women, and it didn't show any IFT change at different concentrations. Figure 4-9 shows the IFT change at different concentrations of PGF. In women with early pregnancy, loss these two proteins are shown to have reduced amounts in comparison to control group [6]. Results show a good sensitivity starting at about 50 pg/ml of protein. This result is very promising because we are able to track small amounts of protein using IFT change.

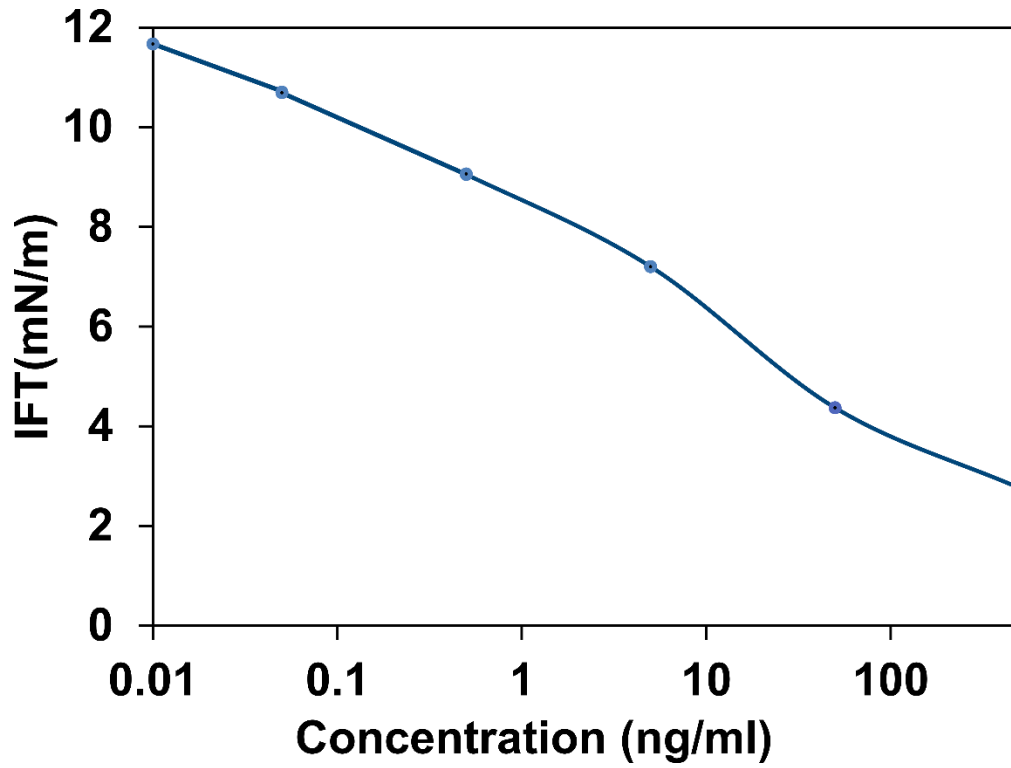


Figure 4-8. Effect of different concentrations of protein LGAL- 14 on IFT (water in oleic acid)

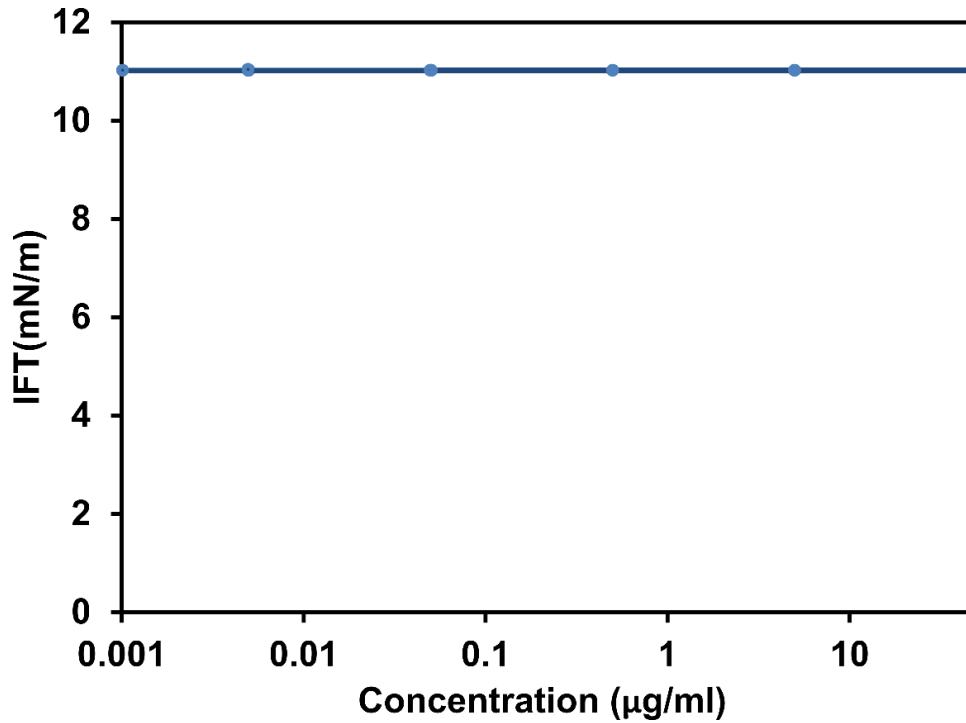


Figure 4-9. Effect of different concentrations of protein PGF on IFT (water in oleic acid)

HPLC Pump Calibration

In this section drop generation using pressure driven flow is investigated. As mentioned in theory section, physics of drop generation is different in pressure driven vs. a flow driven system. Since we are combining a flow driven system (HPLC) with a pressure driven system, we need to confirm the linear behavior of the HPLC pump. We designed the following (Figure 4-10) experiment to check the pump performance. We have measured the number of drops in 5 minutes versus flow rate of the pump. For this purpose, we manually counted the number of drops dispensed from a peek tubing (ID=500 μm) at the outlet of the pump.

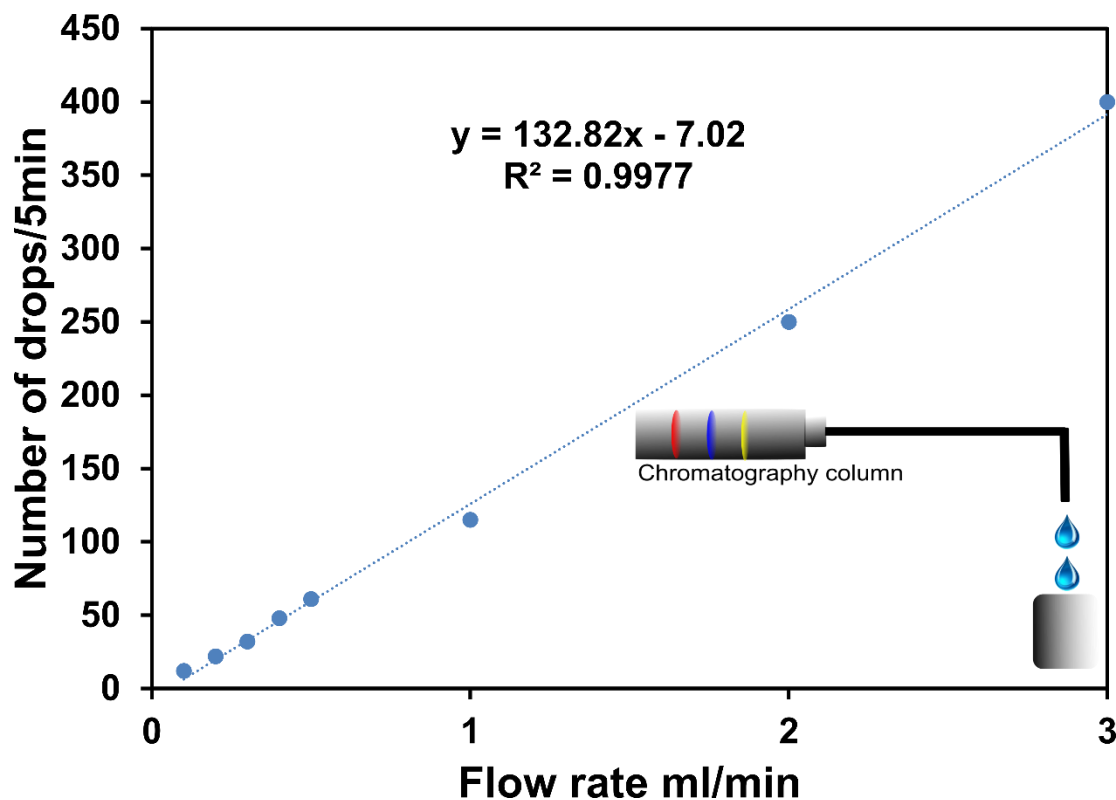


Figure 4-10. HPLC pump calibration with different flow rates

Drop Generation

The next set of experiments investigated droplet generation in a cross junction microfluidic chip with $100\ \mu\text{m}$ width and $100\ \mu\text{m}$ height (Figure 4-11). The goal is to determine under the range of oil and water pressures which are proper for stable drop generation.

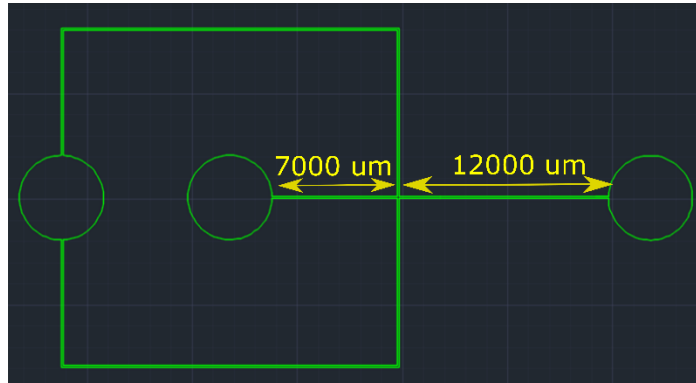


Figure 4-11 Microfluidic chip design and dimensions

Figure 4-12 shows experimental setup including pressure regulators which are responsible for input pressure of oil and water to the microfluidic chip. Using a LabVIEW program (developed in our lab) it is possible to control the amount of pressure on each pressure regulator.

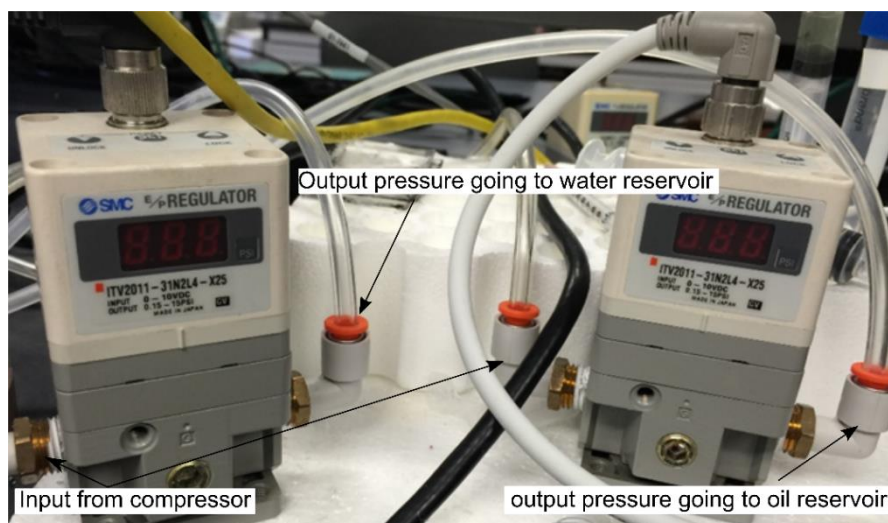


Figure 4-12. Pressure regulators used for oil and water input

Figure 4-13 shows the block diagram for the labview program we used for controlling the pressure regulators. Using a power supply and a National instrument BNC 2120 input voltage is converted to pressure and the result is continuously graphed in the output charts.

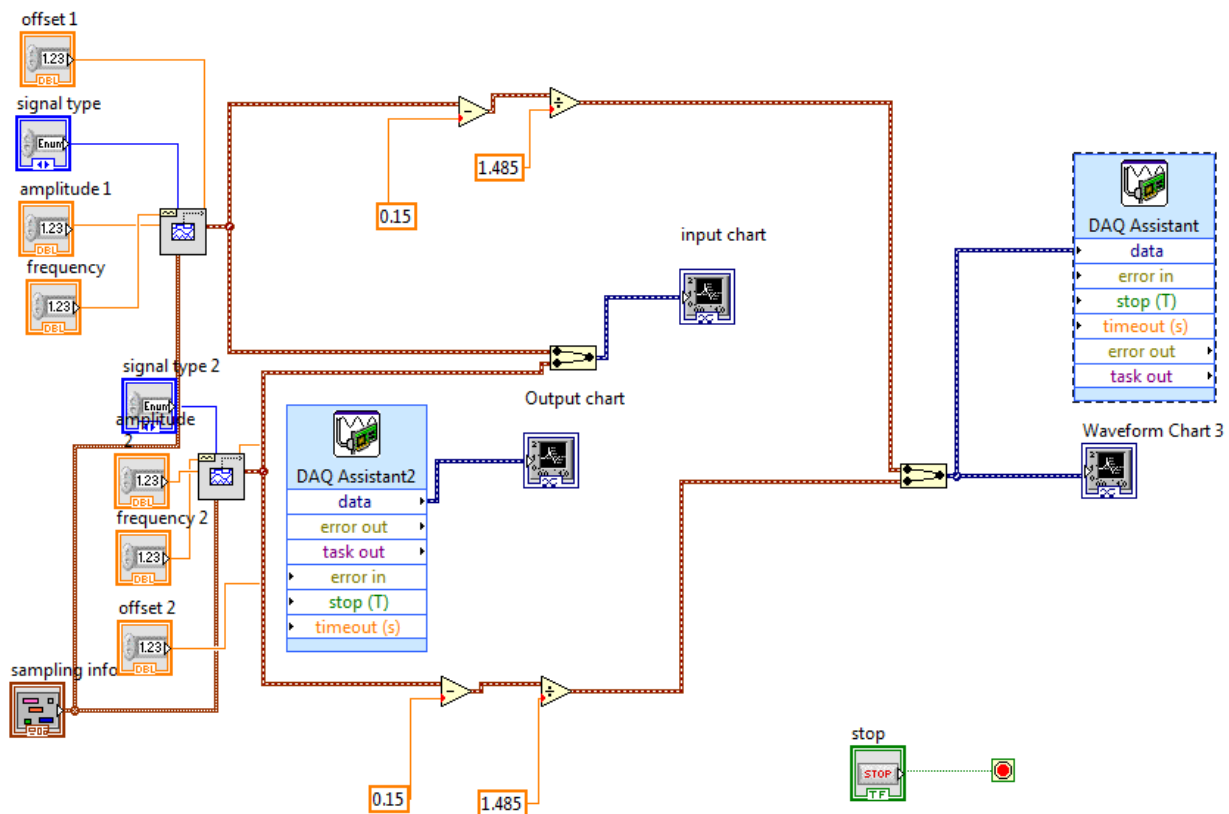


Figure 4-13. Schematic of the block diagram used for controlling pressure regulators

Figure 4-14 shows the drop generation zone at different water to oil ratios. The maximum and minimum pressure ratios for drop generation vary from low to high pressure ranges. At higher pressure ranges this ratio can go as low as 0.5 while at lower oil pressures there will be no drop generation at this ratio. This is because Ca number changes with the velocity of droplet.

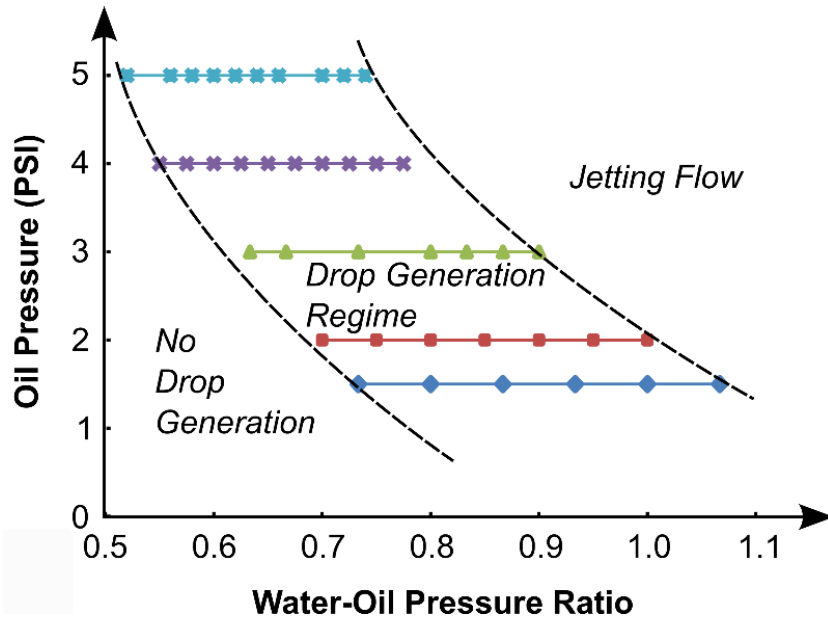


Figure 4-14. The drop generation zone considering the water/oil pressure ratio

Using the constant pressure in oil phase and tuning the water pressure, we are able to track the changes in droplet velocity, major axis length, area and shape eccentricity. We have performed this experiment in a range of different pressures from 1-6 psi ($Ca=0.004-0.014$). Results show that jetting regime occurs above pressure 5 Psi, where no droplets are formed. Pressures 1-5 Psi exhibit the dripping regime in which droplet size is highly dependent on the geometry of the channel. At low pressures, when we are still in dripping regime ($Ca < 0.01$) by applying the constant oil pressure of 2 psi and water pressure=1.6 Psi, velocity decreases by increase in the length of the plugs. However, when $Ca > 0.01$, the plug velocity is independent of the length of plugs.

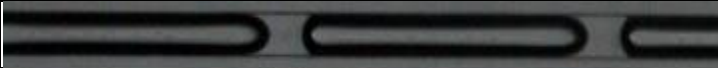

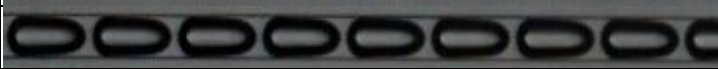
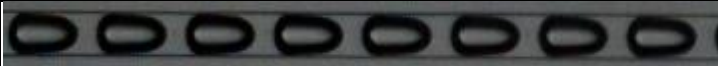
These results can be explained by considering the fact that in dripping regime, plugs (drops) block the whole channel before break up and this can cause fluctuations in the pressure downstream the channel. At higher pressures (higher Ca numbers) plugs (drops) can only block a portion of the channel and this will cause a uniform pressure range upstream and downstream the channel. This uniformity is the reason for constant

velocity while water pressure is changing with a saw tooth wave. Understanding different flow regimes can lead to getting benefit of some key parameters such as interfacial tension in modifying droplet size.

System is less sensitive to interfacial tension between oil/water at higher pressures. This can be due to higher Ca number in which the inertial forces compensate the effect of interfacial forces. The range of drop generation area is also much wider at higher pressures in comparison to lower pressures. This means the system is more flexible to changes in pressure at higher pressures. In other words, increase in viscous forces can mask the effect of interfacial forces at higher pressures.

Table 4-1 shows the size of generated plugs versus water and oil pressures and their ratios. Decreasing water to oil ratio will cause decrease in the size of plugs. Higher pressure ratios will cause smaller plugs. This table shows that the size of droplets can change almost 7X when the pressure is tuned from about 1 psi to 5 psi. Also frequency and velocity increases at higher pressures (images in table 4-1).

Table 4-1. Experimental results for change in drop size versus pressure ratio

Water (PSI)	Oil (PSI)	Ratio	Drop size (μm)	Velocity ($\mu\text{m/S}$)	Image of one frame
0.9	1	0.9	707.82 73	1.6E04	
1.6	2	0.8	243.87 24	1.74E04	
3	4	0.75	207.14 23	2.64E4	
3.4	5	0.68	165.63 75	4.56E4	

In each pressure level, drop generation zone is shown (figure 4-6), below this zone no drop is generated and above this zone instable drop formation (in which droplets form in the middle of the channel) or jetting flow happens and droplet size becomes

unpredictable. As reported in previous research [90] drop generation zone is narrower in pressure driven flow than flow rate driven systems. Increase in velocity will cause decrease in Ca number and droplets tend to produce spherical ends at higher Ca numbers. Drop Generation Control System

We have developed a control system for our pressure regulators using LabVIEW. This control system is able to perform both in closed loop and open loop operations. Our closed loop drop generator is based on a pressure-driven flow focusing junction. Previous reports (as discussed in theory section [90]) show that in pressure-driven generators, contrary to the flow-driven systems, the plug length has a stronger dependence on the water/oil pressure ratio. In pressure-driven system respond time is within 100 milliseconds, compared to >2min with a syringe pump. When used in a closed loop system, a pressure-driven junction can provide both a larger tuning range as well as a faster tuning time[98], [90].

The closed loop drop generation system (Figure 4-15) utilizes morphometric image feedback to detect plug length in real time and dynamically tunes a pressure-controlled drop generator. We previously reported Droplet Morphometry and Velocimetry (DMV), a software algorithm for tracking drop sizes in digital videos [89]. In this work, we developed a real-time version of the software which can be used for feedback control. A machine-vision CMOS camera acquires images from an inverted microscope and sends the images via FireWire to the real-time DMV software. The software measures the plug length and compares it to the desired plug length (set point). The difference is fed to a proportional/integral/derivative (PID) controller which tunes the water pressure while

keeping the oil pressure constant. The tuning process continues until the measured and desired plug lengths are equal.

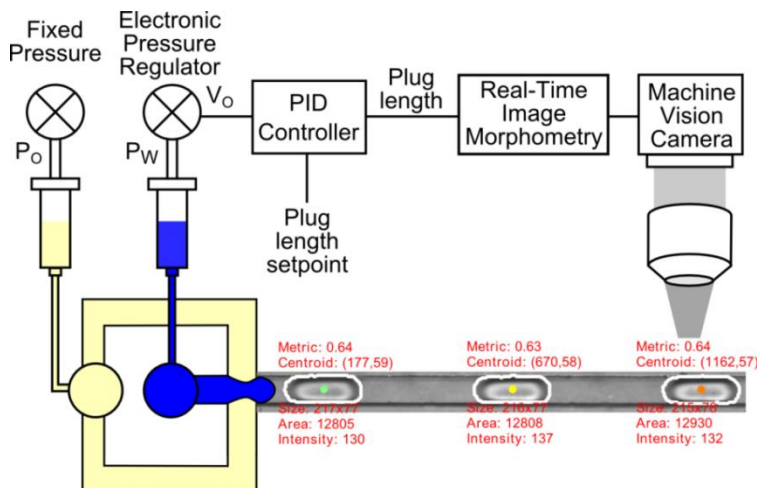


Figure 4-15. Schematic of the closed loop drop generation system

The microfluidic drop generator component consists of a confined cross junction microfluidic chip with 100 μm width. The chip is fabricated with polydimethylsiloxane (PDMS) using soft lithography. Two electronic pressure regulators (SMC ITV2011) control pressurized vials for injecting water and oil into the microfluidic chip. The oil syringe is maintained at a fixed pressure, while the feedback loop dynamically tunes the water pressure. Teflon microtubing with 500 μm ID is used to connect the syringes of water and oil to the microfluidic chip. The dispersed phase is deionized water and the continuous phase is a fluorinated phase (FC-40, 3M). The plug length and other characteristics are imaged in real time using a FireWire CMOS camera (Allied Vision Technologies Marlin F-131B) and measured using DMV as described in reference [89].

The open-loop system exhibits a nonlinear response which is difficult to calibrate, whereas the closed-loop system precisely provides the desired plug length with <5% polydispersity.

Open Loop Characterization

In the open loop system (Figure 4-16 A), the water pressure (PW) is controlled manually by providing a voltage to the pressure regulator. This system is inherently nonlinear due to the flow focusing junction, which has a nonlinear relation between plug length and pressure ratio (Figure 4-16B). As shown in this graph, the plug length can be tuned over a 10 fold dynamic range. Less than 10% change in the dispersed phase pressure can cause more than 4 fold change in plug size.

To test the open loop time constant, a square wave is applied to the pressure regulator, and the corresponding changes in plug characteristics are measured using DMV (Figure 4-16C). The time constant is about 100 ms when the system shifts from low to high pressure and it is about 200 ms in reverse transition. The open loop time constant is limited by the pressure regulator. Figure 4-16E shows that while the plug length and spacing are quite sensitive to changes in the water pressure, the plug velocity remains relatively unchanged (<10%).

We have used open loop system for most of the future experiments because we wanted to characterize the droplet size at constant pressure (without pressure fluctuation interference) with changes in interfacial tension.

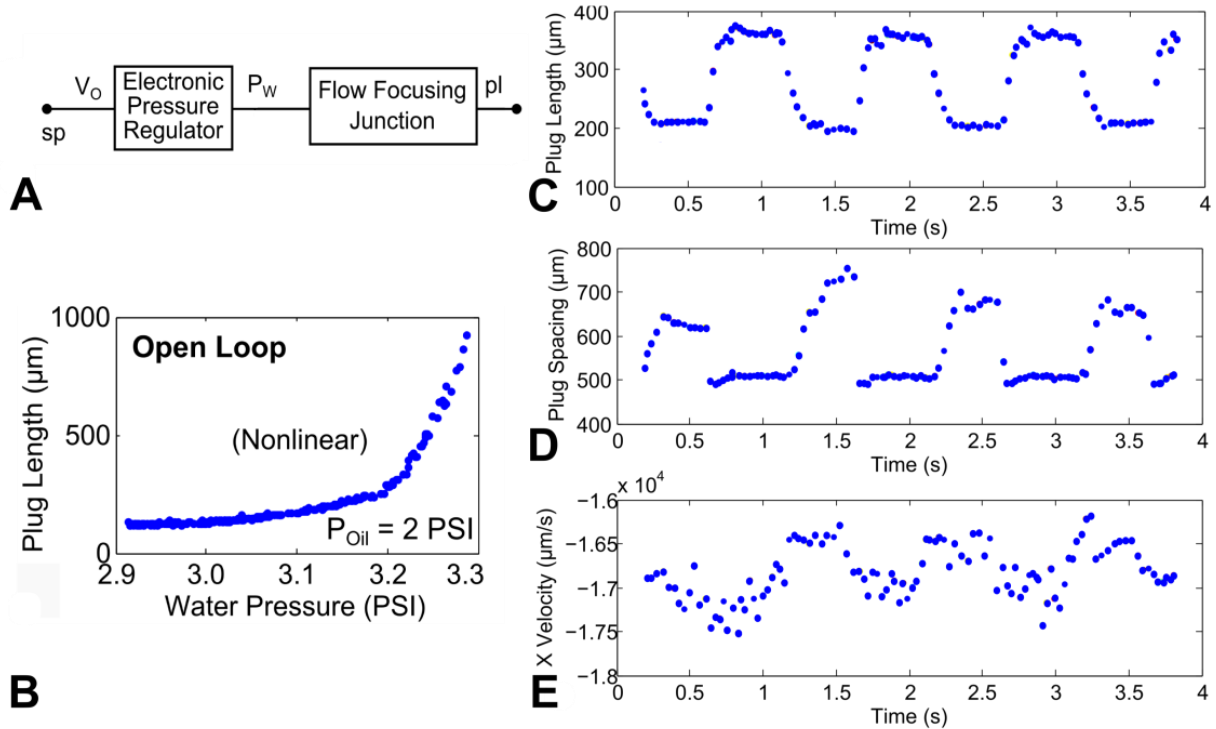


Figure 4-16. Characterization of open loop system. (A) Model. (B) The open-loop system shows a nonlinear relation between water pressure and plug length (C) open loop testing of response time, using a 3-3.2 PSI pressure and step function at 1Hz. (D, E) Open loop characterization of plug spacing and plug velocity, under the same experimental conditions as (C).

Closed Loop Characterization

In the closed loop system (Figure 4-17A), the plug length (measured by DMV) is fed into a PID controller which tunes the water pressure to obtain the desired length. Feedback based on shape metrics or area is also possible. The feedback control produces a precise linear relationship between plug length and plug set point (Figure 4-17 B) eliminating the nonlinearities of the open loop system. Four fold dynamic tuning range is achieved.

Closed loop stability is tested by applying a step change in the plug length set point (Figure 4-17 C-D), and monitoring the response of the system. Open-loop tests show that the controller gain varies from 2-20,000 $\mu\text{m/PSI}$, the process time constant is 0.1s and

the dead time is negligible. In closed-loop mode, the PID parameters were tuned using the Ziegler-Nichols method [99], where K_P is used to decrease the rise time, K_D to reduce overshoot and settling time, and K_I to eliminate the steady state error. If the set point is $250\ \mu\text{m}$ and $K_P=K_I=0.0005$, the system exhibits overdamped behavior with a response time $<10\text{s}$ (Figure 4-17C). If the proportional gain is doubled to 0.001 , the system becomes underdamped and begins to oscillate. It is notable that the oscillation only occurs on the low to high transition.

In general, a large plug length set point (upper end of the tuning range) can cause the system to oscillate. This can be attributed to the nonlinear gain of the flow focusing junction (Figure 4-17B). At higher pressures, the plug length is more sensitive to pressure changes, and the higher effective gain can cause the loop to become unstable. This can be compensated by simply reducing the proportional gain in the PID controller, or by introducing a linearizing function into the feedback loop.

The settling or response time of the system ranges from $7\text{-}10\ \text{s}$. This depends on the damping parameters as well as the physical time constants of the image acquisition ($<500\text{ms}$), data transfer ($<10\text{ms}$), DMV measurement of plug length ($0.1\text{-}1\text{s}$), pressure regulation ($100\text{-}200\text{ms}$), and the flow focusing junction ($<10\text{ms}$). The response time can therefore be improved by optimizing the software and image acquisition, and by tuning the PID parameters for fast settling time.

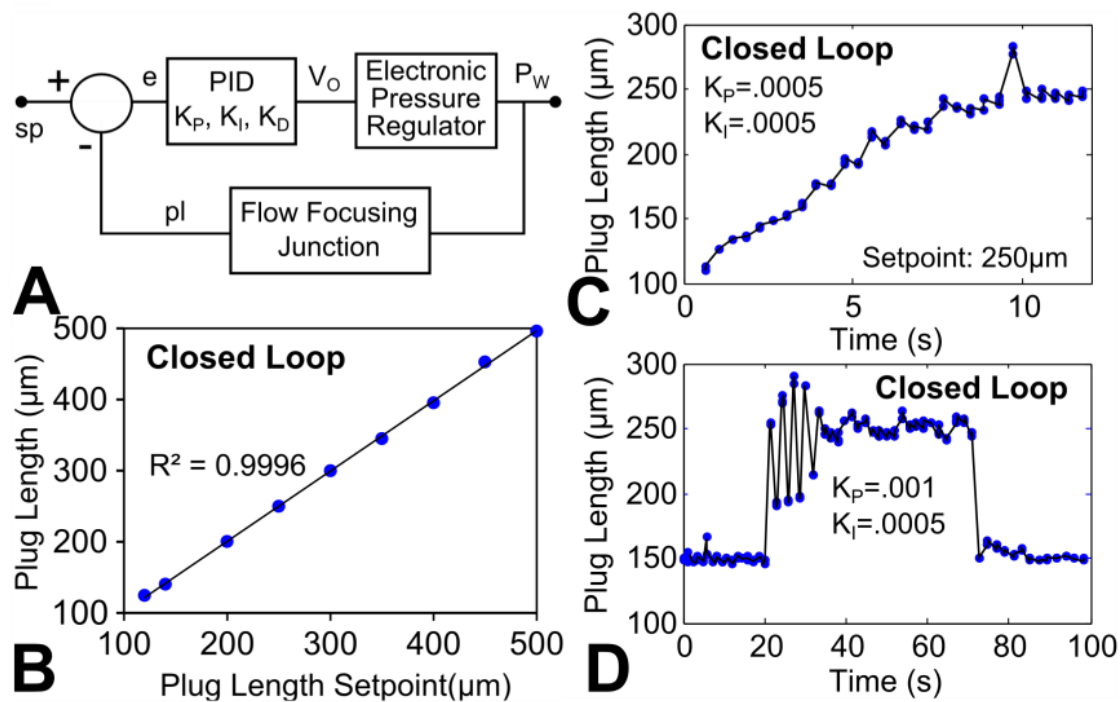


Figure 4-17. Characterization of closed loop system. (A) Model. (B) The closed-loop system provides precise, linear control of drop size. (C) Step response with proportional gain (K_P) set to 0.0005, showing a critically damped response. (D) Step response with K_P doubled to 0.001, resulting in oscillations on the low to high transition.

Figure 4-18 demonstrates the ability of the system to generate a tri-disperse population. The set point was sequentially changed from 150 μm to 200 μm and 250 μm (Figure 4-18A). The histogram (Figure 4-18B) shows 3 distinct populations, each with normal distributions. Being able to precisely generate multiple plug sizes is useful for metered assays or titrations.

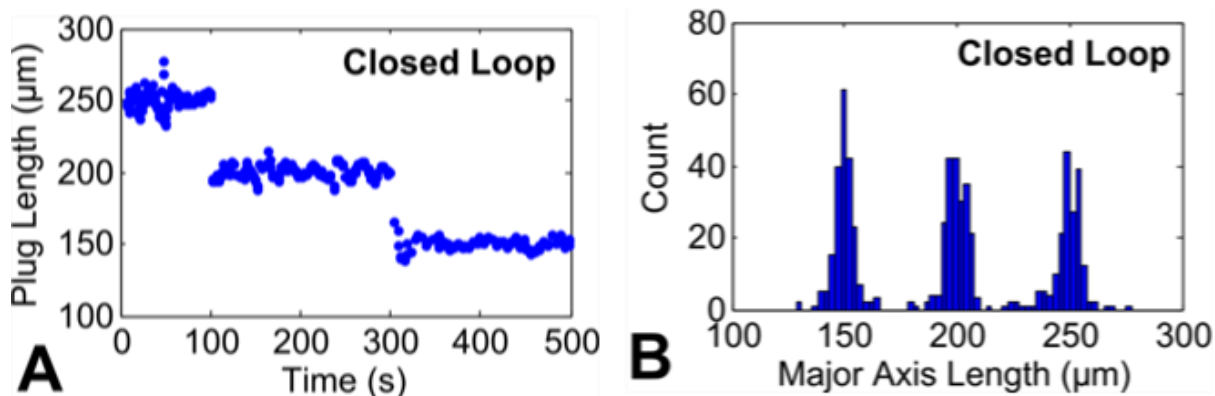


Figure 4-18. Dynamic, in situ tuning. The closed loop system is used to generate a tri-disperse population 150, 200, and 250 μm plugs. (A) Plug length vs. time, (B) histogram of plug lengths.

Effect of Proteins on Drop Size

Being able to generate monodispersed droplets using pressure driven flow, we are ready to investigate the effect of proteins on drop size. Since we were expecting that proteins can change the IFT like surfactants, we performed experiments with different concentrations of protein at different pressures to prove this theory.

Figure 4-19 shows drop size change versus protein concentration. We also needed to confirm that this change in the drop size is clearer at certain pressures. This figure also shows the dynamic range and limit of detection at different concentrations. Dynamic range is wider at lower pressure levels versus higher pressure levels. Limit of detection is also smaller at lower pressures. We decided to perform protein experiment with different carrier phases to understand the effect of carrier phase on protein adsorption.

We have also investigated the effect of other carrier phases such as Hexadecane, FC40 and Octanol in this experiment. As described in previous chapter, chemistry of protein in terms of polarity is very important. For testing different proteins we have experimented with BSA, Thyroglobulin, Uridine and blood plasma.

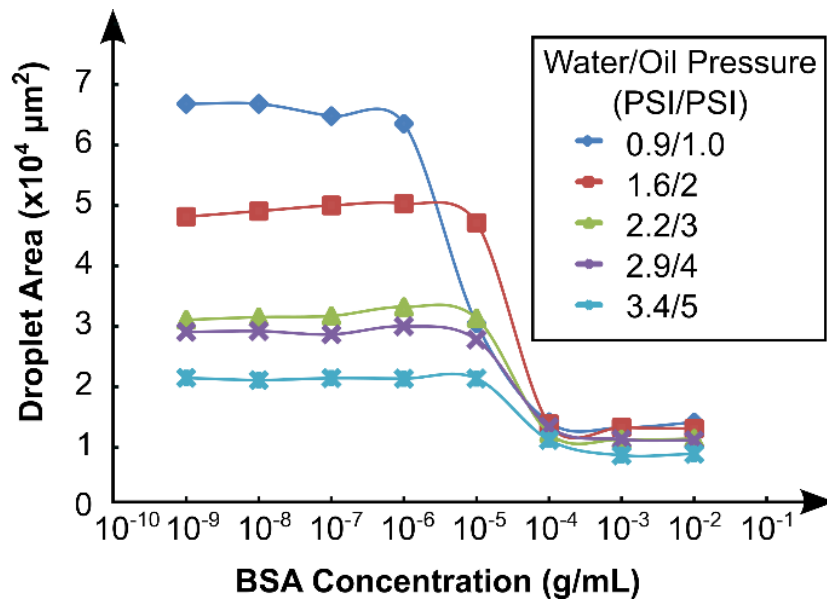


Figure 4-19. The drop generation zone considering the water/oil pressure ratio

The impact of oils on this experiment is investigated in Figure 4-20. Hexadecane doesn't show drop size change at all. Oleic acid shows better limit of detection than octanol. The reason that octanol shows drop size change is because of its polarity. If the alkane is completely nonpolar it cannot bond to protein through the polar groups in its structure (This phenomena is discussed in previous chapter [94], [100]). Limit of detection depends on various parameters such as chemical structure of oil and protein, molecular weight of protein, existence of certain amino acids (cysteine and lysine) and the sum of polar groups in the protein.

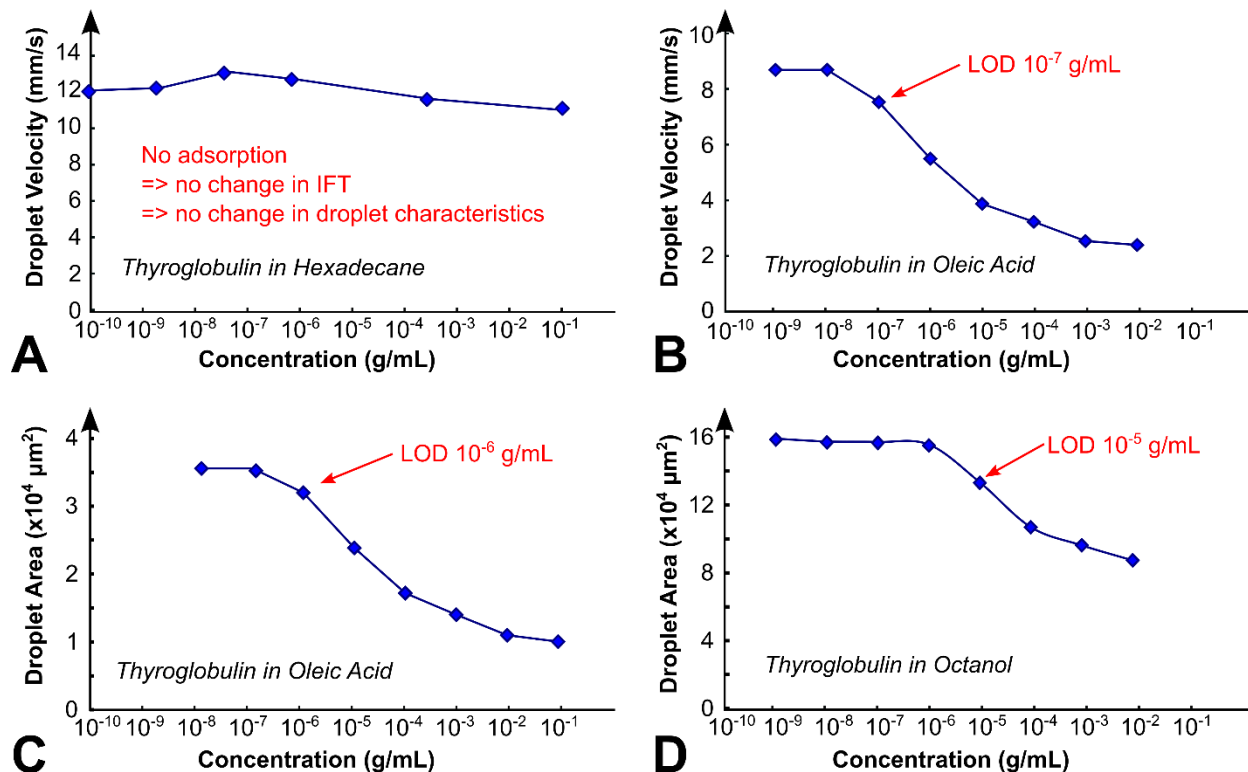


Figure 4-20. A. Using Hexadecane as carrier phase doesn't cause considerable change in drop size B. Oleic acid shows a limit of detection of 10⁻⁷ g/ml with Thyroglobulin. Velocity of droplets also changes with the amount of protein D Using octanol the limit of detection is about 10⁻⁵ g/ml.

Figure 4-22 shows a comparison between different detection systems versus our developed method. Our developed method is called IFTD (Interfacial Tension Detection). This method stands in pg-fg range in comparison with other methods such as refractive index, conductivity, light scattering, corona discharge, UV, visible, photodiode array, fluorescent, radioactivity and electrochemical. Electrochemical detectors are also providing the similar limit of detection; however, they have their own problems such as fouling. IFTD is inexpensive, fast and label free. Since we are measuring 1 μg/ml of protein in a 1nL droplet the total amount of protein detected would be equal to 1 fg as shown in Figure 4-21.

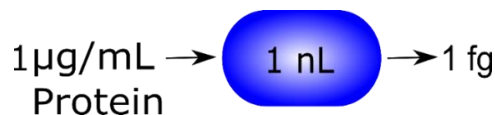


Figure 4-21. Total amount of protein detected

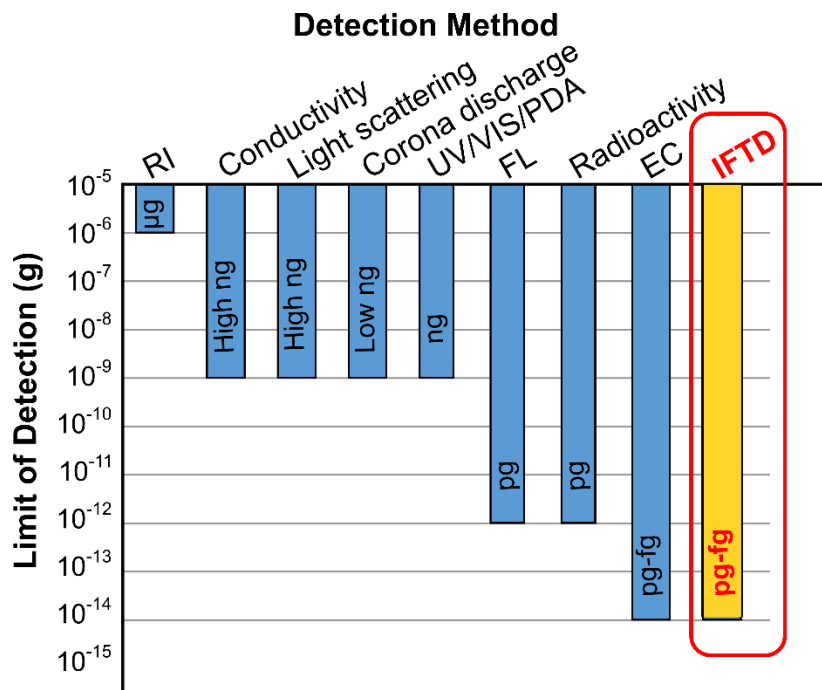


Figure 4-22. Comparison between various detection methods

HPLC System Connected To Microfluidic Chip

Interfacial tension detection (IFTD) method can integrate into other continuous detection methods. In fact, this is a great advantage for this method because more than one detection method can offer better sensitivity and selectivity.

We have used Zenix size exclusion column (7.8*300 mm) with pore size of 300 Å and particle size of 3 µm. The standard flow rate used for this column was 1 ml/min with maximum back pressure of 3500 psi and protein molecular weight range of 5,000 – 1,250,000. Flow rate was 1 mL/min water with 20 µL injection and UV 214-280 nm detection [101].

We have connected the outlet of HPLC system to drop generator (Figure 4-23) in order to quantify the changes in sizes of droplets (based on the amount of proteins eluted from the HPLC column).

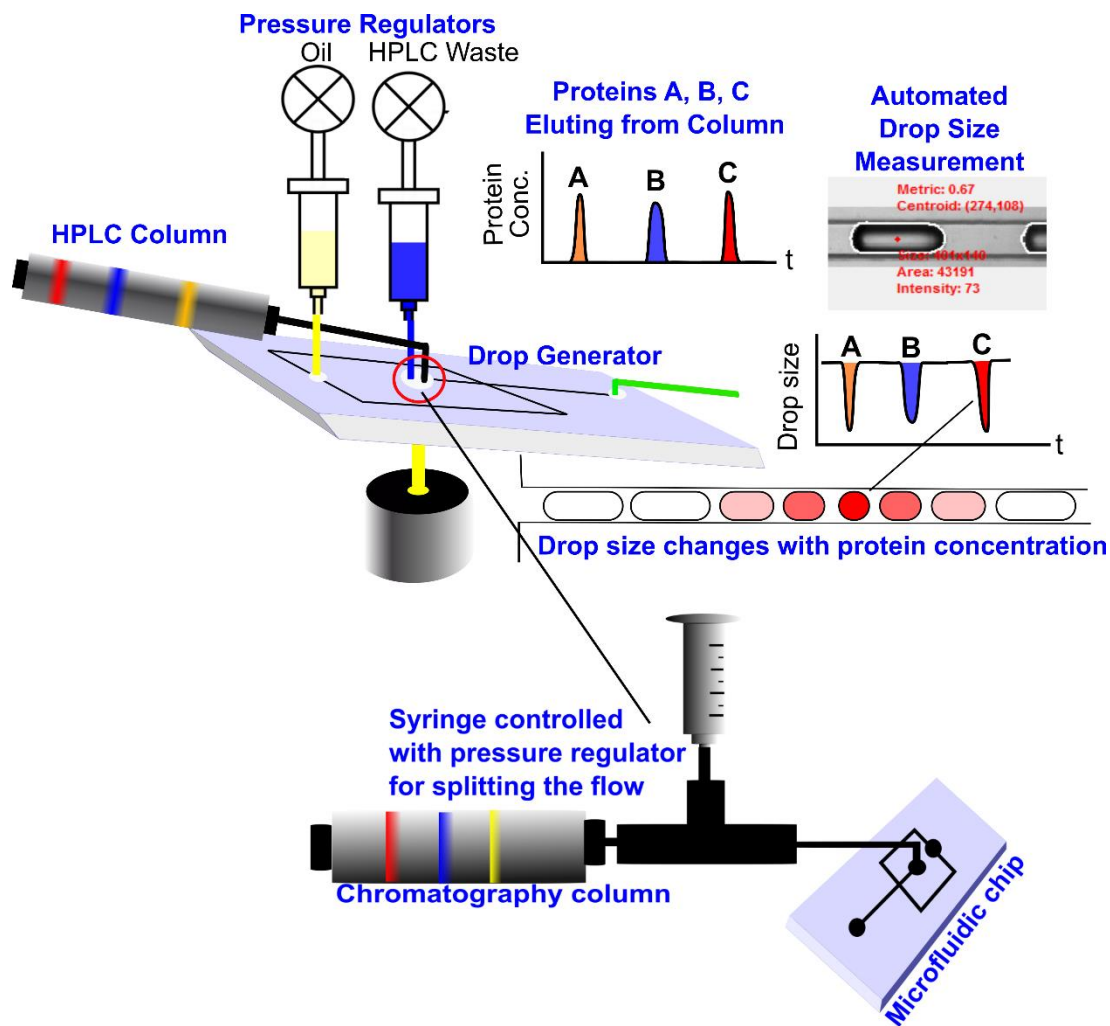


Figure 4-23. HPLC detector based on drop shape morphometry. A drop generator is attached inline after the HPLC column, and the drop shape/size is monitored in real time.

Proteins A, B and C are injected into the HPLC column and as they are eluting from the outlet they are encapsulated inside droplets. Our detection system is based on the concept that the interfacial tension of an oil-water interface is inversely related to protein

concentration. Globular proteins such as bovine serum albumin (BSA) adsorb to the interface, reducing its interfacial tension [2], [3].

In this research, we utilize a cross junction drop generator coupled to the HPLC column. The size of the drops produced in the drop generator is highly sensitive to interfacial tension. The drop size in a microchannel is determined mainly by the balance between shear and interfacial forces, given by the capillary number. In this formula: μ , v_c , Q_c , γ , and A are (respectively) the viscosity, velocity, and flow rate of the continuous phase, the interfacial tension between two phases, and the cross sectional area of the micro-channel. They have investigated the relation between drop size and Ca ($D_p \sim Ca^{0.235}$) by varying the interfacial tension using different surfactant concentrations [91].

$$Ca = \frac{\mu v_c}{\gamma} = \frac{\mu Q_c}{A\gamma} \quad (4-1)$$

We use two types of microfluidic drop generators. The confined geometry has the same height and width for the oil and water channels as well as the downstream channel (100x100 μ m). The unconfined geometry has a narrower water channel (50x100 μ m) in comparison to the oil channel and the downstream channel (both 50x500 μ m). To maintain low Ca number, the large flow rate from the outlet of HPLC is bypassed with a 20:1 flow splitter inside the chip. The ratio of flow splitting can be tuned during the experiment by changing the pressure on the waste port. At lower flow rates, the expansion time for each drop is longer, allowing more time for proteins to adsorb to the interface. A UV absorbance detector (Waters 486 tunable absorbance detector with sensitivity of 0.01 absorbance units and the path length of 10 mm) is placed upstream of the drop generator for comparison.

Figure 4-24 shows droplets containing protein and how proteins saturate the surface of droplet. Proteins tend to accumulate on the back of droplet and cause shape eccentricity change with concentration. This phenomena also impacts the size of droplet. This can happen at high capillary numbers ($Ca > 0.01$) just with surfactants or oils too. We have seen this while IFT is very low (using octanol with buffer) or using 10% V/V surfactant in FC-40.

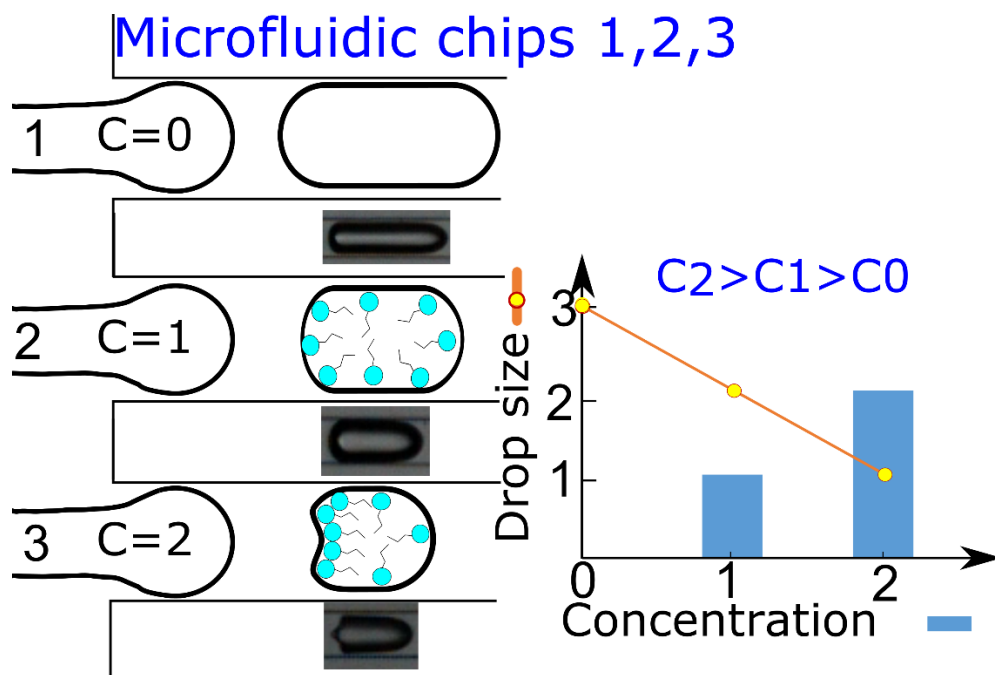


Figure 4-24. Proteins accumulate at the end of droplet. This is due to Marangoni flows inside the droplet.

Figure 4-25 shows the drop size change with protein elution from the HPLC column. The chromatogram is matched with corresponding times in the saved movie of generated droplets in the chip.

The amount of lag time between peak of the chromatogram and drop size change depends on the length of tubing and amount of diffusion in the path. In this experiment we used 30 cm of peek tubing (ID=500 μm) which caused about 0.01 ml dead volume.

Different inlets and tubes are shown in Figure 4-26. The outlet of HPLC goes to the inlet of the chip. The other tube (with resistance) is to bypass the extra liquid to a syringe.

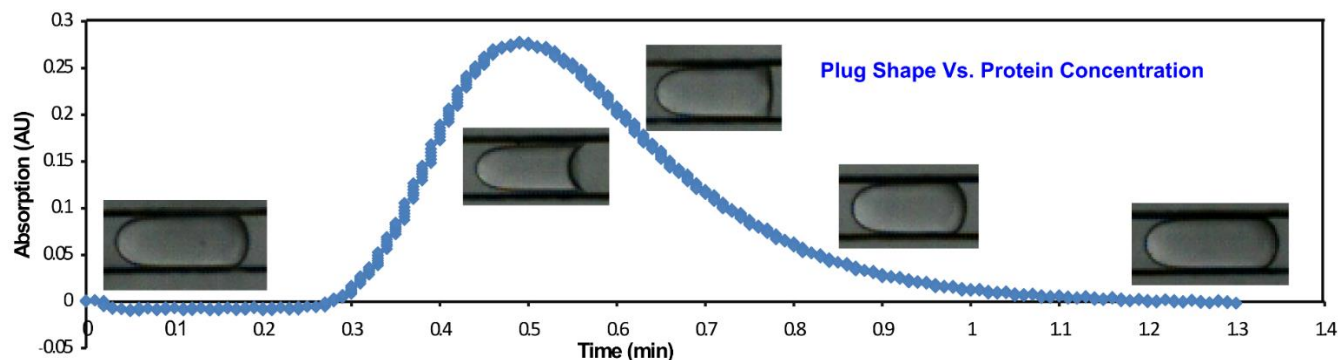


Figure 4-25. Drop size change with protein elution in HPLC

To measure drop parameters, we use an image processing software developed in our group which determines drop size, length and eccentricity, and creates chromatograms based on those parameters. For all experiments, we inject a 50 μl BSA sample at various concentrations, while maintaining a continuous flow rate of 0.5 ml/min in the HPLC.

The first experiment (Figure 4-27) compares the sensitivity of the drop generator and the UV absorbance detector, using an unconfined drop generator. Three samples of 0.1, 0.3, and 0.6 mg/ml BSA were sequentially injected into the HPLC. At the lowest concentration (0.1 mg/ml), the UV absorbance detector does not show any signal, while our system shows a 20% increase in drop size. This occurs because the non-uniform distribution of proteins in the drop causes it to stretch at the tailing end [102].

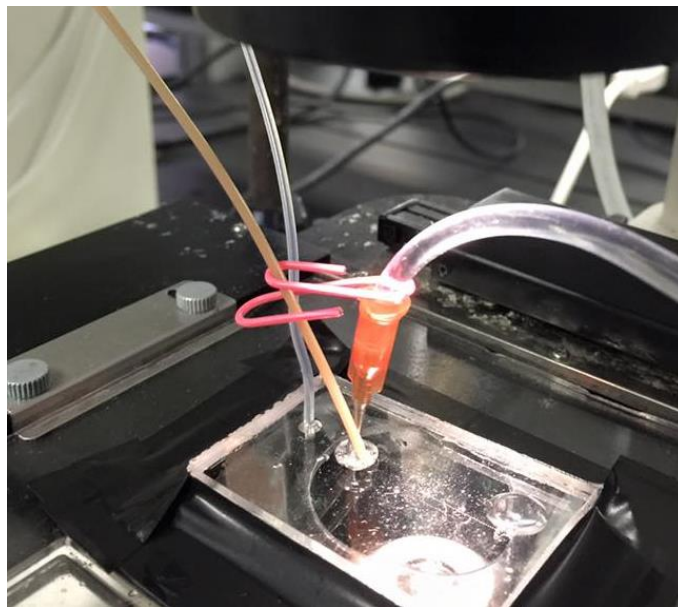


Figure 4-26. The outlet of HPLC goes to the inlet of the chip. The other tube (with resistance) is to bypass the extra liquid to a syringe.

As a result, both the drop length (Figure 4-27B) and the shape eccentricity (deformation from circular shape, Figure 4-27C) increase when proteins elute from the column [103].

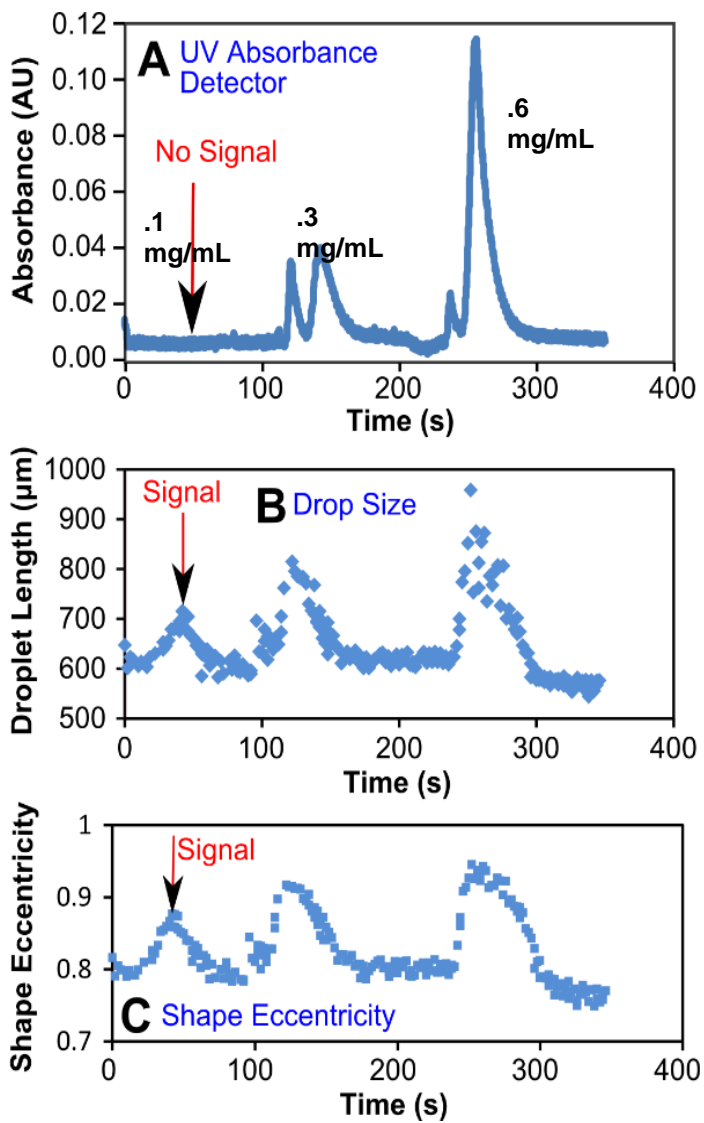


Figure 4-27 (A) The UV absorbance detector shows no signal for the 0.1 mg/ml; (B) Drop length vs. time (C) Shape eccentricity vs. time.

In addition to checking the peak height we have also investigated the area under each peak by integration using MATLAB.

$$\text{Area} = \int \text{Droplet length} \times dt \quad (4-2)$$

Using this method we show a linear increase in the peak area by increasing concentration.

Figure 4-28 shows the bar graph of peak area for major axis length vs. concentration.

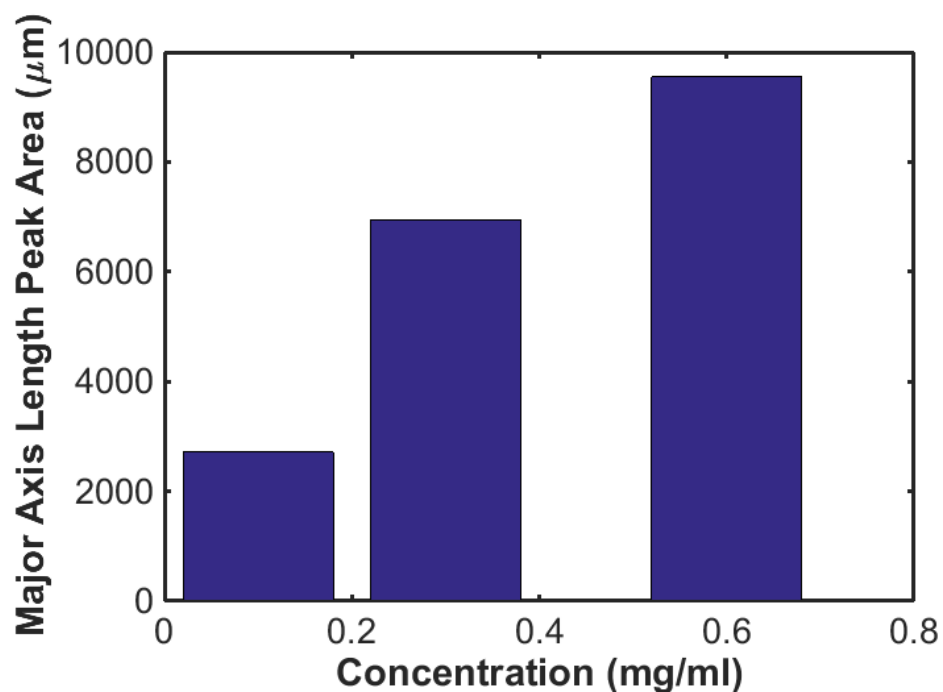


Figure 4-28. Major axis length peak area vs. concentration for three different injections

Figure 4-29 shows peaks of shape eccentricity vs. concentration. The same integration method is used for generating this figure.

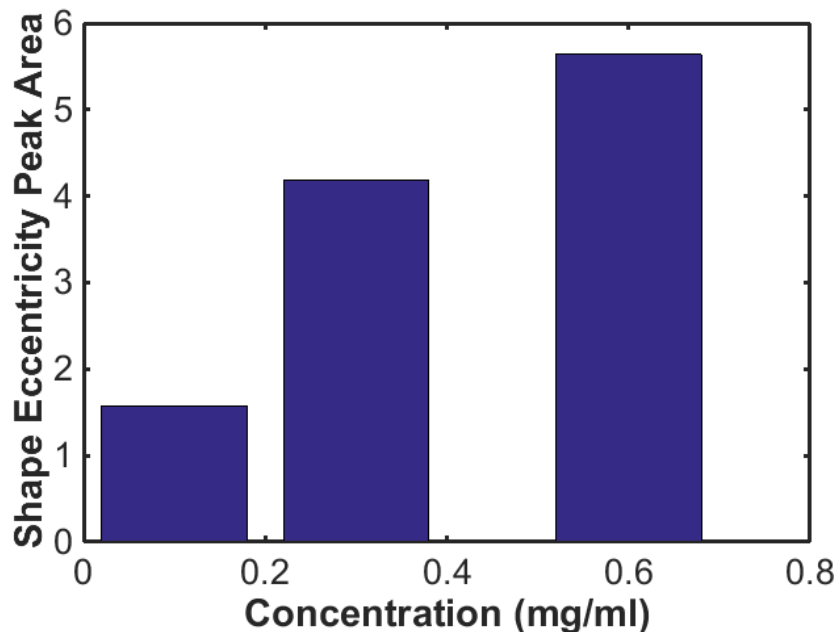


Figure 4-29. Shape Eccentricity peak area vs. concentration for three different injections

The second set of experiments is performed in a confined channel, where the oil and water channels have the same cross section. Three samples of 1, 3, 6 mg/ml BSA (10X larger than the first experiment) are injected to the HPLC. In contrast to the unconfined geometry, here the plug length decreases with protein concentration, although the drop/plug area decreases in both cases (Figure 4-27A). Figure 4-27B shows changes in shape eccentricity versus time. The decrease is consistent with previous studies, and is due to the decreased interfacial tension at higher protein concentrations [8].

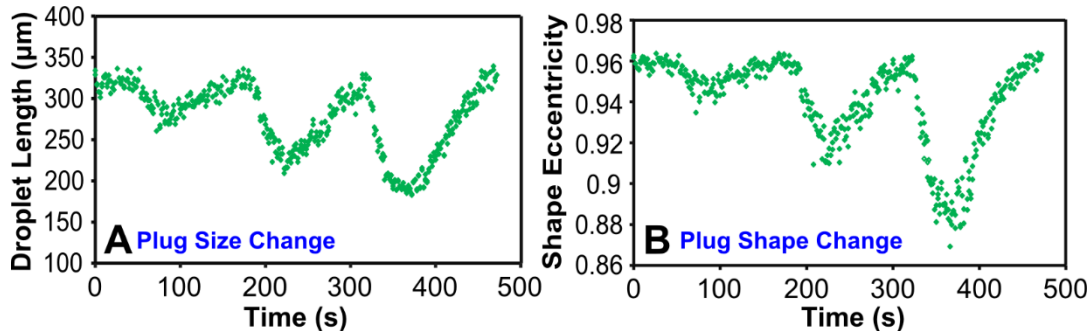


Figure 4-30. Confined drop (plug) generator. (A) Plug length vs. time (B) Plug shape eccentricity vs. time.

The unconfined channel geometry is at least 5 times more sensitive than the confined channel. The unconfined system has a smaller cross section and higher Ca . According to Ca number equation, when Ca is large, it is more sensitive to changes in γ . Therefore drop size, which has a reverse relation with Ca , will be more sensitive to protein concentration. Calibration curves (Figure 4-31) show that the changes in drop size are roughly linear with protein concentration, below the critical micelle concentration (CMC).

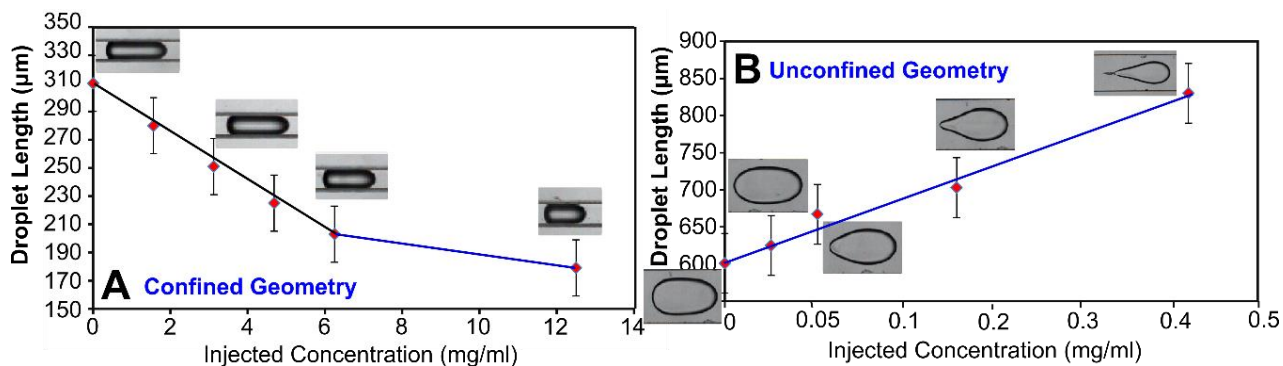


Figure 4-31. (A) Plug length vs. injected protein concentration in a confined drop generator. As the protein concentration increases, the plug length decreases. (B) Drop shape vs. protein concentration in an unconfined drop generator. With increasing protein, the drop elongates to a teardrop shape.

Protein Measurement without HPLC

Using HPLC before drop generator can separate proteins from the mixture before eluting to drop generator. We were curious to see if we will see the same effect if we inject proteins directly to the tubing or the chip. By injecting proteins to the tube (Figure 4-32) we experienced considerable amount of dead volume (50 μL or more) and diffusion. This can prevent forming a peak of protein concentration in droplets.

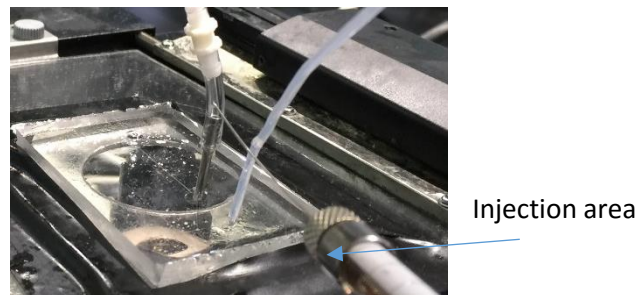


Figure 4-32. Injection to the tube using a 10 μl Hamilton syringe

Figure 4-33 shows the trend of drop size change using injection to tube method. It is clear that drop size doesn't return to its original size. However, the fact that drop size decreases more than half its original size shows the impact of interfacial tension on drop generation.

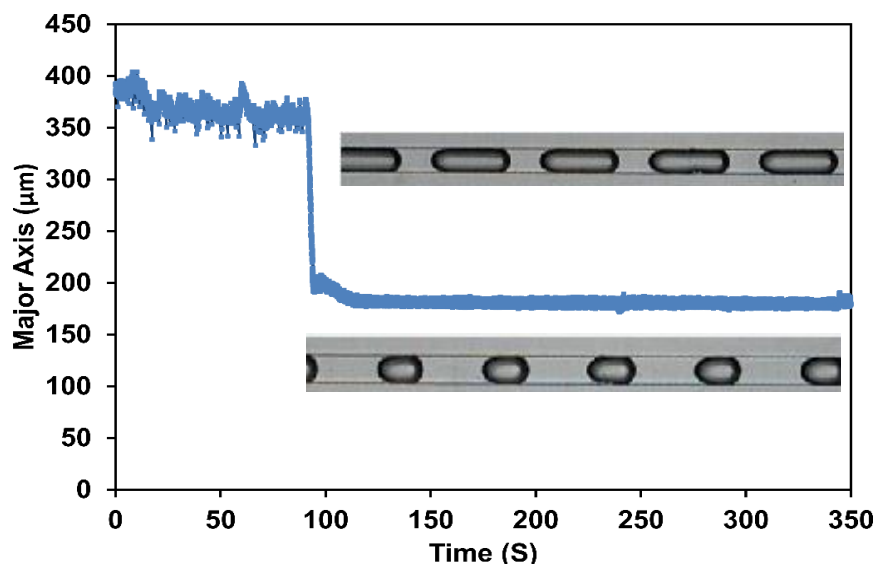


Figure 4-33. The pattern of drop size change by injecting protein to the tube. This graph represents drop size change at concentration 0.001 gr/ml

We were curious to see if the similar pattern of size variation happens when we inject the protein directly to the chip (Figure 4-34). This approach is useful when we want to measure the amounts of only one protein. It is very sensitive since the dead volume is almost zero and proteins reach the cross sectional area almost instantly (10 seconds). We also tested this theory by using pristine buffer or water in the chip. Figure 4-35 shows no considerable change in droplet size. Figure 4-36 shows different tests and the dependence of peak time to concentration. Graphs in this figure show variation of peak time with concentration of protein (The higher the concentration the longer the peak time). Based on these results we have tried to generate a linear calibration curve for predicting unknown amount of protein in the microfluidic chip.

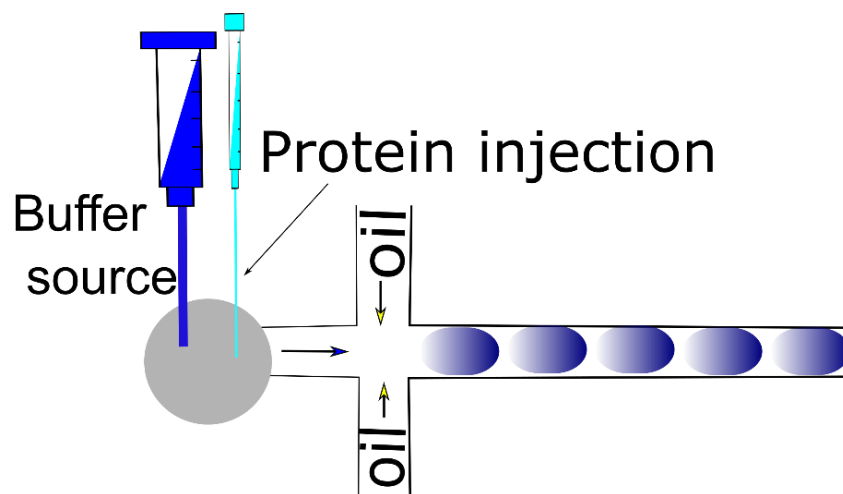


Figure 4-34 Schematic of protein injection to the chip. We are using the buffer inlet to inject protein to the chip.

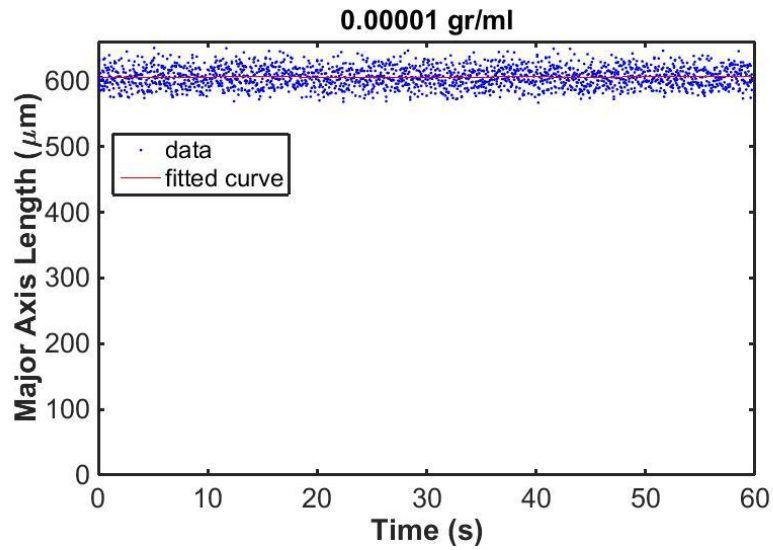


Figure 4-35. Drop size doesn't show any change with pristine solution or very low concentrations (10^{-5} gr/ml) of protein

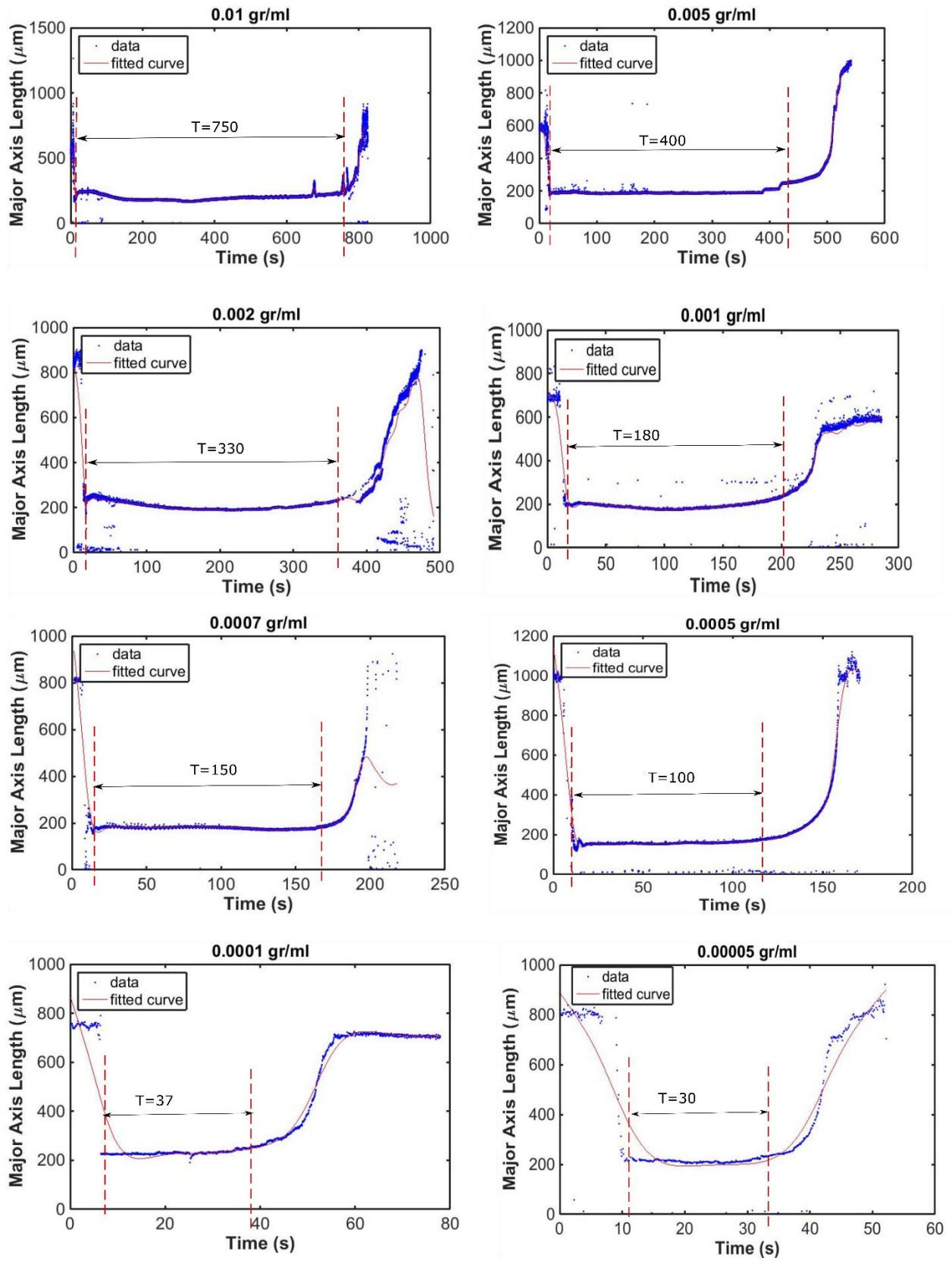


Figure 4-36. Graphs show the change in major axis length change with protein injection. The peak time varies with concentration.

In order to correlate between peak time and concentration, we need a calibration curve. Data must be linearized (using logarithms) in order to fit the results. So we are not solving for: $y = ax + b$ Instead we are solving for:

$$y = ax^b \text{ or } y = ae^{bx} \text{ or possibly something else,}$$

We shall attempt to fit using the first equation and can be done using linear regression and logarithms:

$$y = ax^b \quad (4-3)$$

$$\text{Log } y = \text{log } ax^b \quad (4-4)$$

$$\text{log } y = \text{log } a + \text{log } x^b \quad (4-5)$$

$$\text{log } y = b \times \text{log } x + \text{log } a \quad (4-6)$$

Then the original data is fit by:

$$y = (10a) \times b \quad (4-7)$$

So performing linear regression on the Log Concentration (x) and Log Peak Time (y) we see that:

$$\text{log } a = 4.1033 \rightarrow a = 12686.33 \quad b = 0.6202$$

So then the fit curve is:

$$y = 12686.33x^{0.6202}$$

Or on a Log-Log graph it would be seen as:

$$\text{log } y = 0.6202 \text{ log } X + 4.1033 \quad (4-8)$$

Figure 4-37 shows the graph with regular scale vs. logarithmic scale (MATLAB). The logarithmic scale trend line has the slope of 0.6202 and intercept of 4.1033.

Since this experiment is repeated two times with similar conditions, Figure 4-36 shows the error bars. Injection happens at about 15 S and the initial drops after injection carry

the maximum amount of protein. They have a little tail at the end which shows the saturation of protein inside droplets (Figure 4-38). This calibration line is only valid between minimum and maximum available data points and there is no guarantee that extrapolation presents accurate information.

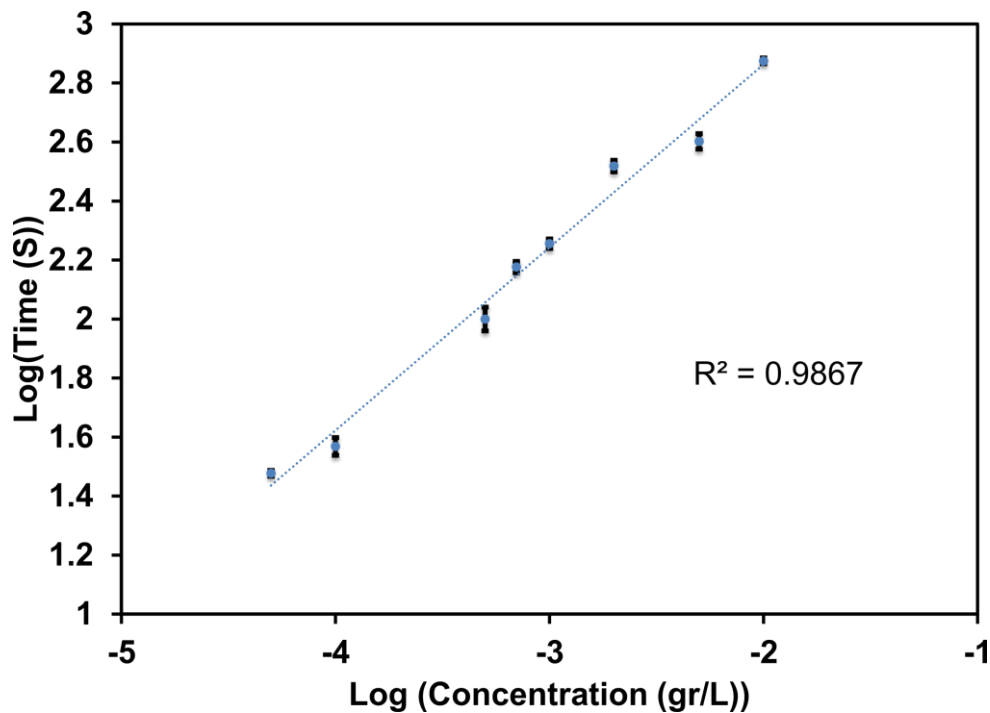


Figure 4-37. Calibration curve for Log (time) Vs. Log (concentration)

This phenomena happens because of marangoni flows [70], [104](due to gradient in interfacial tension) on the surface of the droplet. Since proteins reduce interfacial tension at the interface they migrate to the back of droplet along the interface of oil-water and they may even separate from the droplet at higher concentrations. These masses of concentrated protein can also stick to the walls of channel. This can make the channels hydrophilic at high concentrations of protein. During the period of 124S-540S drop size doesn't change which shows the diffusion of protein during that time. Depending on the concentration of injected protein, this period of time can be shorter or longer. Calibration

of protein quantity based on this time interval can be considered as a new approach to protein quantification.

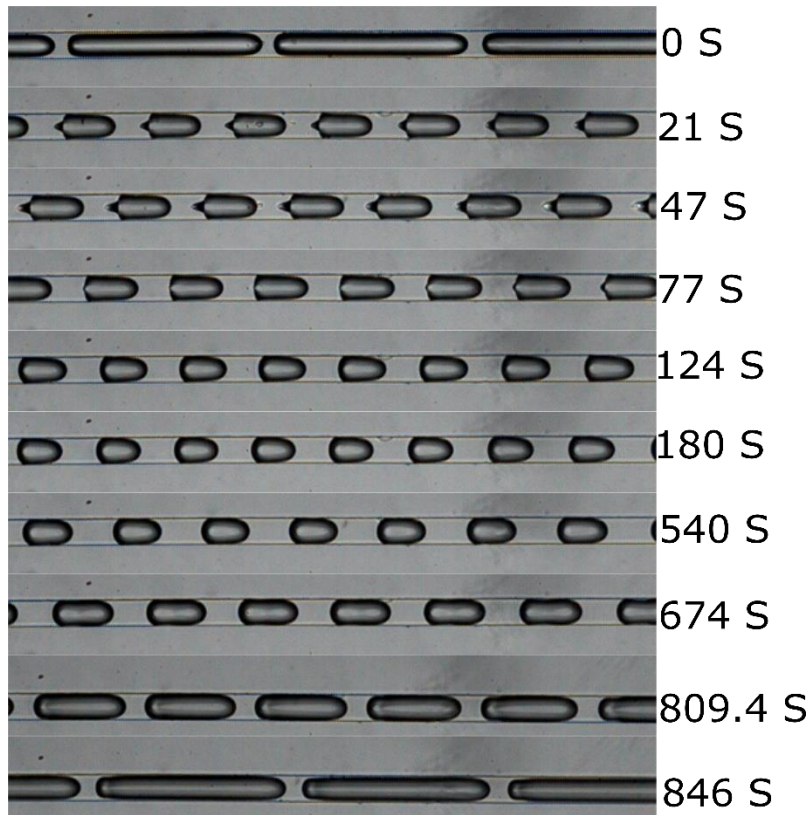


Figure 4-38. Drop size during different times after injection of protein. This figure shows that drop size returns to its original size at about 846 seconds.

Chapter 5. SIMULATION

Simulation results confirm the experimental results shown in previous section. Concept of drop generation both in pressure driven and flow driven systems is described in chapter 2. This section presents the effect of interfacial tension changes in a drop generator both with fixed flow and fixed pressure conditions. All simulation models have used COMSOL Multiphysics 5.0.

Fixed Flow System

As described in chapter 2, flow rate is always kept constant and other parameters such as pressure are considered as dependent variables in fixed flow systems. The fixed flow simulations are performed with constant velocity of continuous phase= 0.1 m/s and dispersed phase=0.03 m/s.

Level set method was used for modeling this laminar two phase flow. This method is considered as one of the precise methods for studying curved shaped boundaries such as droplets. Steps in this simulation include phase initialization (step 1) and time dependent (step 2). This simulation utilizes the Navier Stokes equations with assumptions such as:

- Laminar flow regime
- Constant density of the fluid
- Newtonian fluid

In finite element methods finer mesh will provide more elements and as a result more accurate solution [105] . Here we have used normal mesh due to time limitation but similar trend can be achieved using fine mesh. The channel geometry is similar to the actual channel that we used in our experiments (width=100 μm), the height of the channel (for

3D simulation) is also 100 μm . Figure 5-1 shows the change in drop size with increase in water flow rate. At 0.01 m/s ($Ca=0.005$) there is no drop generation; however, increasing the velocity to above 0.02 ($Ca=0.01$) can cause dripping regime and above 0.07 m/s ($Ca=0.035$) we will have jetting regime. At 0.1 m/s where $Ca=0.05$ we will observe a stable co-flow regime. Similar results has reported in previous research [106].

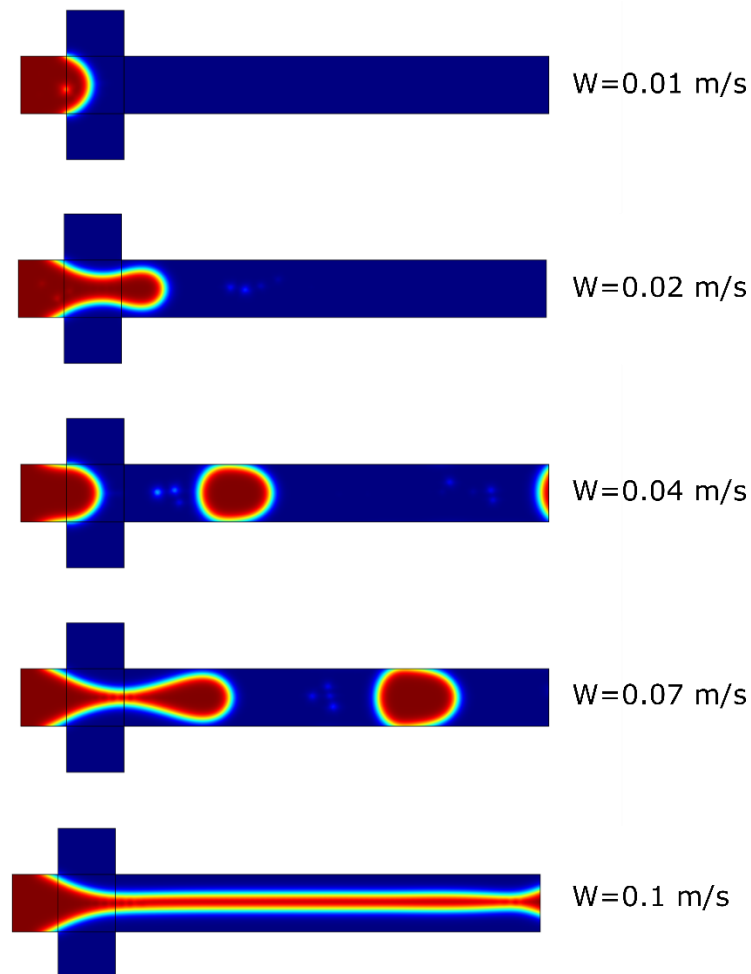


Figure 5-1. Change in drop size with increasing water flow rate (oil flow rate is kept constant at 0.02 m/s)

Figure 5-2 shows drop formation channels at different interfacial tensions. It is clear that higher interfacial tensions will cause larger size droplets. This can be explained through the process of drop break up (described in chapter 2). In this figure red regions

have higher pressure and dark blue regions have minimum pressure. At the inlets pressure is higher. Also pressure inside droplets is higher than their surroundings. Eventually at the outlet of the channel pressure reaches its minimum amount.

Each droplet creates a resistance in the pressure path and decreases the initial inlet pressure inside the channel. However the pressure inside each droplet is higher than its surrounding due to curvature in droplet surface and Young- Laplace model (described in chapter 2).

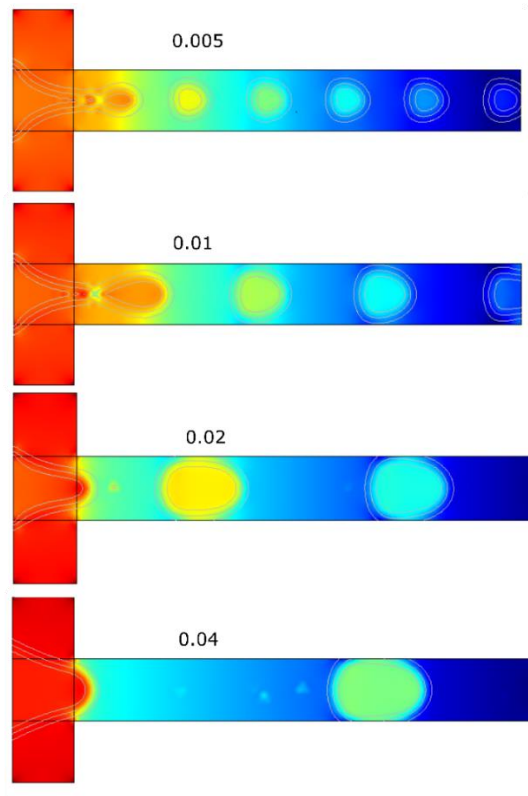


Figure 5-2 Demonstration of increase in drop size with increase in interfacial tension, the amounts of interfacial tension are shown on each channel

Fixed Pressure System

In fixed pressure system pressure of the inlets is kept constant pressure and the rest of the parameters such as velocity of the fluids are considered as dependent variables.

Similar to fixed flow system, laminar two phase flow boundary conditions are applied with level set method. The simulation steps and geometry of the channel are also similar to the fixed flow system. Figure 5-3 shows how increase in water pressure can increase droplet size at constant oil pressures. In this simulation oil pressure is kept constant at 2400 Pa and water pressure is varied from 1000-2500 Pa. IFT is also kept constant (0.02mN/m) at different water pressures.

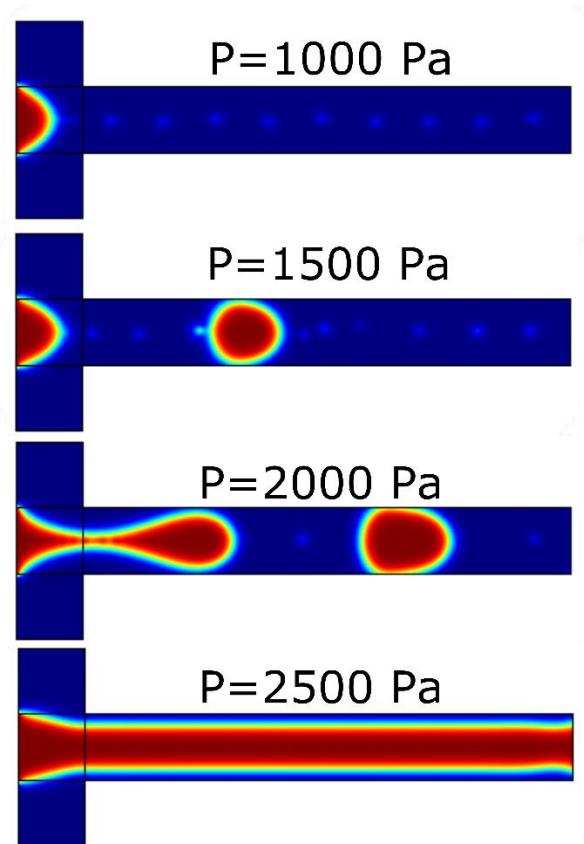


Figure 5-3. Drop size increase with increase in water pressure at constant oil pressure

Materials are water and oleic acid pressure on water inlet is 2000 Pa and oil pressure is 2400 Pa. Mesh is normal and tolerance is 0.01. Boundary conditions are considered as wetted wall with 0.349 rad angle [107]. The study includes two steps of phase

initialization and time dependent time ((0, 0.0001, 0.01)) S. This means we had time intervals of 0.0001 S for the total time of 0.01 S which will include 100 time steps.

Figure 5-4 demonstrates the increase in drop size with increase in interfacial tension in fixed pressure model. The results of simulation agree with experimental results presented in previous sections.

Figure 5-5 shows the drop size change versus interfacial tension in flow driven and pressure driven systems. Changes in drop size are much sharper in pressure driven systems than flow driven systems. This is confirmed both by our experiments and previous literature [87], [108]. The increase in velocity with pressure is much sharper than increase in velocity with flow rate [107].

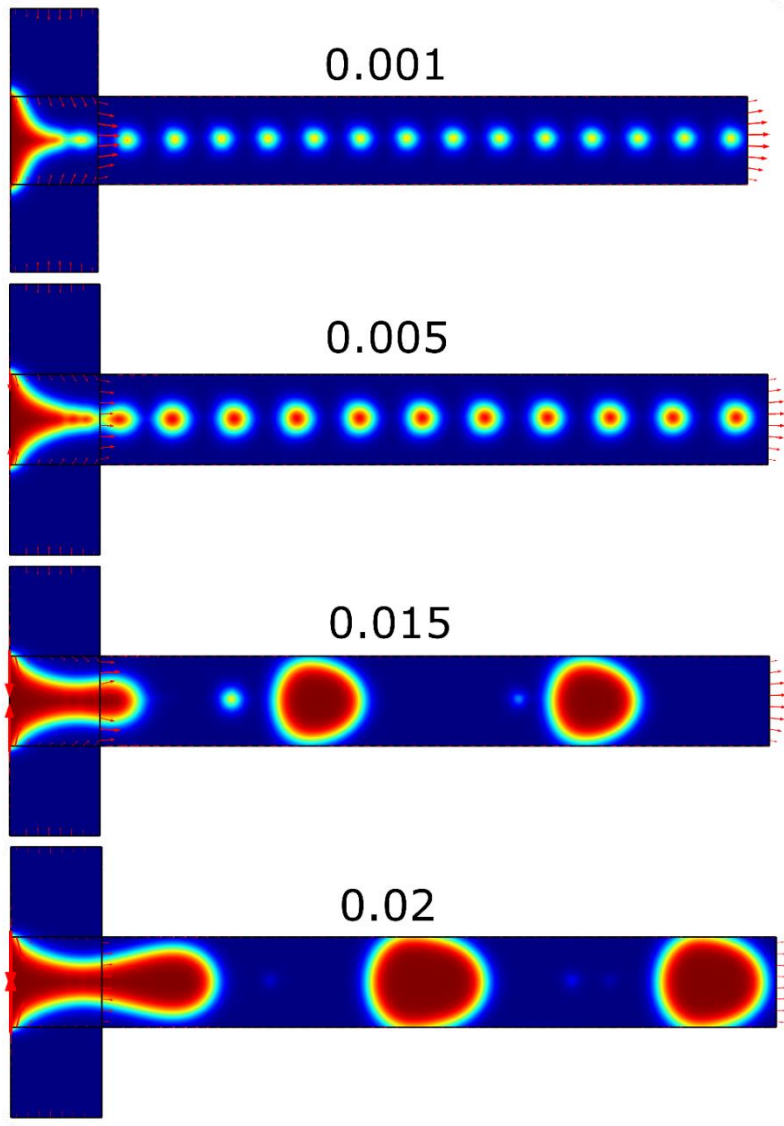


Figure 5-4 Shows a schematic of fluid fraction inside microfluidic channel with different amounts of interfacial tension

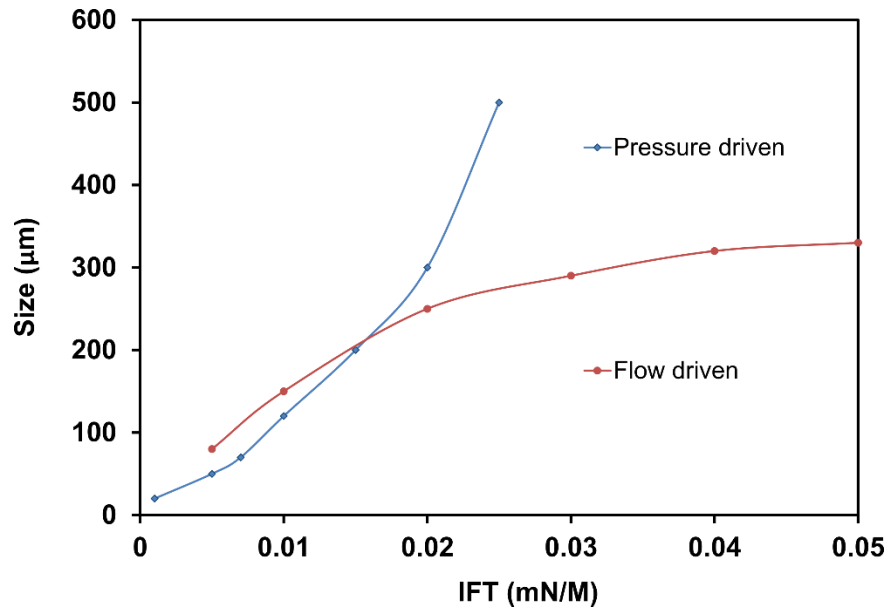


Figure 5-5. Comparison of droplet size vs. interfacial tension both in flow driven and pressure driven systems

Comparison of Pressure Profiles

To understand the physics of pressure driven system versus flow rate driven system we have compared pressure profiles at the inlets of microfluidic chip.

Figure 5-6 shows the pressure profile at 1 point of the microfluidic channel. Maximum and minimum of the pressure profile depends of the concave or convex shape of the droplet proceeding to the cross section of the channel.

The first step is Nucleation when a curved surface of dispersed phase is formed at the end of water channel. At this point, pressures of oil and water are related to the amount of interfacial tension ($P_W - P_O = \frac{\gamma}{2R}$ where P_W is the pressure of water inside the curved surface, P_O is the pressure of oil which is outside the curved surface, γ is the interfacial tension at the surface and R is the radius of the curved surface). In this step, pressure inside the droplet is larger than the pressure outside the droplet. This will lead

to the second step which is called expansion and at this stage the dispersed phase expands more into the middle of the junction. Pressure inside the dispersed phase will cause more expansion and as a result more elongation and eventually droplet pinch off happens. During the third step elongation of the drop will cause concave surfaces on both sides of the elongated drop. Inside these concave surfaces pressure of water is less than pressure of oil. If the oil pressure is high enough it can pinch off the droplet.

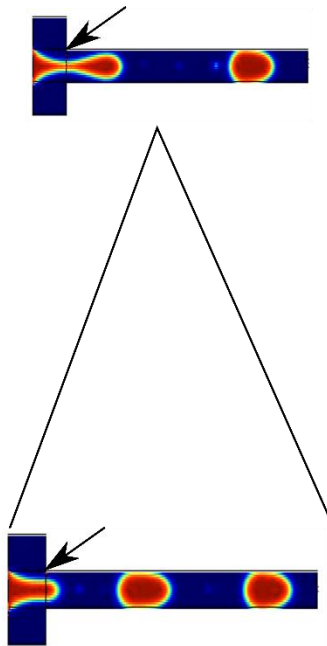


Figure 5-6 Pressure profile at one point of the microfluidic chip

Figure 5-7 shows the pressure profile at three different points of the microfluidic channel in flow driven system versus pressure driven system. The number of positive peaks are equal to the number of droplets in each system. Point 4 in pressure driven flow has the same pressure as inlet while the same point in flow driven system undergoes pressure fluctuations with similar trend as the two other points. Pressure fluctuations in

pressure driven system are 200-400 Pa versus 1000 Pa in flow driven system.

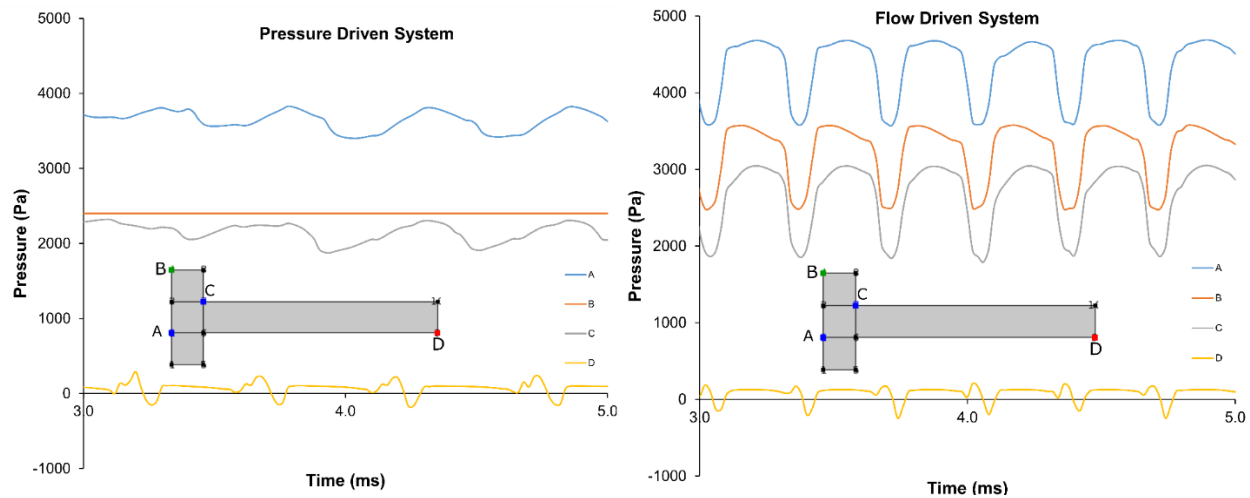


Figure 5-7. Comparison of pressure profiles at three different inlet points

3D simulations

The 3D simulation can be used to confirm the validity of the 2D results. The chosen physics is laminar two phase flow, level set. The study is done in two steps: stationary (step 1) and time dependent (step 2). Other parameters such as materials and pressure at the inlets are the same as 2D. The height of the channel is 100 μm . The mesh size was defined as extra course since calculation time is more than 120 hours for this case. Figure 5-8 shows the volume fraction of droplets at $\sigma=0.02$.

Due to calculation time and system limitations, it was not possible to investigate drop sizes for 3D simulation. Extra coarse mesh causes a vague barrier for drops and it is not possible to estimate the drop size.

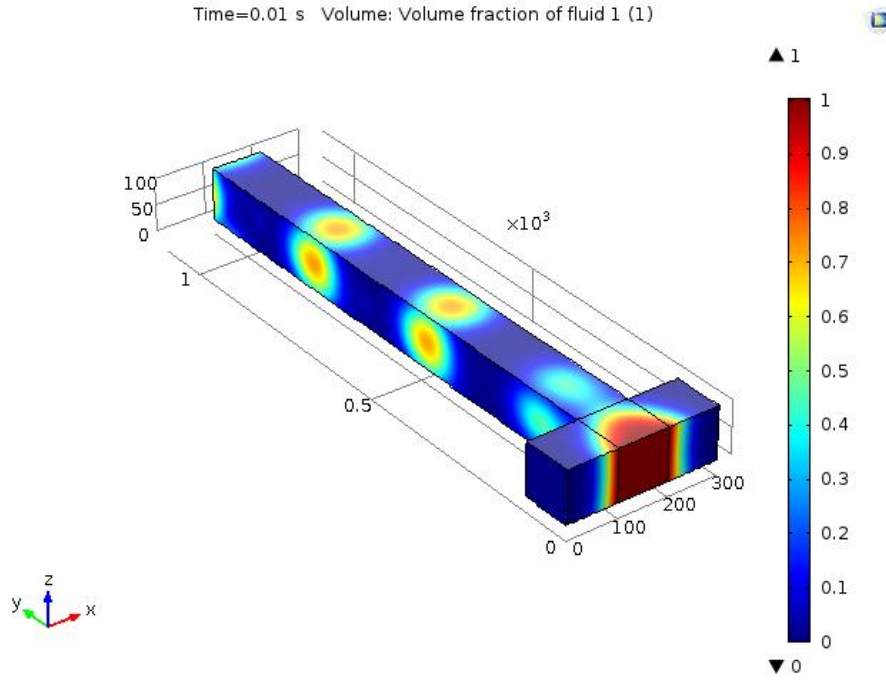


Figure 5-8. 3D simulation of drop generation with $\sigma=0.02$

Chapter 6. APPLICATION

There is a sea of applications for protein detection methods. Serious disease processes are caused by lack of function, out of balance concentrations or sequence mutations of plasma proteins. Considering this fact, better protein detection and characterization methods can save individuals lives. One of the major challenges in quantifying analysis is the highly concentrated protein matrix which may cause interference in quantification and detection of a certain protein.

Quantitative monitoring of proteins is shown to be one of the most promising approaches for biomarker discovery. One of the biomarkers that can be quantified using this method is human Galectin (LGAL-14). Galectins (lectin family) regulate cellular procedures such as cellular growth and immune reactions. Galectins bind to glycoproteins, beta-galactosides (like lactose) and lipids [109], [110]. Unlike many other proteins they do not require metal ions for activity. They are mostly found in mammals [111]. Galectin 14 is also known as placental protein. This protein is placenta specific and it induces the apoptosis of T lymphocytes. This can reduce the maternal immune attacks on fetal [112], [113].

There are no research studies available on chemical interactions between LGAL-14 and oleic acid or even other fatty acids. Cysteine and Lysine are the amino acid residues which bind to fatty acids [97]. Galectin has smaller size (16KDa) in comparison to BSA (66.5 KDa) and it has 6 Cysteine residues which are accessible to the solvent.

Other biomarkers such as placental growth factor (PGF) didn't show successful favorable results. This may be because of the interface which is largely hydrophobic and

bury the amino acids inside. There are only 3 polar interactions in the structure of PGF which include hydrogen bonds, Aspartic acid and Arginine [114].

Pendent drop experiment results have proven that this method is sensitive to very small amounts of LGAL-14 (50 pg). This approach can be used for quantification of very small amounts of this biomarker. For this purpose the sample can be injected to HPLC and eluted to the microfluidic chip.

Chapter 7. FUTURE WORK

Having presented a background, theory, experimental, simulation and application of our protein detection technique, this thesis now proposes future goals and research outcomes.

1. Based on previous results for LGAL-14, IFT measurement, this protein can directly be injected to the chip for drop size measurement and calibration.
2. It is also possible to develop a separation unit inside the chip by coating antibody in the chip and capturing LGAL-14 in a defined area of the chip.

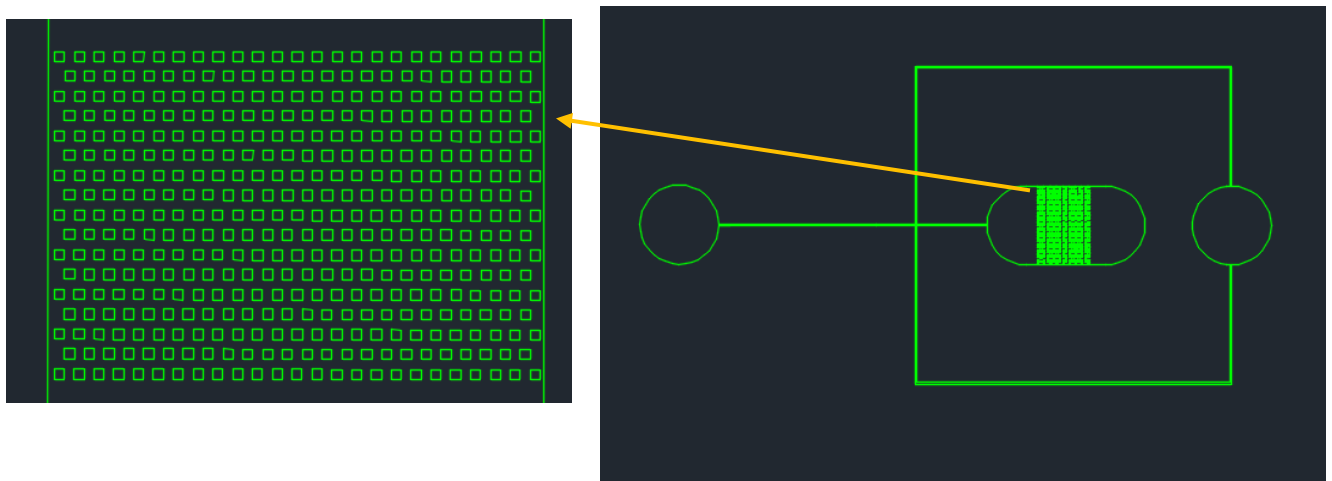


Figure 7-1 Chip design for antibody coating

3. Further investigation can be done on 3D simulation of the drop generation and drop size change Vs. IFT. Improving hardware such as computer's RAM and CPU will help to achieve this goal.
4. This method can potentially be used for detection and quantification of other biomarkers in body fluids such as urine, plasma, tears and sweat.

5. Modification of carrier phases is another important parameter for this work. Table 7-1 shows a list of possible carrier phases which can potentially be used as a continuous phase. A proper carrier phase should have ignorable solubility in water because we want the two phases to be immiscible. IFT value shouldn't be very high or very low. Since at high IFT we will need surfactants for drop generation and surfactants can saturate the surface of droplet not letting proteins to enter the interface. At low values of IFT we may not be able to generate drops at all. Chemical structure of continuous phase is also important because proteins need to adsorb to the interface of oil (continuous phase) water (dispersed phase). If carrier phase is very neutral like Hexadecane there is no partitioning of protein inside carrier phase.

Table 7-1. Possible continuous phases for drop generation [115]

Compound	Formula	IFT (mN/m)	Density (g/ml)	Solubility of organic	Solubility of water
Pentane	C ₆ H ₁₂	49	0.6262	1*10 ⁻³	4.4*10 ⁻²
Hexane	C ₆ H ₁₄	51.10	0.6603	2.91*10 ⁻⁴	4.27*10 ⁻²
Heptane	C ₇ H ₁₆	50.2	0.6837	5*10 ⁻⁵	7.03*10 ⁻²
Octane	C ₈ H ₁₈	50.81	0.7025	1.13*10 ⁻⁴	6.02*10 ⁻²
Decane	C ₁₀ H ₂₂	52	0.7300	1.9*10 ⁻⁷	5.684*10 ⁻²
Hexadecane	C ₁₆ H ₃₄	53.3	0.7733	7.0*10 ⁻⁹	6.784*10 ⁻²
1-heptyne	C ₇ H ₁₂	28.15	0.7328	1.761*10 ⁻³	NA
2-Chloro-2-methylpropane	C ₄ H ₉ Cl	23.75	0.8420	1.04*10 ⁻³	1.30*10 ⁻¹
3-methylbutyronitrile	C ₅ H ₉ N	14.14	0.7914	1.24*10 ⁻²	3.71*10 ⁻¹
1-Octanol	C ₈ H ₁₈ O	8.52	0.8270	6.25*10 ⁻³	1.94*10
2-Octanol	C ₈ H ₁₈ O	9.42	0.8216	6*10 ⁻²	2.2*10
Oleic acid	C ₁₈ H ₃₄ O ₂	15.59	0.8935	6.77*10 ⁻⁹	4.65*10 ⁻¹
Cinnamic acid, Ethyl ester	C ₁₁ H ₁₂ O ₂	21.36	1.0491	2.49*10 ⁻³	5.98*10 ⁻¹
3-phenyl propionic acid, ethyl ester	C ₁₁ H ₁₄ O ₂	20.19	1.0147	6.39*10 ⁻⁴	4.45*10 ⁻¹
Nonanoic acid, ethyl ester	C ₁₁ H ₂₂ O ₂	23.88	0.8657	2.9*10 ⁻⁴	NA

6. Investigation of other microfluidic chip materials can be considered for future work. We have performed all the experiments using PDMS; however, other elastomers, paper or silicon.

Chapter 8. CONCLUSION

This research describes a novel, label-free inline method to detect proteins after a chemical separation. The initial chapter in the thesis begins by describing existing protein separation and purification techniques to give the reader appropriate context. It then presents and compares continuous flow detection methods used in chemical separations and purifications. The second chapter describes the chemical structure of proteins and their behavior in the interface of two immiscible fluids. Some conceptual models related to protein adsorption, including the Young- Laplace model and Beer- Lambert law, are derived and presented. Our detection method is based on a microfluidic droplet generator, and consequently the following section introduces various designs and geometries of drop generators. In particular, we describe fixed flow and fixed pressure drop generators, focusing on the inherent differences in the nature of each system. The drop generation regime for pressure driven systems is calculated and effect of inlet pressures on droplet sizes is demonstrated.

Following the introduction to fundamentals, Chapter 3 introduces our new method for protein detection/ quantification. This technique offers a better (up to 100X) limit of detection than conventional UV absorbance detectors (used in HPLC systems). The effect of different carrier phases on drop size change versus the amount of protein is also investigated. These experiments are performed in different pressure ranges to optimize the best pressure range for this operation.

The effect of different carrier phases is investigated and it has shown that some of the carrier phases don't display any change in droplet size with changes in protein

concentration. Modifying the carrier phase can offer better limit of detection since proteins show different partitioning coefficients in different carrier phases.

Simulation models have shown excellent agreement with experimental results. Simulation results both in pressure driven and flow driven systems show an increase in droplet size with increase in interfacial tension however these changes are sharper in pressure driven flow. We plan to develop a model for investigating the effect of pressure on droplet sizes as well.

In chapter 7 one of the target biomarkers which can be measured by this method is introduced as an application for this technique.

Looking ahead, this type of protein detection system described in the thesis could be used not only in chromatography applications, but also in other chemical separations, including capillary electrophoresis. The low dead volume and high sensitivity of the technique makes it amenable to miniaturization, and is therefore suitable for low flow separations like ultra-performance liquid chromatography (UPLC) and electrophoresis. Future work will seek to integrate our system with these detection systems.

BIBLIOGRAPHY

- [1] R. Aebersold and M. Mann, "Mass spectrometry-based proteomics," *Nature*, vol. 422, no. 6928, pp. 198–207, Mar. 2003.
- [2] C.-P. Jia, X.-Q. Zhong, B. Hua, M.-Y. Liu, F.-X. Jing, X.-H. Lou, S.-H. Yao, J.-Q. Xiang, Q.-H. Jin, and J.-L. Zhao, "Nano-ELISA for highly sensitive protein detection," *Biosens. Bioelectron.*, vol. 24, no. 9, pp. 2836–2841, May 2009.
- [3] J. J. Coon, P. Zürbig, M. Dakna, A. F. Dominiczak, S. Decramer, D. Fliser, M. Frommberger, I. Golovko, D. M. Good, S. Herget-Rosenthal, J. Jankowski, B. A. Julian, M. Kellmann, W. Kolch, Z. Massy, J. Novak, K. Rossing, J. P. Schanstra, E. Schiffer, D. Theodorescu, R. Vanholder, E. M. Weissinger, H. Mischak, and P. Schmitt-Kopplin, "CE-MS analysis of the human urinary proteome for biomarker discovery and disease diagnostics," *PROTEOMICS – Clin. Appl.*, vol. 2, no. 7–8, pp. 964–973, Jul. 2008.
- [4] D. T. Wong, "Salivary diagnostics powered by nanotechnologies, proteomics and genomics," *J. Am. Dent. Assoc.*, vol. 137, no. 3, pp. 313–321, Mar. 2006.
- [5] S. I. Stoeva, J.-S. Lee, J. E. Smith, S. T. Rosen, and C. A. Mirkin, "Multiplexed Detection of Protein Cancer Markers with Biobarcode Nanoparticle Probes," *J. Am. Chem. Soc.*, vol. 128, no. 26, pp. 8378–8379, Jul. 2006.
- [6] R. Fritz, H.-R. Kohan-Ghadr, J. M. Bolnick, A. D. Bolnick, B. A. Kilburn, M. P. Diamond, S. Drewlo, and D. R. Armant, "Noninvasive detection of trophoblast protein signatures linked to early pregnancy loss using trophoblast retrieval and isolation from the cervix (TRIC)," *Fertil. Steril.*, vol. 104, no. 2, p. 339–346.e4, Aug. 2015.
- [7] E. Dickinson and Y. Matsumura, "Proteins at liquid interfaces: Role of the molten globule state," *Colloids Surf. B Biointerfaces*, vol. 3, no. 1–2, pp. 1–17, Sep. 1994.

- [8] F. M. Richards, "Areas, Volumes, Packing, and Protein Structure," *Annu. Rev. Biophys. Bioeng.*, vol. 6, no. 1, pp. 151–176, 1977.
- [9] S. Tia and A. E. Herr, "On-chip technologies for multidimensional separations," *Lab. Chip*, vol. 9, no. 17, pp. 2524–2536, Sep. 2009.
- [10] R. R. Burgess and M. P. Deutscher, Eds., *Guide to Protein Purification, Volume 436, Second Edition*, 2 edition. Amsterdam: Academic Press, 2009.
- [11] B. Domon and R. Aebersold, "Mass Spectrometry and Protein Analysis," *Science*, vol. 312, no. 5771, pp. 212–217, Apr. 2006.
- [12] J. M. Walker, *The Protein Protocols Handbook*. Towota, N.J: Humana Pr, 1996.
- [13] R. Pieper, C. L. Gatlin, A. J. Makusky, P. S. Russo, C. R. Schatz, S. S. Miller, Q. Su, A. M. McGrath, M. A. Estock, P. P. Parmar, and others, "The human serum proteome: Display of nearly 3700 chromatographically separated protein spots on two-dimensional electrophoresis gels and identification of 325 distinct proteins," *Proteomics*, vol. 3, no. 7, pp. 1345–1364, 2003.
- [14] E. Cimetta, S. Cagnin, A. Volpatti, G. Lanfranchi, and N. Elvassore, "Dynamic culture of droplet-confined cell arrays," *Biotechnol. Prog.*, vol. 26, no. 1, pp. 220–231, 2010.
- [15] T. G. Henares, F. Mizutani, and H. Hisamoto, "Current development in microfluidic immunosensing chip," *Anal. Chim. Acta*, vol. 611, no. 1, pp. 17–30, Mar. 2008.
- [16] A. H. C. Ng, U. Uddayasankar, and A. R. Wheeler, "Immunoassays in microfluidic systems," *Anal. Bioanal. Chem.*, vol. 397, no. 3, pp. 991–1007, Jun. 2010.
- [17] J. Mok, M. N. Mindrinos, R. W. Davis, and M. Javanmard, "Digital microfluidic assay for protein detection," *Proc. Natl. Acad. Sci.*, vol. 111, no. 6, pp. 2110–2115, Feb. 2014.
- [18] N. Pamme, "Continuous flow separations in microfluidic devices," *Lab. Chip*, vol. 7, no. 12, pp. 1644–1659, Nov. 2007.
- [19] D. Pavia, G. Lampman, G. Kriz, and J. Vyvyan, *Introduction to Spectroscopy*. Cengage Learning, 2008.

- [20] "Modern Analytical Chemistry by David T Harvey: McGraw-Hill Science/Engineering/Math 9780072375473 Hardcover, 1 - ExtremelyReliable." [Online]. Available: http://www.abebooks.com/Modern-Analytical-Chemistry-David-T-Harvey/11787597990/bd?cm_mmc=gmc-_-gmc-_-PLA-_-v01. [Accessed: 22-Apr-2015].
- [21] S. K. Chapman and G. A. Reid, Eds., "UV-Visible Spectroscopy as a Tool to Study Flavoproteins - Springer," Humana Press, 1999.
- [22] X. Casadevall i Solvas, X. Niu, K. Leeper, S. Cho, S.-I. Chang, J. B. Edel, and A. J. deMello, "Fluorescence detection methods for microfluidic droplet platforms," *J. Vis. Exp.*, no. 58, Dec. 2011.
- [23] G. Zizak, "Flame Emission Spectroscopy: Fundamentals and Applications."
- [24] "Fundamentals of Modern UV-Visible Spectroscopy Agilent Book," *Scribd*. [Online]. Available: <https://www.scribd.com/doc/136846022/Fundamentals-of-Modern-UV-Visible-Spectroscopy-Agilent-Book>. [Accessed: 23-Apr-2015].
- [25] F. A. Bovey, P. A. Mirau, and H. S. Gutowsky, *Nuclear Magnetic Resonance Spectroscopy*. Elsevier, 1988.
- [26] C. Mariani and G. Stefani, "Photoemission Spectroscopy: Fundamental Aspects," in *Synchrotron Radiation*, S. Mobilio, F. Boscherini, and C. Meneghini, Eds. Springer Berlin Heidelberg, 2015, pp. 275–317.
- [27] "2.2.46. Chromatographic Separation Techniques," *Scribd*. [Online]. Available: <https://www.scribd.com/doc/91384694/2-2-46-Chromatographic-Separation-Techniques>. [Accessed: 28-Apr-2015].
- [28] V. Bansal, "HIGH PERFORMANCE LIQUID CHROMATOGRAPHY: A SHORT REVIEW," *J. Glob. Pharma Technol.*, vol. 2, no. 5, Jun. 2010.
- [29] T. Kupiec, "Quality-Control Analytical Methods: High-Performance Liquid Chromatography," *Int. J. Pharm. Compd.*, vol. 8, no. 3, pp. 223–227, Jun. 2004.

- [30] R. Z. Ráfliné, S. H. Kószeginé, I. Török, and T. Paál, “[Chromatographic methods in the European Pharmacopoeia],” *Acta Pharm. Hung.*, vol. 71, no. 2, pp. 205–212, Aug. 2001.
- [31] J. C. Bellot and J. S. Condoret, “Liquid chromatography modelling: a review,” *Process Biochem.*, vol. 26, no. 6, pp. 363–376, Dec. 1991.
- [32] W. Christie, “Detectors for high-performance liquid chromatography of lipids with special reference to evaporative light-scattering detection,” *Advances in lipid methodology*, vol. one, pp. 239–271, 1992.
- [33] R. Nuber, H. Maucher, and E. F. Stange, “Size exclusion chromatography for extraction of serum bile acids,” *J. Lipid Res.*, vol. 31, no. 8, pp. 1517–1522, Aug. 1990.
- [34] A. E. K. My Hedhammar, “Chromatographic methods for protein purification.”
- [35] J.-L. Ochoa, “Hydrophobic (interaction) chromatography,” *Biochimie*, vol. 60, no. 1, pp. 1–15, Mar. 1978.
- [36] *Protein Chromatography - Methods and Protocols*. .
- [37] M. Hamidi and N. Zarei, “A reversed-phase high-performance liquid chromatography method for bovine serum albumin assay in pharmaceutical dosage forms and protein/antigen delivery systems,” *Drug Test. Anal.*, vol. 1, no. 5, pp. 214–218, May 2009.
- [38] P. Cuatrecasas, “Protein Purification by Affinity Chromatography DERIVATIZATIONS OF AGAROSE AND POLYACRYLAMIDE BEADS,” *J. Biol. Chem.*, vol. 245, no. 12, pp. 3059–3065, Jun. 1970.
- [39] M. Zachariou, *Affinity Chromatography: Methods and Protocols*. Springer Science & Business Media, 2008.
- [40] T. Hatano, M. Hori, R. W. Hemingway, and T. Yoshida, “Size exclusion chromatographic analysis of polyphenol-serum albumin complexes,” *Phytochemistry*, vol. 63, no. 7, pp. 817–823, Aug. 2003.
- [41] G. Alvarez-Manilla, Atwood, Y. Guo, N. L. Warren, R. Orlando, and M. Pierce, “Tools for Glycoproteomic Analysis: Size Exclusion Chromatography Facilitates Identification of Tryptic

- Glycopeptides with N-linked Glycosylation Sites," *J. Proteome Res.*, vol. 5, no. 3, pp. 701–708, Mar. 2006.
- [42] A. B. Theberge, F. Courtois, Y. Schaerli, M. Fischlechner, C. Abell, F. Hollfelder, and W. T. S. Huck, "Microdroplets in Microfluidics: An Evolving Platform for Discoveries in Chemistry and Biology," *Angew. Chem. Int. Ed.*, vol. 49, no. 34, pp. 5846–5868, 2010.
- [43] N. Gasilova, Q. Yu, L. Qiao, and H. H. Girault, "On-Chip Spyhole Mass Spectrometry for Droplet-Based Microfluidics," *Angew. Chem. Int. Ed.*, vol. 53, no. 17, pp. 4408–4412, Apr. 2014.
- [44] M. Swartz, "Hplc Detectors: A Brief Review," *J. Liq. Chromatogr. Relat. Technol.*, vol. 33, no. 9–12, pp. 1130–1150, Jul. 2010.
- [45] M. F. Smiechowski, V. F. Lvovich, S. Roy, A. Fleischman, W. H. Fissell, and A. T. Riga, "Electrochemical detection and characterization of proteins," *Biosens. Bioelectron.*, vol. 22, no. 5, pp. 670–677, Dec. 2006.
- [46] Y. Zhou and J. Yoon, "Recent progress in fluorescent and colorimetric chemosensors for detection of amino acids," *Chem. Soc. Rev.*, vol. 41, no. 1, p. 52, 2012.
- [47] "About fluorescence - 998-0050.pdf." [Online]. Available: <http://www.turnerdesigns.com/t2/doc/appnotes/998-0050.pdf>. [Accessed: 25-Aug-2016].
- [48] T. H. Mourey and L. E. Oppenheimer, "Principles of operation of an evaporative light-scattering detector for liquid chromatography," *Anal. Chem.*, vol. 56, no. 13, pp. 2427–2434, Nov. 1984.
- [49] H. Wu and D. Y. Wu, "Nature of Heat Denaturation of Proteins," *J. Biol. Chem.*, vol. 64, no. 2, pp. 369–378, Jun. 1925.
- [50] W. Völkel, A. Pähler, and W. Dekant, "Gas chromatography-negative ion chemical ionization mass spectrometry as a powerful tool for the detection of mercapturic acids and DNA and protein adducts as biomarkers of exposure to halogenated olefins," *J. Chromatogr. A*, vol. 847, no. 1–2, pp. 35–46, Jun. 1999.

- [51] S. Matsumura, H. Kataoka, and M. Makita, "Capillary gas chromatographic analysis of protein amino acids as their N(O,S)-isobutoxycarbonyl methyl ester derivatives," *Biomed. Chromatogr.*, vol. 9, no. 5, pp. 205–210, Sep. 1995.
- [52] M. E. Swartz, "UPLC™: An Introduction and Review," *J. Liq. Chromatogr. Relat. Technol.*, vol. 28, no. 7–8, pp. 1253–1263, Apr. 2005.
- [53] L. Nováková, L. Matysová, and P. Solich, "Advantages of application of UPLC in pharmaceutical analysis," *Talanta*, vol. 68, no. 3, pp. 908–918, Jan. 2006.
- [54] D. A. Wolters, M. P. Washburn, and J. R. Yates, "An Automated Multidimensional Protein Identification Technology for Shotgun Proteomics," *Anal. Chem.*, vol. 73, no. 23, pp. 5683–5690, Dec. 2001.
- [55] J. Štěpánek, M. Příbyl, D. Šnita, and M. Marek, "Microfluidic chip for fast bioassays—evaluation of binding parameters," *Biomicrofluidics*, vol. 1, no. 2, Apr. 2007.
- [56] M. He, J. S. Edgar, G. D. M. Jeffries, R. M. Lorenz, J. P. Shelby, and D. T. Chiu, "Selective Encapsulation of Single Cells and Subcellular Organelles into Picoliter- and Femtoliter-Volume Droplets," *Anal. Chem.*, vol. 77, no. 6, pp. 1539–1544, Mar. 2005.
- [57] L. Mazutis, A. F. Araghi, O. J. Miller, J.-C. Baret, L. Frenz, A. Janoshazi, V. Taly, B. J. Miller, J. B. Hutchison, D. Link, A. D. Griffiths, and M. Ryckelynck, "Droplet-Based Microfluidic Systems for High-Throughput Single DNA Molecule Isothermal Amplification and Analysis," *Anal. Chem.*, vol. 81, no. 12, pp. 4813–4821, Jun. 2009.
- [58] D. T. Chiu and R. M. Lorenz, "Chemistry and Biology in Femtoliter and Picoliter Volume Droplets," *Acc. Chem. Res.*, vol. 42, no. 5, pp. 649–658, May 2009.
- [59] G. H. Qing Xiang, "Miniaturized Immunoassay Microfluidic System with Electrokinetic Control," *Biosens. Amp Bioelectron.*, vol. 21, no. 10, pp. 2006–9, 2006.

- [60] Z. Li, S. Y. Mak, A. Sauret, and H. C. Shum, "Syringe-pump-induced fluctuation in all-aqueous microfluidic system implications for flow rate accuracy," *Lab. Chip*, vol. 14, no. 4, p. 744, 2014.
- [61] R. Dingreville and J. Qu, "Interfacial excess energy, excess stress and excess strain in elastic solids: Planar interfaces," *J. Mech. Phys. Solids*, vol. 56, no. 5, pp. 1944–1954, May 2008.
- [62] J. W. Gibbs, *The collected works / of J. W. Gibbs,...* Green (New-York), 1928.
- [63] J. Berthier and K. Brakke, *Physics of Microdroplets*. Somerset, NJ, USA: John Wiley & Sons, 2012.
- [64] H. J. Lee and C.-J. Kim, "Surface-tension-driven microactuation based on continuous electrowetting," *J. Microelectromechanical Syst.*, vol. 9, no. 2, pp. 171–180, Jun. 2000.
- [65] R. Blossey, "Self-cleaning surfaces — virtual realities," *Nat. Mater.*, vol. 2, no. 5, pp. 301–306, May 2003.
- [66] C. N. Baroud, F. Gallaire, and R. Danga, "Dynamics of microfluidic droplets," *Lab. Chip*, vol. 10, no. 16, pp. 2032–2045, Aug. 2010.
- [67] S. L. Anna and H. C. Mayer, "Microscale tipstreaming in a microfluidic flow focusing device," *Phys. Fluids 1994-Present*, vol. 18, no. 12, p. 121512, Dec. 2006.
- [68] D. N. Breslauer, P. J. Lee, and L. P. Lee, "Microfluidics-based systems biology," *Mol. Biosyst.*, vol. 2, no. 2, p. 97, 2006.
- [69] J. H. Xu, S. W. Li, J. Tan, Y. J. Wang, and G. S. Luo, "Controllable Preparation of Monodisperse O/W and W/O Emulsions in the Same Microfluidic Device," *Langmuir*, vol. 22, no. 19, pp. 7943–7946, Sep. 2006.
- [70] A. S. Basu and Y. B. Gianchandani, "Virtual microfluidic traps, filters, channels and pumps using Marangoni flows," *J. Micromechanics Microengineering*, vol. 18, no. 11, p. 115031, Nov. 2008.
- [71] J. A. Hamilton and D. P. Cistola, "Transfer of oleic acid between albumin and phospholipid vesicles.," *Proc. Natl. Acad. Sci. U. S. A.*, vol. 83, no. 1, pp. 82–86, Jan. 1986.

- [72] Z. W. Ulissi, J. Zhang, V. Sresht, D. Blankschtein, and M. S. Strano, "2D Equation-of-State Model for Corona Phase Molecular Recognition on Single-Walled Carbon Nanotube and Graphene Surfaces," *Langmuir*, vol. 31, no. 1, pp. 628–636, Jan. 2015.
- [73] *Molecular Thermodynamics of Fluid-Phase Equilibria*, 3 edition. Upper Saddle River, N.J: Prentice Hall, 1998.
- [74] M. D. LeVan and T. Vermeulen, "Binary Langmuir and Freundlich isotherms for ideal adsorbed solutions," *J. Phys. Chem.*, vol. 85, no. 22, pp. 3247–3250, Oct. 1981.
- [75] P. Atkins and J. de Paula, *Atkins' Physical Chemistry*. OUP Oxford, 2014.
- [76] B. Kirby, *Micro- and Nanoscale Fluid Mechanics: Transport in Microfluidic Devices*. Cambridge University Press, 2010.
- [77] J. Berthier and P. Silberzan, *Microfluidics for Biotechnology*. Artech House, 2010.
- [78] J. Berthier, *Micro-Drops and Digital Microfluidics*. William Andrew, 2012.
- [79] P. Garstecki, M. J. Fuerstman, H. A. Stone, and G. M. Whitesides, "Formation of droplets and bubbles in a microfluidic T-junction—scaling and mechanism of break-up," *Lab. Chip*, vol. 6, no. 3, p. 437, 2006.
- [80] *Transport Phenomena, Revised 2nd Edition*, 2nd edition. John Wiley & Sons, Inc., 2006.
- [81] J. Atencia and D. J. Beebe, "Controlled microfluidic interfaces," *Nature*, vol. 437, no. 7059, pp. 648–655, Sep. 2005.
- [82] T. Thorsen, "Microfluidic technologies for high-throughput screening applications," phd, California Institute of Technology, 2003.
- [83] S. N. Bhatia and D. E. Ingber, "Microfluidic organs-on-chips," *Nat. Biotechnol.*, vol. 32, no. 8, pp. 760–772, Aug. 2014.

- [84] "Wiley: The Physics of Microdroplets - Jean Berthier, Ken Brakke." [Online]. Available: <http://www.wiley.com/WileyCDA/WileyTitle/productCd-0470938803.html>. [Accessed: 19-Jun-2015].
- [85] J. Xu and D. Attinger, "Drop on demand in a microfluidic chip," *J. Micromechanics Microengineering*, vol. 18, no. 6, p. 65020, Jun. 2008.
- [86] H. Gu, M. H. G. Duits, and F. Mugele, "Droplets Formation and Merging in Two-Phase Flow Microfluidics," *Int. J. Mol. Sci.*, vol. 12, no. 4, pp. 2572–2597, Apr. 2011.
- [87] G. F. Christopher and S. L. Anna, "Microfluidic methods for generating continuous droplet streams," *J. Phys. Appl. Phys.*, vol. 40, no. 19, pp. R319–R336, Oct. 2007.
- [88] P. Garstecki, H. Stone, and G. Whitesides, "Mechanism for Flow-Rate Controlled Breakup in Confined Geometries: A Route to Monodisperse Emulsions," *Phys. Rev. Lett.*, vol. 94, no. 16, Apr. 2005.
- [89] A. S. Basu, "Droplet morphometry and velocimetry (DMV): a video processing software for time-resolved, label-free tracking of droplet parameters," *Lab. Chip*, vol. 13, no. 10, p. 1892, 2013.
- [90] T. Ward, M. Faivre, M. Abkarian, and H. A. Stone, "Microfluidic flow focusing: Drop size and scaling in pressure versus flow-rate-driven pumping," *ELECTROPHORESIS*, vol. 26, no. 19, pp. 3716–3724, 2005.
- [91] K. Wang, Y. C. Lu, J. H. Xu, and G. S. Luo, "Determination of Dynamic Interfacial Tension and Its Effect on Droplet Formation in the T-Shaped Microdispersion Process," *Langmuir*, vol. 25, no. 4, pp. 2153–2158, Feb. 2009.
- [92] T. Thorsen, R. W. Roberts, F. H. Arnold, and S. R. Quake, "Dynamic Pattern Formation in a Vesicle-Generating Microfluidic Device," *Phys. Rev. Lett.*, vol. 86, no. 18, pp. 4163–4166, Apr. 2001.
- [93] "PubMed entry." .
- [94] A. A. Spector, K. John, and J. E. Fletcher, "Binding of long-chain fatty acids to bovine serum albumin," *J. Lipid Res.*, vol. 10, no. 1, pp. 56–67, Jan. 1969.

- [95] F. K. Hansen and G. Rødsrud, "Surface tension by pendant drop," *J. Colloid Interface Sci.*, vol. 141, no. 1, pp. 1–9, Jan. 1991.
- [96] Pubchem, "UDP-glucose | C15H24N2O17P2 - PubChem." [Online]. Available: <https://pubchem.ncbi.nlm.nih.gov/compound/UDP-glucose#section=Chemical-and-Physical-Properties>. [Accessed: 27-Aug-2016].
- [97] Y. A. Gryzunov, A. Arroyo, J.-L. Vigne, Q. Zhao, V. A. Tyurin, C. A. Hubel, R. E. Gandley, Y. A. Vladimirov, R. N. Taylor, and V. E. Kagan, "Binding of fatty acids facilitates oxidation of cysteine-34 and converts copper–albumin complexes from antioxidants to prooxidants," *Arch. Biochem. Biophys.*, vol. 413, no. 1, pp. 53–66, May 2003.
- [98] R. Kebriaei and A. S. Basu, "Autosizing, closed-loop drop generator using morphometric image feedback," presented at the 17th International Conference on Miniaturized Systems for Chemistry and Life Sciences, MicroTAS 2013, 2013, vol. 3, pp. 1944–1946.
- [99] "Xue d Chen y Atherton d p Linear Feedback Control Analysis A," *Scribd*. [Online]. Available: <https://www.scribd.com/doc/47280441/Xue-d-Chen-y-Atherton-d-p-Linear-Feedback-Control-Analysis-A>. [Accessed: 10-Aug-2015].
- [100] R. G. Reed, "Location of long chain fatty acid-binding sites of bovine serum albumin by affinity labeling," *J. Biol. Chem.*, vol. 261, no. 33, pp. 15619–15624, Nov. 1986.
- [101] [Online]. Available: https://www.sepax-tech.com/usermanual/UserManual_Zenix.pdf. [Accessed: 05-May-2016].
- [102] G. K. Kurup and A. S. Basu, "Field-free particle focusing in microfluidic plugs," *Biomicrofluidics*, vol. 6, no. 2, pp. 22008-22008–10, Apr. 2012.
- [103] R. Kebriaei and A. S. Basu, "Label-free inline hplc detector using a drop generator," presented at the 18th International Conference on Miniaturized Systems for Chemistry and Life Sciences, MicroTAS 2014, 2014, pp. 2375–2377.

- [104] A. S. Basu and Y. B. Gianchandani, "Shaping high-speed Marangoni flow in liquid films by microscale perturbations in surface temperature," *Appl. Phys. Lett.*, vol. 90, no. 3, p. 34102, 2007.
- [105] K. Donovan, "Computational Fluid Dynamics Modeling of Two-Dimensional and Three-Dimensional Segmented Flow in Microfluidic Chips," *Masters Theses*, Jan. 2014.
- [106] H. Gu, M. H. G. Duits, and F. Mugele, "Droplets Formation and Merging in Two-Phase Flow Microfluidics," *Int. J. Mol. Sci.*, vol. 12, no. 4, pp. 2572–2597, Apr. 2011.
- [107] "A COMSOL Multiphysics® Model of Droplet Formation at a Flow Focusing Device - abrishamkar_abstract.pdf." [Online]. Available: https://www.comsol.com/paper/download/181817/abrishamkar_abstract.pdf. [Accessed: 28-Aug-2016].
- [108] G. F. Christopher, N. N. Noharuddin, J. A. Taylor, and S. L. Anna, "Experimental observations of the squeezing-to-dripping transition in T-shaped microfluidic junctions," *Phys. Rev. E*, vol. 78, no. 3, p. 36317, Sep. 2008.
- [109] N. N. Pejnovic, J. M. Pantic, I. P. Jovanovic, G. D. Radosavljevic, A. L. Djukic, N. N. Arsenijevic, and M. L. Lukic, "Galectin-3 is a regulator of metaflammation in adipose tissue and pancreatic islets," *Adipocyte*, vol. 2, no. 4, pp. 266–271, Oct. 2013.
- [110] "The Role of Galectins in Protein Trafficking - Delacour - 2009 - Traffic - Wiley Online Library." [Online]. Available: <http://onlinelibrary.wiley.com/doi/10.1111/j.1600-0854.2009.00960.x/pdf>. [Accessed: 25-Aug-2016].
- [111] K. Drickamer, "Evolving views of protein glycosylation," *Trends Biochem. Sci.*, vol. 23, no. 9, pp. 321–324, Sep. 1998.
- [112] S. H. Barondes, V. Castronovo, D. N. W. Cooper, R. D. Cummings, K. Drickamer, T. Felzi, M. A. Gitt, J. Hirabayashi, C. Hughes, K. Kasai, H. Leffler, F.-T. Liu, R. Lotan, A. M. Mercurio, M. Monsigny, S. Pillai,

- F. Poirer, A. Raz, P. W. J. Rigby, J. M. Rini, and J. L. Wang, "Galectins: A family of animal β -galactoside-binding lectins," *Cell*, vol. 76, no. 4, pp. 597–598, Feb. 1994.
- [113] N. G. Than, R. Romero, M. Goodman, A. Weckle, J. Xing, Z. Dong, Y. Xu, F. Tarquini, A. Szilagy, P. Gal, Z. Hou, A. L. Tarca, C. J. Kim, J.-S. Kim, S. Haidarian, M. Uddin, H. Bohn, K. Benirschke, J. Santolaya-Forgas, L. I. Grossman, O. Erez, S. S. Hassan, P. Zavodszky, Z. Papp, and D. E. Wildman, "A primate subfamily of galectins expressed at the maternal-fetal interface that promote immune cell death," *Proc. Natl. Acad. Sci.*, vol. 106, no. 24, pp. 9731–9736, Jun. 2009.
- [114] H. W. Christinger, G. Fuh, A. M. de Vos, and C. Wiesmann, "The Crystal Structure of Placental Growth Factor in Complex with Domain 2 of Vascular Endothelial Growth Factor Receptor-1," *J. Biol. Chem.*, vol. 279, no. 11, pp. 10382–10388, Mar. 2004.
- [115] A. H. Demond and A. S. Lindner, "Estimation of interfacial tension between organic liquids and water," *Environ. Sci. Technol.*, vol. 27, no. 12, pp. 2318–2331, Nov. 1993.

ABSTRACT

SUB-PICOGRAM, INLINE DETECTION OF PROTEINS USING MICROFLUIDIC DROP GENERATORS AND SHAPE-BASED DETECTION

by

RAZIEH KEBRIAEI

December 2016

Advisor: Dr. Amar S. Basu

Major: Biomedical Engineering

Degree: Doctor of Philosophy

Proteomic workflows rely on sensitive and precise methods for purifying and detecting proteins, and one of the most popular methods is liquid chromatography (LC) followed by an inline detector. However, the most commonly used method, UV-Vis absorbance, provides relatively low sensitivity and requires long path lengths in the flow cell. Mass spectrometry-based detectors provide high sensitivity, but are more expensive and require some optimization of protein ionization and fragmentation. Other sensitive detection methods (such as ELISA) cannot be easily integrated into 'inline' continuous measurement, as is needed for LC. In this thesis, we present a highly sensitive, label-free method to detect proteins in continuous flow, using a pressure-driven microfluidic droplet generator. The system consists of a cross junction or flow focusing structure where the flowing stream of proteins is combined with two coflowing streams of oil which break up the former stream into a train of droplets. In such a system, the droplet size predictably scales with interfacial tension (IFT) of the oil-water interface. When globular proteins (eg BSA) enter the junction, they adsorb to the interface and reduce IFT, and

thereby the droplet radius. Temporal variations in droplet size therefore correlate with changes in protein concentration. Using microfluidic drop generators as an inline detection method provides two benefits: 1) it can improve available limits of detection, because the high surface area to volume ratio enhances adsorption phenomena, and 2) it provides fast time resolution, due to the high rate of drop generation.

To test and implement our system, we designed and operated a pressure driven system which can work both in closed loop and open loop versions. Inlet pressure can be actuated and controlled precisely depending on the requirements for the size of droplets. To maximize the effect of interfacial tension, we operate a 100 μm drop generator at small Capillary number ($Ca= 0.00135\text{-}0.007739$). Four different carrier phases (oleic acid, octanol, hexadecane, and FC-40) were tested with four proteins (BSA, thyroglobulin, uridine, placental growth factor, galectin and blood plasma). Image processing software developed in our group tracks droplet size, length, frequency, shape eccentricity, and creates chromatograms based on these parameters. Droplet sizes were found to decrease when a hydrophobic protein was combined with a hydrophobic carrier. Calibration curves show that the changes in drop size, velocity, and shape eccentricity are linear with protein concentration, provided the protein concentration is less than the critical micelle concentration. The best limit of detection is $\sim 1 \mu\text{g/mL}$ in a 1 nL droplet, which equates to 1 fg of total protein. The low detection limits are due to favorable scaling: the high surface area to volume ratio in droplet systems increases the probability of adsorption, and therefore changes drop size even at low concentration. When used as a detector for high performance liquid chromatography (HPLC), it demonstrates sensitivity

up to 100X better than conventional UV-Vis detectors. This detection method can potentially serve as a label-free, universal detector for proteins.

AUTOBIOGRAPHICAL STATEMENT

Razieh Kebraei received her Bachelor degree in Chemical Engineering from Bahonar University of Kerman, IRAN, 2007 and her master degree in Biotechnology Engineering from IUST (Iran University of Science and Technology) IRAN, 2010. Currently, she is pursuing her PhD degree in Biomedical Engineering from Wayne State University. Her dissertation is in the field of droplet microfluidics entitled “Sub-Picogram, Inline Detection of Proteins Using Microfluidic Drop Generators and Shape-Based Detection” under supervision of Prof. Amar S. Basu.

Besides her research work at WSU she has also served as teaching assistant during her PhD degree. She has been awarded Garrett T. Heberlein Excellence in Teaching Award (March 2016), summer dissertation fellowship from Wayne State Graduate School (February 2016), Wayne State University professional travel award (2014, 2015), one of the ten selected research posters in SWE national conference (October 2015) and society of laboratory automation and screening (Tony B. Award, among 10 participating countries in SLAS 2013).